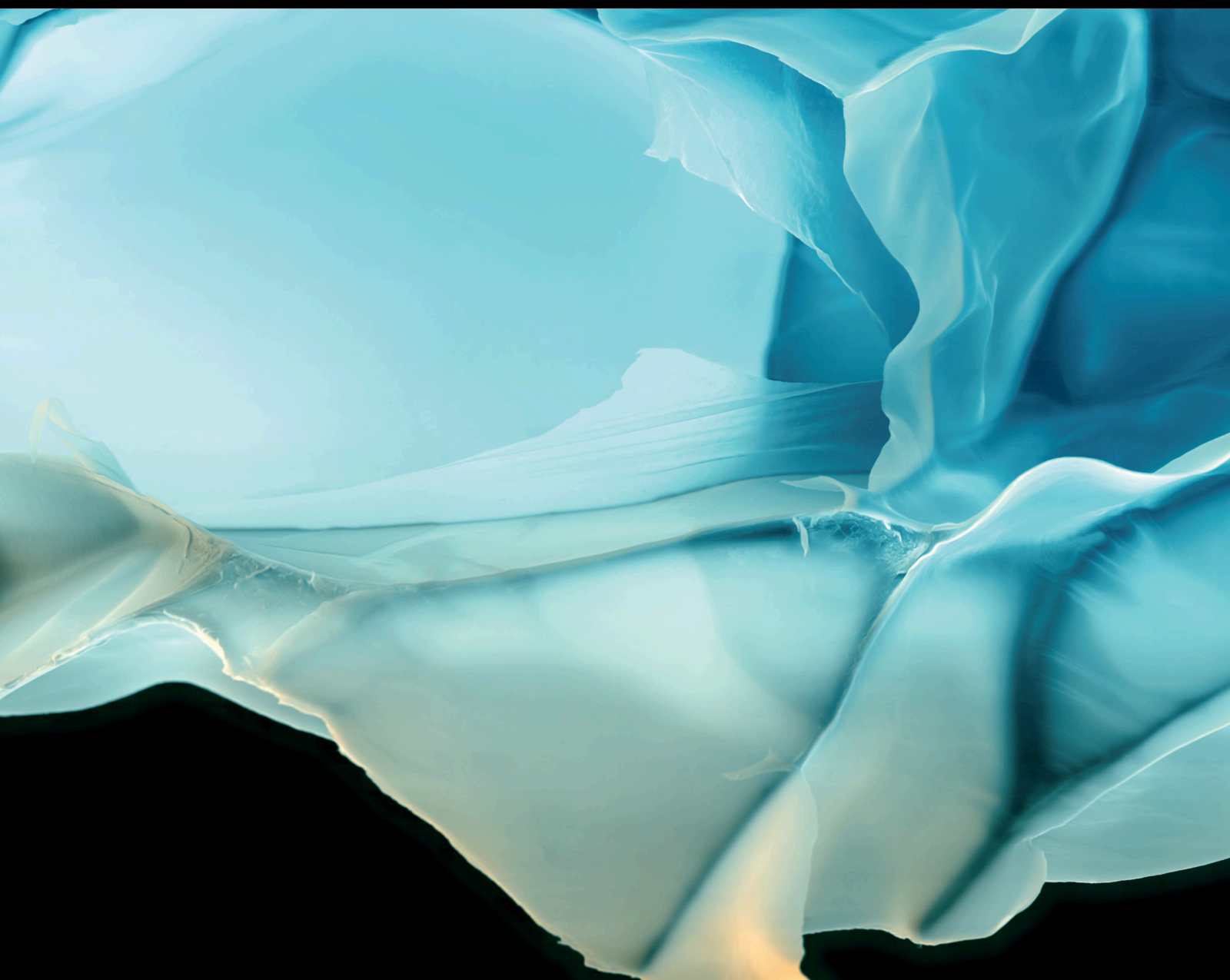


Advances in Polymer Technology

Functionalized Polymeric Materials for Catalytic Upgrading of Biobased Feedstocks

Lead Guest Editor: Song Yang,
Guest Editors: Chunbao Xu, and Heng Zhang





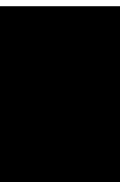
Functionalized Polymeric Materials for Catalytic Upgrading of Biobased Feedstocks

Advances in Polymer Technology

**Functionalized Polymeric Materials
for Catalytic Upgrading of Biobased
Feedstocks**

Lead Guest Editor: Song Yang,

Guest Editors: Chunbao Xu, and Heng Zhang



Copyright © 2021 Hindawi Limited. All rights reserved.

This is a special issue published in "Advances in Polymer Technology." All articles are open access articles distributed under the Creative Commons Attribution License, which permits unrestricted use, distribution, and reproduction in any medium, provided the original work is properly cited.

Chief Editor




Ning Zhu, China

Editorial Board

Nasir M. Ahmad, Pakistan
Paul Andersen, USA
Xianglan Bai, USA
Lucia Baldino, Italy
Matthias Bartneck, Germany
Anil K. Bhowmick, India
Marcelo Calderón, Spain
Federico Carosio, Italy
Teresa Casimiro, Portugal
Sébastien Déon, France
Alain Durand, France
Coro Echeverria, Spain
Thomas J. Farmer, United Kingdom
María Fernández-Ronco, Switzerland
Volkan Filiz, Germany
Maria L. Focarete, Italy
E. Johan Foster, USA
Wenxin Fu, USA
Behnam Ghalei, Japan
Camino Giovanni, Italy
Chiara Gualandi, Italy
Leandro Gurgel, Brazil
Minna Hakkarainen, Sweden
Christian Hopmann, Germany
Daniel J. Keddie, United Kingdom
Sam Kenig, Israel
Adam Kiersnowski, Poland
Ick Soo Kim, Japan
Yohei Kotsuchibashi, Japan
L. James Lee, USA
Siu N. Leung, Canada
Wen Li, China
Haiqing Lin, USA
Katja Loos, The Netherlands
Hong-Yang Ma, China
Milan Marić, Canada
Tamilselvan Mohan, Slovenia
Alexandra Muñoz-Bonilla, Spain
Rafael Muñoz-Espí, Spain
Kenichi Nagase, Japan
Mohamad A. Nahil, United Kingdom
Ngoc A. Nguyen, Vietnam
Daewon Park, USA
Kinga Pielichowska, Poland
Sikander Rafiq, Pakistan
Filippo Rossi, Italy
Sagar Roy, USA
Júlio Santos, Brazil
Mona Semsarilar, France
Lu Shao, China
Gaurav Sharma, India
Sang E. Shim, Republic of Korea
Melissa F. Siqueira, Brazil
Mark A. Spalding, USA
Gyorgy Szekely, Saudi Arabia
Vijay K. Thakur, USA
Leonard D. Tijing, Australia
Lih-sheng Turng, USA
Costas Tzoganakis, Canada
Micaela Vannini, Italy
Surendar R. Venna, USA
Pierre Verge, Luxembourg
John Vlachopoulos, Canada
Yu Wang, USA
Ren Wei, Germany
Chunfei Wu, United Kingdom
Bingang Xu, Hong Kong
Yun Yu, Australia
Szczepan Zapotoczny, Poland
Martin Zatloukal, Czech Republic
Xinyu Zhang, USA
Liqun Zhang, China
Li Zibiao, Singapore



Contents

Functionalized Polymeric Materials for Catalytic Upgrading of Biobased Feedstocks

Heng Zhang , Chunbao Charles Xu , and Song Yang 



Editorial (2 pages), Article ID 5036404, Volume 2021 (2021)

3-Bromopyridine-Heterogenized Phosphotungstic Acid for Efficient Trimerization of Biomass-Derived 5-Hydroxymethylfurfural with 2-Methylfuran to C21 Fuel Precursor

Yufei Xu, Zhaozhuo Yu, Hu Li , and Song Yang 

Research Article (12 pages), Article ID 6438490, Volume 2020 (2020)

Functionalized Metal-Organic Framework Catalysts for Sustainable Biomass Valorization

Xiaofang Liu , Zhigang Liu, and Rui Wang 






Review Article (11 pages), Article ID 1201923, Volume 2020 (2020)

Progress of Catalytic Valorization of Bio-Glycerol with Urea into Glycerol Carbonate as a Monomer for Polymeric Materials

Heng Zhang , Hu Li , Anping Wang , Chunbao (Charles) Xu , and Song Yang 

Review Article (17 pages), Article ID 7207068, Volume 2020 (2020)

Adsorption of Chelerythrine from *Toddalia asiatica* (L.) Lam. by ZSM-5

Yunlong Liu , Jie Guo , Zhuobing Xiao , Dazhao Peng , and Ke Song 

Research Article (9 pages), Article ID 9408921, Volume 2020 (2020)

Efficient Production of Methyl Oleate Using a Biomass-Based Solid Polymeric Catalyst with High Acid Density

Anping Wang , Heng Zhang , Hu Li , and Song Yang 

Research Article (11 pages), Article ID 4041631, Volume 2019 (2019)

Editorial

Functionalized Polymeric Materials for Catalytic Upgrading of Biobased Feedstocks

Heng Zhang ¹, Chunbao Charles Xu ², and Song Yang ¹

¹State Key Laboratory Breeding Base of Green Pesticide & Agricultural Bioengineering, Key Laboratory of Green Pesticide & Agricultural Bioengineering, Ministry of Education, State-Local Joint Laboratory for Comprehensive Utilization of Biomass, Center for Research & Development of Fine Chemicals, Guizhou University, Guiyang, Guizhou 550025, China

²Institute for Chemicals and Fuels from Alternative Resources (ICFAR), Department of Chemical and Biochemical Engineering, Western University, London, Ontario, Canada N6A 5B9

Correspondence should be addressed to Heng Zhang; hzhang23@gzu.edu.cn, Chunbao Charles Xu; cxu6@uwo.ca, and Song Yang; hzx.msm@gmail.com

Received 2 March 2021; Accepted 3 March 2021; Published 19 March 2021

Copyright © 2021 Heng Zhang et al. This is an open access article distributed under the Creative Commons Attribution License, which permits unrestricted use, distribution, and reproduction in any medium, provided the original work is properly cited.

Modern life depends on polymers, from materials applied in the manufacture of clothing, houses, cars, and airplanes to those demonstrating complex adhibitions in medicine, diagnostics, and electronics. More importantly, both natural and synthetic polymeric materials bearing versatile functionalities are gaining research interest for applications in catalysis, especially in the catalytic valorization of renewable biomass feedstocks (the abundant, natural, and low-cost biopolymers on the earth) to value-added chemicals and liquid biofuels [1–3]. As an important class of heterogeneous catalysts, functionalized polymeric materials with tailorable and attractive catalytic properties exhibit dramatic improvement of catalytic activity and selectivity in biomass refinery to produce energy and chemicals, compared with conventional counterparts.

The Special Issue “Functionalized Polymeric Materials for Catalytic Upgrading of Biobased Feedstocks” focuses on the introduction of polymer/polymeric catalysts preparation, functionalization of polymeric materials, and applications to guide the development and application of functionalized polymeric materials in biomass transformation. Five eminent research groups in the field of polymeric materials and biomass valorization have kindly accepted our invitation to participate in this special issue, briefly listed as follows:

In the paper entitled “Progress of Catalytic Valorization of Bio-Glycerol with Urea into Glycerol Carbonate as a Monomer for Polymeric Materials,” Zhang et al. summarized

the state-of-the-art accomplishments made in the efficient transformation of bioglycerol and urea into glycerol carbonate as a polymer monomer. Emphasis was given to the catalytic performance of the relevant catalysts such as zinc, magnesium, tungsten, ionic liquid-based catalysts, and waste-derived materials, reaction conditions, and possible pathways. Besides, how to modify the reaction conditions that will influence the related activities and selectivity to glycerol carbonate was also depicted [4].

In the paper entitled “Functionalized Metal-Organic Framework Catalysts for Sustainable Biomass Valorization,” Liu et al. depicted metal-organic frameworks (MOFs), also identified as micro- and mesoporous coordination polymers (PCPs) to be employed as versatile heterogeneous polymeric catalysts for biomass upgrading. They highlighted recently developed four types of MOFs like pristine MOFs and their composites, MOF-supported metal nanoparticles, acid-functionalized MOFs, and biofunctionalized MOFs for the production of green, sustainable, and industrially acceptable biomass-derived platform molecules: (1) upgrading of saccharides, (2) upgrading of furan derivatives, and (3) upgrading of other biobased compounds [5].

In the paper entitled “Efficient Production of Methyl Oleate Using a Biomass-Based Solid Polymeric Catalyst with High Acid Density,” Wang et al. investigated the biomass-based chitosan polymer acid catalyst (CS-SO₃H) for biodiesel production. The results showed that CS-SO₃H morphology

exhibited a sphere of about 10 μm diameter, and the acid density was as high as 3.81 mmol/g. The catalyst demonstrated good catalytic activity in the esterification of oleic acid and methanol, which is a model reaction of the preesterification process in the preparation of biodiesel from feedstocks with high acid values. Under the optimum reaction conditions (15/1 methanol/oleic acid mole ratio and 3 wt% catalyst dosage at 75°C for 3 h), the yield of methyl oleate came up to 95.7%. After four times of reuse, the yield of the catalyst could still reach 85.7%, which indicated that the catalyst depicted good catalytic activity and stability and showed potential application prospects [6].

In the paper entitled “Adsorption of Chelerythrine from *Toddalia asiatica* (L.) Lam. by ZSM-5,” Liu et al. performed a study focusing on the separation and purification of active components from biomass by using the micropolymer catalyst zeolite molecular sieves ZSM-5. Batch experiments revealed that the adsorption efficiency was affected by the solution pH, and the optimum initial solution pH was 6. The maximum adsorption capacity of CHE was found at a solid-liquid ratio of 2:15. This material was thought to be a promising adsorbent for purifying alkaloids (especially quaternary ammonium alkaloids) from medicinal herbs. In addition, a technique for isolating active components from the pretreatment process of biomass was also provided [7].

In the paper entitled “3-Bromopyridine-Heterogenized Phosphotungstic Acid for Efficient Trimerization of Biomass-Derived 5-Hydroxymethylfurfural with 2-Methylfuran to C_{21} Fuel Precursor,” Xu et al. employed the halogenated pyridine-heterogenized HPW as a heterogeneous acidic catalyst for the conversion of biomass-derived 5-hydroxymethylfurfural (HMF) and 2-methylfuran (2-MF) to C_{21} fuel precursor (MMBM). Single-factor optimization was utilized to test the catalytic performance of 3-BrPyPW; a good MMBM yield of 57.1% with 82.0% 2-MF conversion could be obtained under optimum reaction conditions. The 3-BrPyPW catalyst could be reused for four cycles without a significant decrease in its activity, which was characterized without obvious structure change after recycles. Moreover, a dominant reaction pathway for the synthesis of MMBM from HMF and 2-MF was elucidated [8].

As Guest Editors, we would like to appreciate all authors for their valuable contributions and the referees for their excellent work in reviewing the submitted manuscripts.

Conflicts of Interest

The editors declare that there is no conflict of interest regarding the publication.

Heng Zhang
Chunbao Charles Xu
Song Yang

References

- [1] H. Zhang, H. Li, C. Xu, and S. Yang, “Heterogeneously chemo/enzyme-functionalized porous polymeric catalysts of high-

performance for efficient biodiesel production,” *ACS Catalysis*, vol. 9, no. 12, pp. 10990–11029, 2019.

- [2] H. Zhang, H. Li, Y. Hu, K. T. Venkateswara Rao, C. (. C.). Xu, and S. Yang, “Advances in production of bio-based ester fuels with heterogeneous bifunctional catalysts,” *Renewable and Sustainable Energy Reviews*, vol. 114, article 109296, 2019.
- [3] H. Li, Z. Fang, R. L. Smith, and S. Yang, “Efficient valorization of biomass to biofuels with bifunctional solid catalytic materials,” *Progress in Energy and Combustion Science*, vol. 55, pp. 98–194, 2016.
- [4] H. Zhang, H. Li, A. Wang, C. Xu, and S. Yang, “Progress of catalytic valorization of bio-glycerol with urea into glycerol carbonate as a monomer for polymeric materials,” *Advances in Polymer Technology*, vol. 2020, Article ID 7207068, 17 pages, 2020.
- [5] X. Liu, Z. Liu, and R. Wang, “Functionalized metal-organic framework catalysts for sustainable biomass valorization,” *Advances in Polymer Technology*, vol. 2020, Article ID 1201923, 11 pages, 2020.
- [6] A. Wang, H. Zhang, H. Li, and S. Yang, “Efficient production of methyl oleate using a biomass-based solid polymeric catalyst with high acid density,” *Advances in Polymer Technology*, vol. 2019, no. 11, Article ID 4041631, 11 pages, 2019.
- [7] Y. Liu, J. Guo, Z. Xiao, D. Peng, and K. Song, “Adsorption of chelerythrine from *Toddalia asiatica* (L.) Lam. by ZSM-5,” *Advances in Polymer Technology*, vol. 2020, Article ID 9408921, 9 pages, 2020.
- [8] Y. Xu, Z. Yu, H. Li, and S. Yang, “3-bromopyridine-heterogenized phosphotungstic acid for efficient trimerization of biomass-derived 5-hydroxymethylfurfural with 2-methylfuran to C_{21} fuel precursor,” *Advances in Polymer Technology*, vol. 2020, no. 12, Article ID 6438490, 12 pages, 2020.

Research Article

3-Bromopyridine-Heterogenized Phosphotungstic Acid for Efficient Trimerization of Biomass-Derived 5-Hydroxymethylfurfural with 2-Methylfuran to C₂₁ Fuel Precursor

Yufei Xu, Zhaozhuo Yu, Hu Li , and Song Yang 

State Key Laboratory Breeding Base of Green Pesticide & Agricultural Bioengineering, Key Laboratory of Green Pesticide & Agricultural Bioengineering, Ministry of Education, State-Local Joint Laboratory for Comprehensive Utilization of Biomass, Center for Research & Development of Fine Chemicals, Guizhou University, Guiyang, Guizhou 550025, China

Correspondence should be addressed to Hu Li; hli13@gzu.edu.cn and Song Yang; jhzx.msm@gmail.com

Received 8 August 2019; Revised 12 April 2020; Accepted 24 April 2020; Published 6 August 2020

Academic Editor: Leandro Gurgel

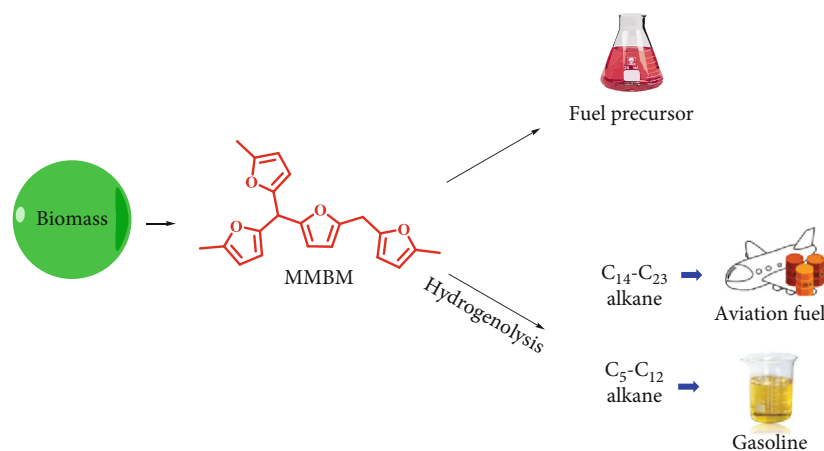
Copyright © 2020 Yufei Xu et al. This is an open access article distributed under the Creative Commons Attribution License, which permits unrestricted use, distribution, and reproduction in any medium, provided the original work is properly cited.

The production of long-chain carbon compounds (C₉-C₂₁) from biomass derivatives to alternate traditional fossil diesel is sustainable, eco-friendly, and potentially economic for modern industry. In this work, phosphotungstic acid heterogenized by 3-bromopyridine was achieved using a solvothermal method, which was demonstrated to be efficient for trimerization of biomass-derived 5-hydroxymethylfurfural (HMF) with 2-methylfuran (2-MF) to C₂₁ fuel precursor (57.1% yield) under mild reaction conditions. The heterogeneous acidic catalyst could be reused for four consecutive cycles without obvious loss of activity, and different characterization techniques (e.g., XRD (X-ray diffraction), TG (thermogravimetric analysis), SEM (scanning electron microscope), FT-IR (Fourier transform infrared spectroscopy), and BET (Brunauer-Emmett-Teller)) were utilized to investigate the performance of the catalyst. In addition, a plausible reaction pathway was postulated, on the basis of results obtained by NMR (nuclear magnetic resonance) and GC-MS (gas chromatography-mass spectrometer). This strategy provides a facile and efficient approach to prepare a recyclable acidic catalyst for the production of diesel fuel precursor from biomass via controllable polymerization.

1. Introduction

To relieve the increasingly severe shortage issues of energy in modern society over the last decade, more and more new conversion systems are established to utilize or explore alternative energy (e.g., wind power, geothermal energy, tidal energy, and solar power) to replace traditional mineral fuels [1–5]. Unfortunately, fossil energy still takes a big part in our daily life especially automobile and jet fuels [6, 7]. Therefore, it is urgent to find a renewable and benign matter for energy production via a new type of synthetic approaches. The terrestrial biomass was regarded as an environmental and sustainable feedstock to produce various platform molecules which can be directly employed for the synthesis of biofuels or value-added chemicals [8–15].

Generally, the jet fuels are composed of long-chain carbon molecules that could be produced from oligomerization of low-carbon molecules via the C-C bond formation such as aldol condensation and alkylation in the presence of a basic or acidic catalyst [16–20]. In this regard, the environmental and energy problems could be addressed effectively by using biomass-derived long-chain carbon molecules to replace the petrochemical molecules as the fuel precursor. A C₂₁ compound named 5-(bis(5-methylfuran-2-yl)methyl)-5'-methyl-2,2'-bifuran (MMBM), which is derived from condensation of biobased 2-methylfuran (2-MF) and 5-hydroxymethylfurfural (HMF) with an acid catalyst, is a cost-effective and promising biochemical for producing drop-in fuels [21] and can be directly employed to increase the fuel combustion efficiency. In addition, after hydrogenolysis, MMBM can be used as high-quality fuels (Scheme 1) [22],

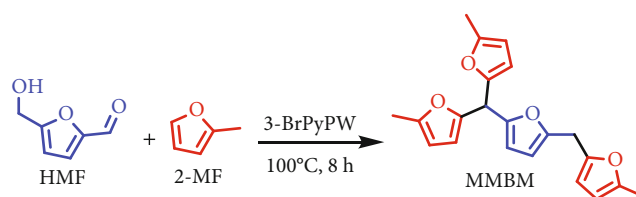


SCHEME 1: The production and application of biomass-based C₂₁ compound (MMBM).

such as aviation [23, 24] and diesel fuels [25]. Therefore, the production of such biomass-based C_n compounds for high-quality biofuels has attracted the researchers' interests in recent years.

In 2011, Corma et al. [24] utilized the 2-MF as the substrate to get the C₁₅ fuel molecule precursor (5,5-bis(5-methylfuran-2-group)penta-2-ketone) using H₂SO₄ as an acid catalyst. A total yield of 87% C_n fuel molecule precursor could be achieved through the hydroxyalkylation/alkylation process. However, the shortcomings are also obvious; for example, (1) the acid catalyst H₂SO₄ is harmful to the environment, and (2) the homogenous catalyst would be lost and could not be reused after one reaction cycle. In 2017, Dutta et al. [25] came up with a modified graphene material to catalyze HMF and 2-MF into MMBM under 63°C for 12 h. In 2018, Wang et al. [26] and Gebresillase et al. [27] also prepared Sn-K-10 and KCC-IAPSO₃H as acidic catalysts for the condensation of 2-MF with acetic anhydride and 2-MF with furfural, *n*-butyraldehyde, or 2-pentanone into C₁₇ or C₁₄-C₁₅ fuel precursors under relatively mild conditions, respectively. These reaction systems can achieve the conversion of biomass platform molecules into long-chain molecule precursors by using acid catalysts, while the main disadvantage is that the catalyst preparation methods are too complicated and the cost is too high.

HPAs (heteropoly acids) with superb strong acidity are extensively used as economic and environmental catalysts in organic synthesis [28–32]. In particular, phosphotungstic acid (HPW, H₃PW₁₂O₄₀) has a tetrahedral PO₄ core in the center of the anion structure, surrounded by twelve WO₆ polyhedra via oxygen atoms to link each other, which exhibits excellent catalytic activity for upgrading biomass-derived compounds into different valuable chemicals and biofuels [33, 34]. However, it should be mentioned that HPW is extremely soluble into most polar solvents, difficult to separate, corrosive to reactors, and polluted to the environment [35–48]. Taking the above problems into consideration, it is highly desirable to heterogenize HPW using a high-efficiency method. For example, Wang et al. [50] and Fang et al. [51] prepared electric flocculation of HPW and silica-supported HPW heterogeneous catalysts for the con-



SCHEME 2: The synthesis of C₂₁ fuel precursor (MMBM) from the trimerization of HMF with 2-MF catalyzed by 3-BrPyPW.

version of glucose into 5-hydroxymethylfurfural (HMF) with a good yield of 61.7% and 78.3%, respectively. Due to heterogeneous functionalization, these catalysts could be reused at least four or five times without significant loss of catalytic activity. The incorporation of organic moieties (e.g., pyridine) is also illustrated to be capable of heterogenizing HPW, which was illustrated to be efficient for the conversion of HMF to 5-ethoxymethylfurfural (EMF) as well as fructose to ML with 90% and 82.5% yield, respectively. In view of the robust structure and good reactivity of the HPW-based acidic catalyst, it is highly promising to design novel solid acid by appropriate modification of HPW to match the desired biomass conversion processes.

In the present study, 3-bromopyridine was found to be effective for heterogenization of HPW, and the resulting acidic catalyst (3-BrPyPW) was active for the trimerization of biomass-derived HMF with 2-methylfuran (2-MF) to produce C₂₁ fuel precursor (MMBM), as shown in Scheme 2. The reaction parameters and relevant mechanism were also investigated.

2. Experimental Section

2.1. Materials. 2-Methylfuran (2-MF, 99%), 5-hydroxymethyl-2-furaldehyde (HMF, 99%), dichloromethane (DCM, 99%), 1,4-dioxane (99%), naphthalene (99%), ethanol (99%), methanol (99%), phosphotungstic acid (HPW, 99.0%), 3-bromopyridine (3-BrPy) (98.0%), pyridine (Py, 98.0%), Amberlyst-15, and Nafion-117 were purchased from Beijing Innochem Technology Co., Ltd. 1,2-Dichloroethane was purchased from Sigma-Aldrich Co. LLC.

2.2. Catalyst Preparation. 3-BrPyPW was prepared by using a solvothermal method. Firstly, 1.1 mmol HPW and 30 mL ethanol were added into a 150 mL round-bottom flask with a magneton and stirred at 25°C to get a clear HPW solution; then, 1 mmol 3-BrPy was added into the solution with continuous stirring for 1.5 h at 25°C. The turbid liquid was poured into a 100 mL Teflon reactor, followed by transfer into a stainless steel autoclave. The sealed stainless steel autoclave was then placed in a muffle furnace set at 90°C for 12 h. Upon completion, precipitation could be obtained after filtration, and the resulting white solid was further washed with 20 mL ethanol for three times to ensure the redundant reactants be removed, and 3-BrPyPW was obtained after drying at 80°C overnight. The HPyPW catalyst was prepared using the same method for the preparation of 3-BrPyPW, in which the organic ligand pyridine was used instead of 3-BrPy under otherwise identical conditions.

2.3. Catalyst Characterization. The FT-IR spectra of the catalysts were recorded by a Fourier transform infrared spectrometer (Nicolet iS50) with KBr disk. An X-ray diffractometer (D8 Advance) with CuK α radiation ($\lambda = 0.1548$ nm) in the range of 5° to 80° was utilized to record the X-ray diffraction (XRD) patterns of catalysts. The SEM images and corresponding mapping images were obtained by a scanning electron microscope (FESEM XL-30; Philips). The TG curves were obtained by using a thermal gravimetric analyzer (STA409) with 10°C min⁻¹ heating rate in an atmosphere of dry air. The N₂ adsorption-desorption experiment was carried out at -196°C using an ASAP 2460 equipment (Micromeritics). Firstly, the catalyst was outgassed for 12 h at 150°C. Then, the specific surface area was got by using the Brunauer-Emmett-Teller (BET) method, and the average pore size was obtained by using the Barrett-Joyner-Halenda (BJH) method. The XPS (X-ray photoelectron spectroscopy) data were collected by a Physical Electronics Quantum 2000 Scanning ESCA Microprobe (Physical Electronics Inc., PHI, MN) equipped with a monochromatic AlK α anode. ICP (inductively coupled plasma emission spectroscopy) analysis was conducted using a 5300 DV device (PerkinElmer Inc., Waltham, MA).

2.6. Catalyst Recycling Study. After each cycle of the reaction, the catalyst was removed from the reaction system by centrifugation and then washed with 20 mL ethanol for three times, which was finally dried at 80°C for 24 h. The recovered catalyst was utilized directly for the next run under identical reaction conditions.

The total acid density of the catalyst was determined by the Na⁺ exchange method. Firstly, 50 mg of solid catalyst was added to a sodium chloride solution (2 mol/L, 15 mL). The catalyst was oscillated by ultrasound for 0.5 h (2 mol/L, 5 mL/time), then washed three times, and the supernatant was collected by using a centrifuge, and the resulting supernatant was placed into a conical flask. Titrating the collected solution with sodium oxide solution (0.08213 mol/L), the solution with phenolphthalein will become red after the last drop of sodium hydroxide solution was added. It could be the endpoint of titration if the solution color remains for 30 seconds. The volume of consumed sodium hydroxide solution also needs to be recorded. The total acid density of the catalyst can be expressed as

$$C(H^+) = (V_{\text{NaOH}} \times C_{\text{NaOH}}) / m. \quad (1)$$

$C(H^+)$ could be used as the total acid density (mol/g) of the catalyst, and m represents the mass (mg) of the catalyst. C_{NaOH} is the concentration of sodium hydroxide (mol/L). V_{NaOH} stands for the volume of consumed NaOH solution (L) during the titration.

2.4. Reaction Procedures for the Synthesis of MMBM from 2-MF and HMF. In a general reaction procedure, 3 mmol 2-MF and 1 mmol HMF, 20 mg 3-BrPyPW catalyst, 2 mL solvent (dichloromethane), and a magnetic bar were added into a 15 mL Ace pressure tube, which was then placed into an oil bath preheated to 100°C. After reaching the desired reaction time, the tube was taken out from the oil bath and cooled to room temperature with flowing tap water. Prior to quantitative analyses with GC (gas chromatography), the reaction solution was diluted with CH₂Cl₂ and filtered to remove solid catalyst with a filter membrane.

2.5. Product Analysis. An Agilent 7890B gas chromatography (GC) with an HP-5 column and FID detector was used to analyze the concentration of reactants and products, and 10 mg naphthalene was added as internal standard. An Agilent 6890N GC/5973 MS (GC-MS (gas chromatography-mass spectrometer)) was utilized to identify by-products. The conversion of 2-MF and yield of MMBM were obtained by using below calculation equations:

$$2 - \text{MF conversion (\%)} = \left[1 - \frac{\text{mole concentration of 2 - MF in product}}{\text{mole concentration of initial 2 - MF}} \right] \times 100\%, \quad (2)$$

$$\text{MMBM yield (\%)} = \left[\frac{\text{mole concentration of MMBM}}{\text{mole concentration of initial 2 - MF}} \right] \times 100\%.$$

3. Results and Discussion

3.1. Catalyst Characterization. In order to understand the crystal structure of the prepared catalysts, the XRD patterns of 3-BrPyPW, HPyPW, and HPW were recorded and are shown in Figure 1. A Keggin anion cubic structure belonging

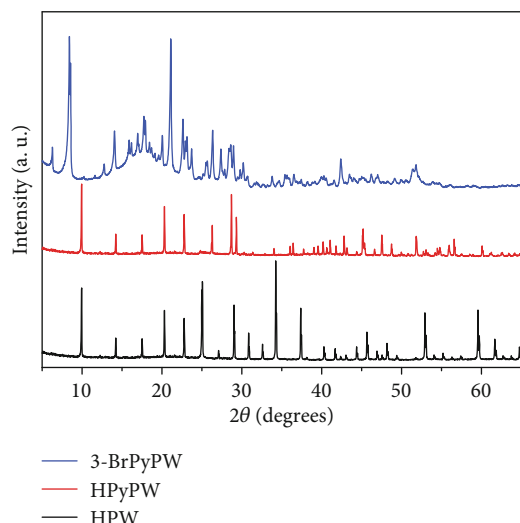


FIGURE 1: XRD patterns of 3-BrPyPW, HPyPW, and HPW.

to HPW with diffraction peaks at 9.9° , 14.1° , 17.6° , 20.3° , 22.7° , 24.8° , 29.1° , and 34.1° [50–56] could also be observed for HPyPW and 3-BrPyPW. This result indicated that even HPW was decorated by different organic species; it could well maintain the original HPW cubic basically. Moreover, due to the introduction of organic ligands, peaks in relatively low intensity appeared for both HPyPW and 3-BrPyPW, with the 2θ values having a negative shift to a lower angle. This phenomenon can be attributed to the electrostatic interaction between HPW and ligands [48, 49]. Moreover, some unknown diffraction peaks could be observed in 3-BrPyPW and HPyPW, and the possible explanation is that two catalysts will absorb some organic moieties, and this phenomenon has been proved by a previous work [51].

The FT-IR spectra of 3-BrPyPW, HPyPW, and HPW are shown in Figure 2. It could be clearly seen that specific peaks of a Keggin structure appear at the fingerprint region of 800 to 1100 cm^{-1} for each catalyst, and the characteristic peaks at 806 cm^{-1} , 892 cm^{-1} , 987 cm^{-1} , and 1082 cm^{-1} are attributed to asymmetric vibrations of the W-O_c , W-O_b , W-O_d , and P-O_a bonds, respectively, with a characteristic peak at 594 cm^{-1} being assigned to bending vibration of the P-O bond [48]. It means the presence of the characteristic structure of HPW in the as-prepared 3-BrPyPW and HPyPW catalysts, which agrees with the XRD results. In addition, the absorption peaks of pyridine structure were observed at 1633 cm^{-1} ($\nu_{\text{C}=\text{C}}$), 1499 cm^{-1} ($\nu_{\text{C}=\text{N}}$), 1262 cm^{-1} ($\delta_{\text{C-H}}$), 1202 cm^{-1} ($\gamma_{\text{C-H}}$), and 3092 cm^{-1} (stretching vibration of benzene C-H bands) in both 3-BrPyPW and HPyPW catalysts, clearly indicating the existence of pyridine moieties.

The SEM image was used to investigate the morphology of 3-BrPyPW and is shown in Figure 3. It could be seen that the 3-BrPyPW displayed a polyhedral block structure, which closely agrees with the XRD results (Figure 1). In addition, when the N, O, P, W, and Br elemental mappings of 3-BrPyPW were analyzed (Figure 3), it was found that each element is well dispersed on the catalyst surface. This also laterally proved the successful preparation of 3-BrPyPW. This result was further confirmed by XPS and ICP analysis. For

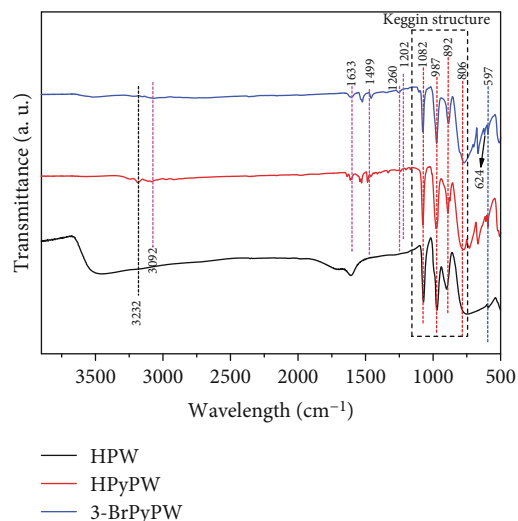


FIGURE 2: FT-IR spectra of 3-BrPyPW, HPyPW, and HPW.

3-BrPyPW, 65 wt% of W species and 4 wt% of P species could be detected by ICP analysis, while 5 wt% of C and 2 wt% of N could be attained by XPS analysis. On the other hand, 69 wt% of W species and 3 wt% of P species could be detected by ICP analysis, while 3 wt% of C and 1 wt% of N could be obtained by XPS analysis in the HPyPW sample. These results show that almost equivalent HPW and ligands are connected to each other through electrostatic interaction.

The N_2 adsorption-desorption isotherms of the 3-BrPyPW, HPyPW, and HPW are shown in Figure 4. Three typical H_4 -type adsorption-desorption isotherm curves could be observed. For the catalyst BET specific surface area, it can be arranged in the following order: 3-BrPyPW ($120.5\text{ m}^2/\text{g}$) > HPyPW ($115.4\text{ m}^2/\text{g}$) > HPW ($4.8\text{ m}^2/\text{g}$), with the arrangement of BJH average pore size as follows: 3-BrPyPW (13.5 nm) > HPyPW (5.6 nm) > HPW (3.5 nm). Moreover, the total acid density of three catalysts was also tested. It could be found that 3-BrPyPW has a relatively high acid density (2.54 mmol/g) compared to HPyPW (0.51 mmol/g) and HPW (1.54 mmol/g) (Table 1). Therefore, in comparison with HPyPW and HPW, a higher specific surface area, larger pore size, and higher total acid density may make 3-BrPyPW have a superior activity in the conversion of 2-MF and HMF to MMBM.

3.2. Catalyst Screening for the Conversion of 2-MF and HMF to MMBM. The synthesis of MMBM from HMF and 2-MF in CH_2Cl_2 under 100°C for 8 h was investigated in the presence of different catalysts, and the obtained results are shown in Table 2. HPW gave 81.7% 2-MF conversion and 32.9% MMBM yield. After being functionalized with pyridine, it was found that the resulting HPyPW catalyst showed poor reactivity with 21.1% 2-MF conversion while just 0.1% MMBM yield. To our surprise, 3-BrPyPW exhibited a superior catalytic performance with 82.0% 2-MF conversion and 57.1% MMBM yield. The introduction of the electronegative substituent was proposed to cause an inductive effect and steric hindrance, which might improve the catalyst structure, thus affording enhanced catalytic activity [49]. Amberlyst-

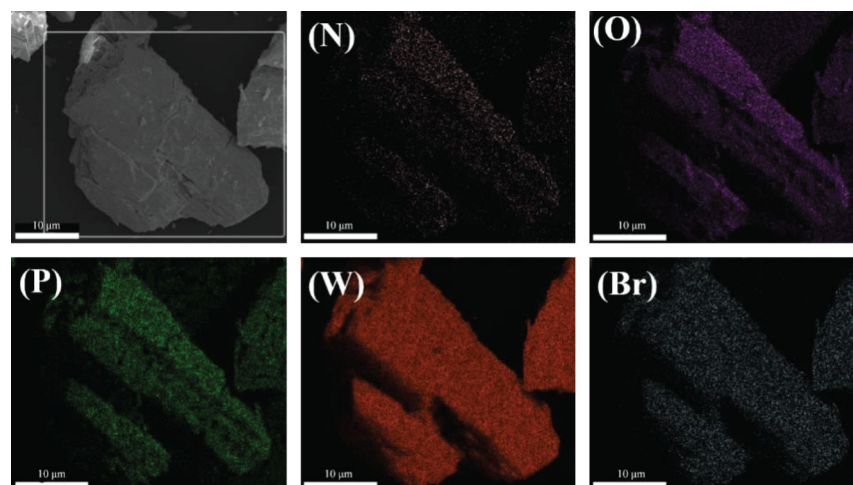


FIGURE 3: SEM image and elemental mappings of the 3-BrPyPW catalyst.

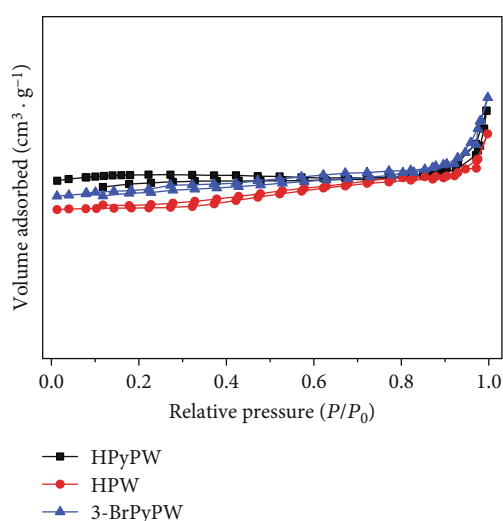
FIGURE 4: The N_2 adsorption-desorption isotherms of 3-BrPyPW, HPyPW, and HPW.

TABLE 1: Acid density, pore size, and specific surface area comparison of 3-BrPyPW, HPyPW, and HPW.

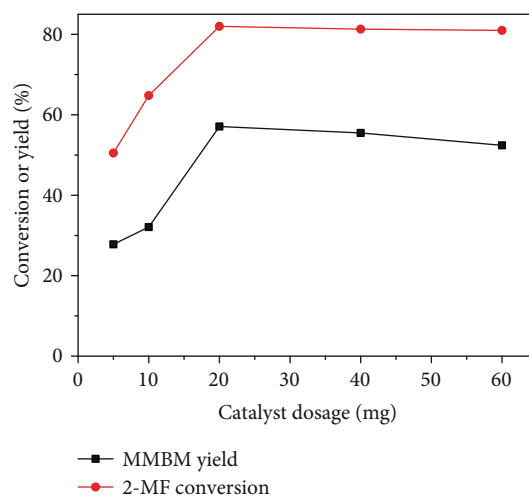
Catalyst	Acid density (mmol/g)	Average pore size (nm)	S_{BET} (m^2/g)
3-BrPyPW	2.54	13.5	120.5
HPyPW	0.51	5.6	115.4
HPW	1.54	3.5	4.8

15 and Nafion-117 were also investigated for comparison, and 37.9% and 76.4% 2-MF conversion with 12.3% and 25.8% MMBM yield could be achieved, respectively. These experimental results are consistent with those of previous reports, with respect to the BET specific surface area, average pore size, and total acid density. By introducing the 3-BrPy ligand, the obtained 3-BrPyPW catalyst has a larger specific surface area and pore size, so that it can get a better reaction activity com-

TABLE 2: Catalytic results for the synthesis of MMBM from 2-MF and HMF over different catalysts.

Catalyst	Yield (MMBM, %)	Conversion (2-MF, %)
HPW	32.9	81.7
HPyPW	0.1	21.1
3-BrPyPW	57.1	82.0
Amberlyst-15	12.3	37.9
Nafion-117	25.8	76.4

Reaction conditions: 3 mmol 2-MF, 1 mmol HMF, 20 mg catalyst, 2 mL solvent, 100°C, and 8 h.

FIGURE 5: The influence of the 3-BrPyPW catalyst dosage on the synthesis of MMBM from HMF and 2-MF. Reaction conditions: 3 mmol 2-MF, 1 mmol HMF, 2 mL CH_2Cl_2 , 100°C, and 8 h.

pared to HPyPW and HPW. Furthermore, a good acid density may also contribute to the pronounced yield of MMBM. Therefore, 3-BrPyPW is a better catalyst for the investigated reaction, which was thus selected for further optimization.

3.3. The Effect of the Catalyst Dosage on the Synthesis of MMBM from HMF and 2-MF. The impact of the 3-

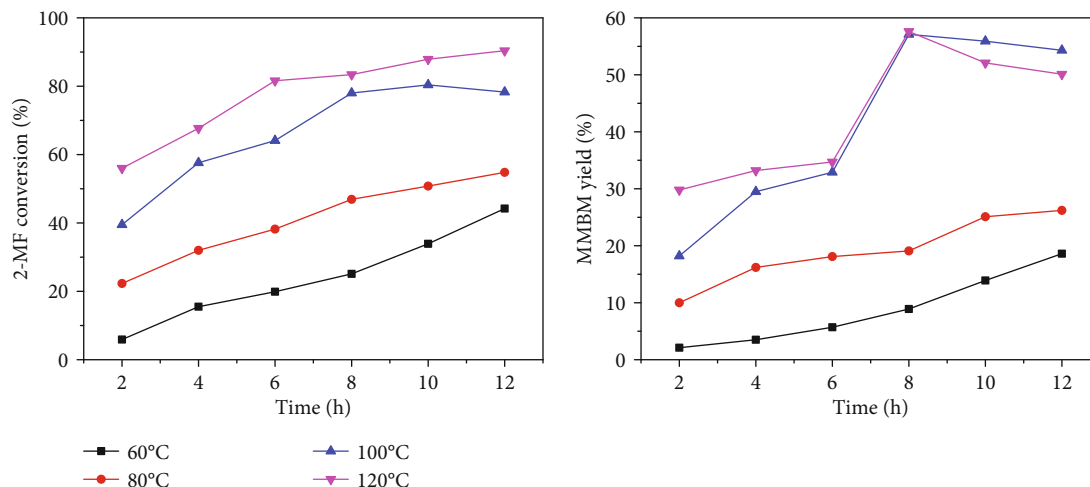


FIGURE 6: Influence of reaction temperature/time on the conversion of HMF and 2-MF to MMBM. Reaction conditions: 3 mmol 2-MF, 1 mmol HMF, 20 mg 3-BrPyPW, and 2 mL CH_2Cl_2 .

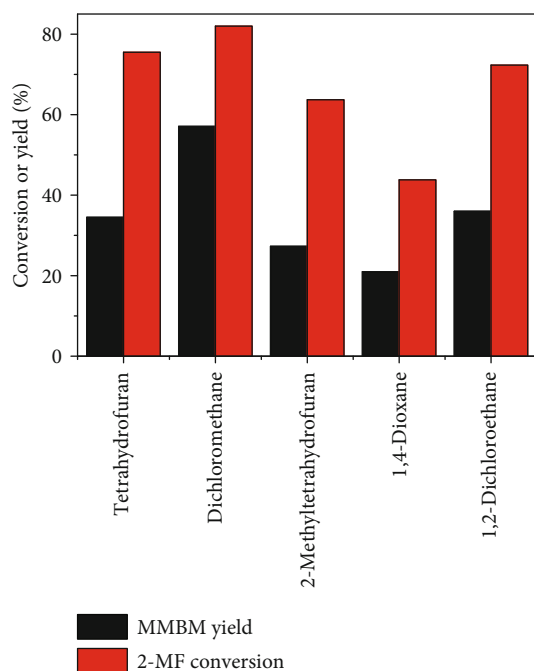


FIGURE 7: The influence of the solvent type on the synthesis of MMBM from HMF and 2-MF. Reaction conditions: 3 mmol 2-MF, 1 mmol HMF, 2 mL solvent, 100°C, and 8 h.

BrPyPW catalyst dose on the conversion of HMF and 2-MF to MMBM was examined (Figure 5). The conversion of 2-MF and yield of MMBM increased from 50.5% to 82.0% and 27.8% to 57.1% with the increase of the catalyst dosage from 5 mg to 20 mg. When a higher amount of catalyst of 40 mg and 60 mg was employed for the reaction, the yield of MMBM decreased to 55.5% and 52.4%, respectively, but no obvious change in 2-MF conversion was observed. This result may be due to the occurrence of side reactions using a relatively higher catalyst dosage. The possible reason is that the substrate HMF would be converted to by-products, such

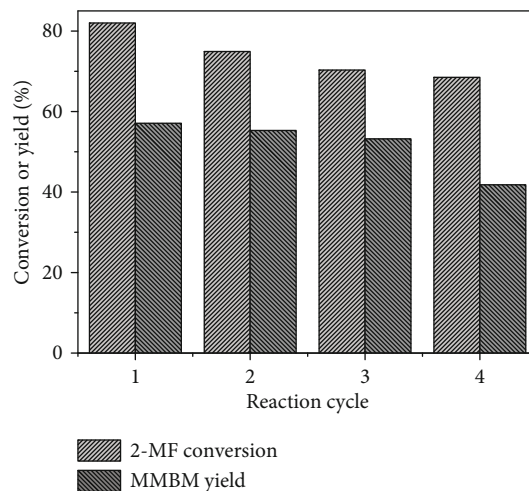


FIGURE 8: The 3-BrPyPW catalyst recycling study. Reaction conditions: 3 mmol 2-MF, 1 mmol HMF, 20 mg 3-BrPyPW, 2 mL CH_2Cl_2 , 100°C, and 8 h.

as maleic acid, as determined by NMR spectra (Figure S1), which is in good agreement with previous works [55, 56]. Therefore, 20 mg 3-BrPyPW was chosen as the best catalyst dosage for the trimerization reaction.

3.4. Influence of Reaction Temperature/Time on the Synthesis of MMBM from HMF and 2-MF. The reaction temperature and time were found to be important for the synthesis of MMBM from HMF and 2-MF. A range of reaction temperatures (60, 80, 100, and 120°C) with varying reaction time from 2 to 12 h was utilized to optimize the reaction conditions (Figure 6). It could be found that with increasing the reaction temperature and time, the conversion of either 2-MF or HMF gradually increased, and a maximum 2-MF conversion of 90.4% was obtained at 120°C for 12 h. The yield of MMBM kept increasing with raising the temperature from 60 to 120°C reacting for 2 to 8 h, where 57.1% and 57.6% yield of MMBM could be achieved at 100 and 120°C for 8 h,

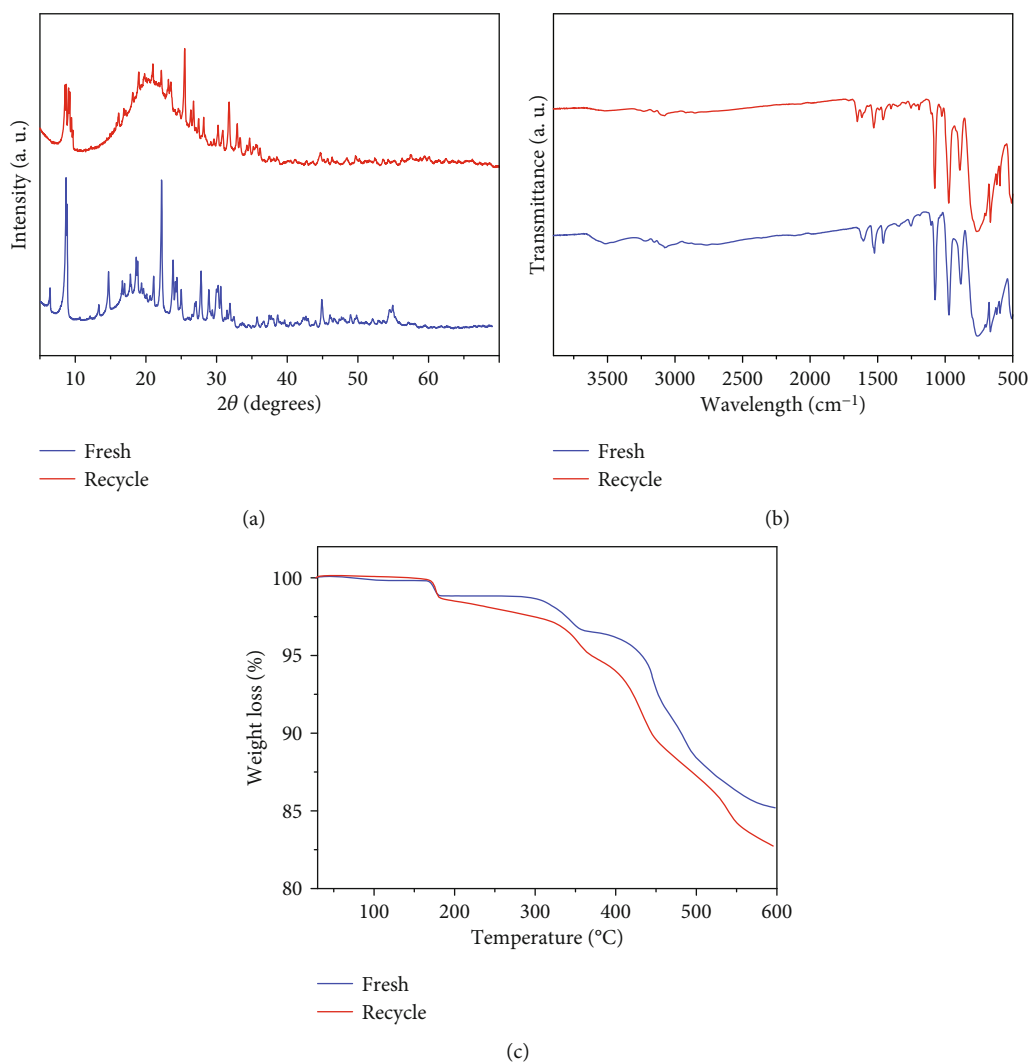
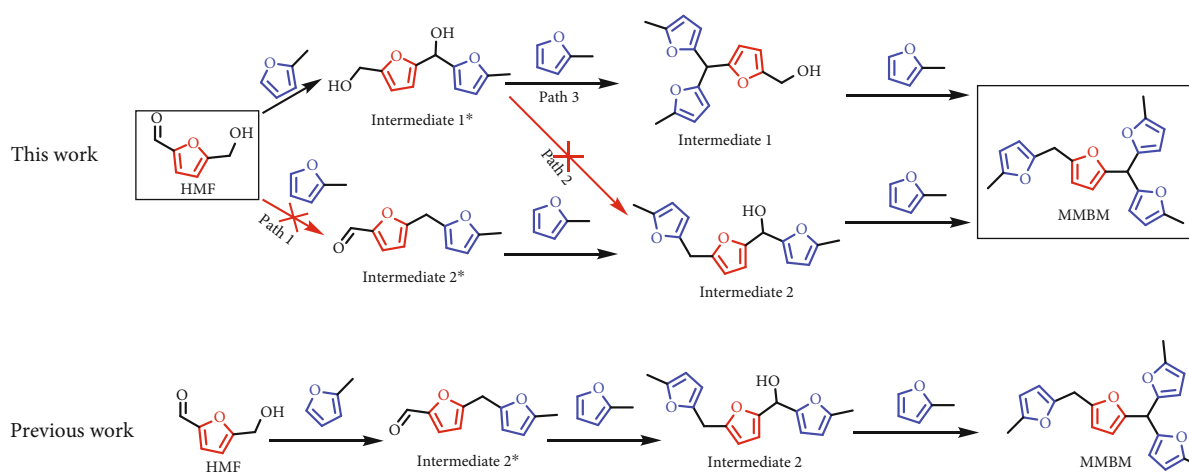


FIGURE 9: XRD patterns (a), FT-IR spectra (b), and TGA curves (c) of the recycled (after the fourth run) and fresh 3-BrPyPW catalysts.



SCHEME 3: Comparison of reaction pathways for the conversion of HMF and 2-MF to MMBM in this work and reported work.

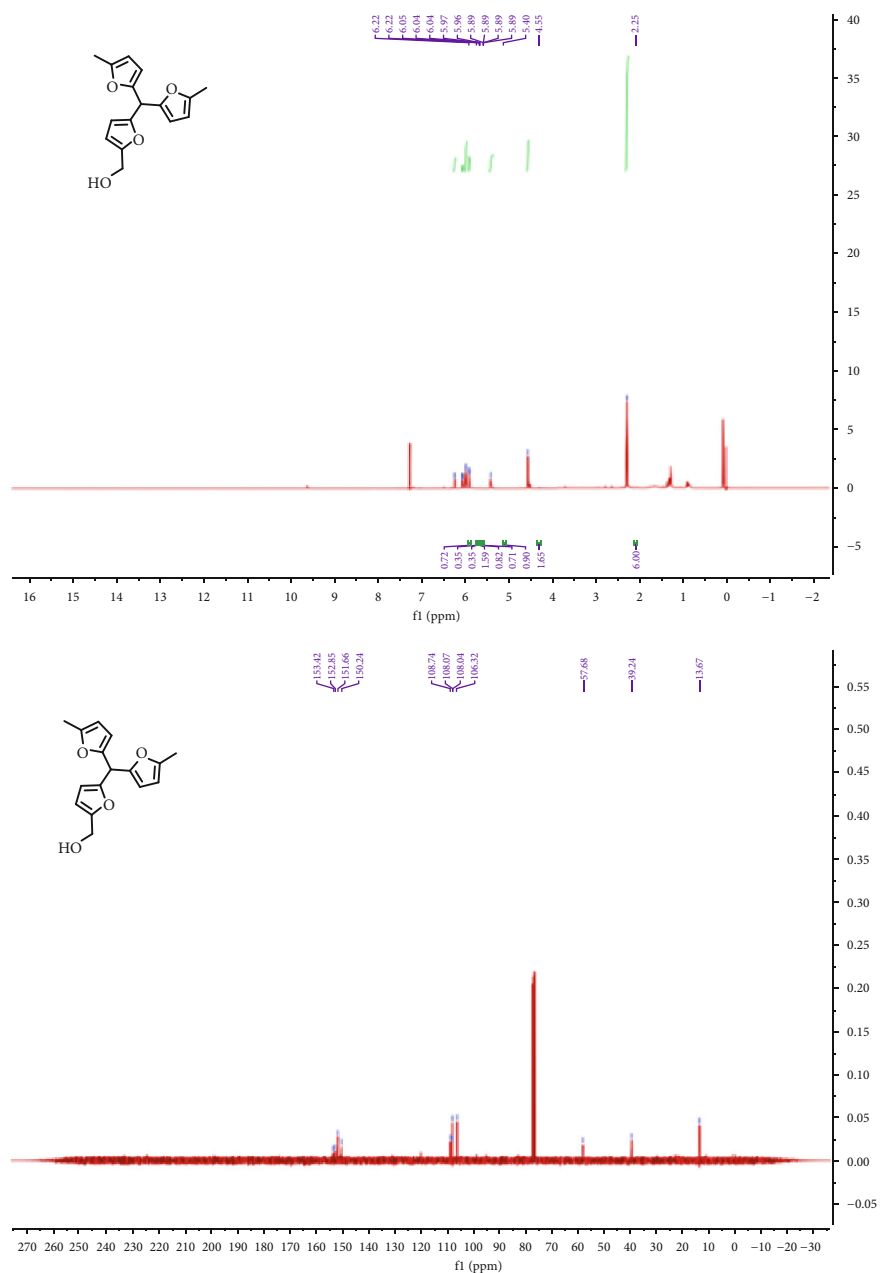


FIGURE 10: ^1H and ^{13}C NMR spectra of intermediate 1. Intermediate 1: ^1H NMR (500 MHz, CDCl_3) δ = 6.22 (*d*, J = 3.2 Hz, 1H), 6.05 (s, 1H), 6.04 (*d*, J = 0.7 Hz, 1H), 5.97 (*d*, J = 3.1 Hz, 2H), 5.89 (*d*, J = 1.0 Hz, 1H), 5.89 (*d*, J = 1.0 Hz, 1H), 5.40 (s, 1H), 4.55 (s, 2H), 2.25 (s, 6H). ^{13}C NMR (126 MHz, CDCl_3) δ = 153.42, 152.85, 151.66, 150.24, 108.74, 108.05, 106.32, 57.68, 39.24, 13.67.

respectively. However, when the reaction time continued to increase from 8 to 12 h, a decline in MMBM yield from 57.1% and 57.6% to 54.3% and 50.1% was detected at 100°C and 120°C, respectively. It was indicated that the extension of reaction time led to a decrease of MMBM yield, which may be due to the happening of side reactions. For example, HMF would be transformed into by-products, like oxidation to maleic acid, as determined by NMR spectra (Figure S1) for long reaction time with an excess amount of the 3-BrPyPW catalyst [55, 56]. So, a higher temperature led to the increase of substrate conversion but with no significant contribution to raising the yield

of MMBM. On account of saving energy consumption, 100°C and 8 h were chosen as the optimum reaction temperature and time, respectively.

3.5. The Effect of the Solvent Type on the Synthesis of MMBM from HMF and 2-MF. The reaction solvent also has a great influence on the synthesis of MMBM from HMF and 2-MF. Figure 7 shows the corresponding screening results of different reaction solvents (tetrahydrofuran, dichloromethane, 2-methyltetrahydrofuran, 1,4-dioxane, and 1,2-dichloroethane). As tetrahydrofuran and dichloromethane were used as solvent, 34.5% and 57.1% yield of MMBM with

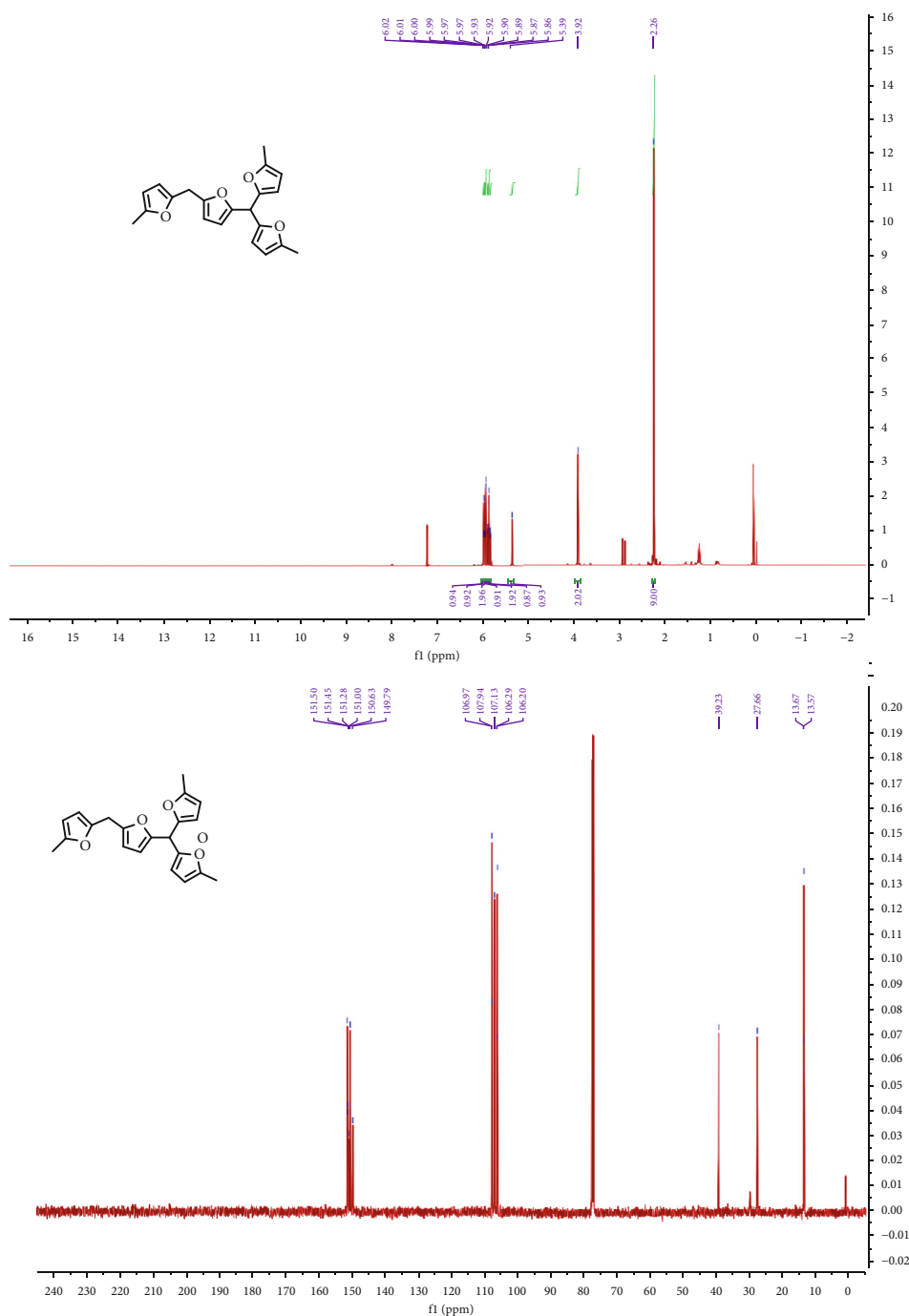


FIGURE 11: ^1H and ^{13}C NMR spectra of MMBM. MMBM: ^1H NMR (500 MHz, CDCl_3) δ = 6.01 (*d*, J = 3.7 Hz, 1H), 6.00 (*d*, J = 3.2 Hz, 1H), 5.97 (*d*, J = 3.1 Hz, 2H), 5.93 (*d*, J = 3.0 Hz, 1H), 5.90 (*d*, J = 3.1 Hz, 2H), 5.87 (*d*, J = 2.9 Hz, 1H), 5.39 (s, 1H), 3.92 (s, 2H), 2.26 (s, 9H). ^{13}C NMR (126 MHz, CDCl_3) δ = 151.50, 151.45, 151.28, 151.00, 150.63, 149.79, 107.97, 107.94, 107.13, 106.29, 106.20, 39.23, 27.66, 13.67, 13.57.

75.5% and 82.0% 2-MF conversion can be achieved, respectively. When 2-methyltetrahydrofuran, 1,4-dioxane, and 1,2-dichloroethane were employed, the yield of MMBM is 27.3%, 21.0%, and 36.0% which can be attained under the same reaction conditions, respectively. It is proposed that CH_2Cl_2 may act as an extractant to separate the target product MMBM from the in situ formed water in the reaction system, thus hindering its further degradation. According to this

solvent screening experiment, dichloromethane was chosen as the best solvent for the reaction system.

3.6. Catalyst Recycling Study. The recyclability of 3-BrPyPW was tested in the synthesis of MMBM from HMF and 2-MF under optimum reaction conditions. Figure 8 shows that the MMBM yield decreased gradually from 57.1% to 41.8% while 2-MF conversion decreased from 82.0% to 68.5% after

four consecutive cycles, showing that the 3-BrPyPW catalyst is relatively stable for the trimerization reaction. Figure 9 collects the XRD patterns (Figure 9(a)), FT-IR spectra (Figure 9(b)), and TGA curves (Figure 9(c)) of the fresh and recycled 3-BrPyPW catalysts. For XRD patterns, it is not difficult to see that the intensity of fresh 3-BrPyPW was higher than that of the recycled counterpart, indicating that organic residues might be absorbed into the catalyst after four reaction cycles [56]. Moreover, the ICP analysis of reused 3-Br-PyPW shows that there has no leaching of W species. Compared to fresh 3-BrPyPW, the FT-IR spectrum of the reused catalyst showed a relatively lower transmittance, which is a good agreement with the results obtained from XRD patterns. The TG curves of fresh and recycled 3-BrPyPW revealed that organic species might adhere to the catalyst after four consecutive reactions, which can be well supported by the result that recycled 3-BrPyPW has a drastic decline in weight loss compared to the fresh counterpart. This further indicated that the deposition of organic moieties is most likely to be the major factor that caused the loss of the catalyst activity. From above experiments, by comparing with previous studies [25, 57], 3-BrPyPW was demonstrated to show superior reactivity and stability in the production of MMBM from HMF and 2-MF under the examined reaction conditions in our work.

3.7. Reaction Mechanism Study. In order to investigate the reaction pathways for the trimerization of HMF with 2-MF to MMBM, the reaction mixture was recorded by GC-MS and NMR. Based on the experimental results, the possible reaction pathways were proposed and are shown in Scheme 3. The proposed reaction path was also compared with that of previous work reported by Dutta et al. [25] and Shinde et al. [57]. As identified by GC/MS, a compound with a molecular weight of 272.1 was formed during the reaction process. It is preliminarily assumed that its structure is intermediate 1, which was further confirmed by ^1H and ^{13}C NMR (Figure 10). On the other hand, MMBM was also detected by GC-MS (molecular weight 336.2) and confirmed by ^1H and ^{13}C NMR (Figure 11). This result revealed that intermediate 1* was formed from HMF and 2-MF, which further rapidly converted intermediate 1 and subsequently afforded the fuel precursor MMBM. However, both intermediates 2* and 2 were not detected by GC-MS, implying the reaction pathway might be neither path 1 nor path 2, and path 3 was most likely the dominant reaction pathway.

4. Conclusion

In summary, a halogenated pyridine-heterogenized HPW was prepared by a simple solvothermal method and used as a heterogeneous acidic catalyst for the conversion of HMF and 2-MF to MMBM. Single-factor optimization was utilized to test the catalytic performance of 3-BrPyPW; a good MMBM yield of 57.1% with 82.0% 2-MF conversion could be obtained under optimum reaction conditions (1 mmol HMF and 3 mmol 2-MF at 100°C for 8 h in 2 mL CH_2Cl_2). The 3-BrPyPW catalyst could be reused for four cycles without significant decreasing of its activity, which was character-

ized without obvious structure change after recycles. Moreover, a dominant reaction pathway for the synthesis of MMBM from HMF and 2-MF was elucidated.

Data Availability

The data used to support the findings of this study are included in the article.

Conflicts of Interest

There are no conflicts of interest regarding the publication of this paper.

Acknowledgments

This work was financially supported by the National Natural Science Foundation of China (21666008, 21576059, and 21908033), Fok Ying-Tong Education Foundation (161030), Key Technologies Research and Development Program of China (2014BAD23B01), and Guizhou Science & Technology Foundation ((2018)1037).

Supplementary Materials

Figure S1: ^1H and ^{13}C NMR spectra of maleic acid. (*Supplementary materials*)

References

- [1] Y. Román-Leshkov, C. J. Barrett, Z. Y. Liu, and J. A. Dumesic, "Production of dimethylfuran for liquid fuels from biomass-derived carbohydrates," *Nature*, vol. 447, no. 7147, pp. 982–985, 2007.
- [2] L. Zhang, B. Zhang, J. Chen et al., "Lawn structured triboelectric nanogenerators for scavenging sweeping wind energy on rooftops," *Advanced Materials*, vol. 28, no. 8, pp. 1650–1656, 2016.
- [3] J. Unternährer, S. Moret, S. Joost, and F. Maréchal, "Spatial clustering for district heating integration in urban energy systems: application to geothermal energy," *Applied Energy*, vol. 190, pp. 749–763, 2017.
- [4] E. Segura, R. Morales, and J. A. Somolinos, "A strategic analysis of tidal current energy conversion systems in the European Union," *Applied Energy*, vol. 212, pp. 527–551, 2018.
- [5] Y. Yang, R. Zhao, T. Zhang et al., "Graphene-based standalone solar energy converter for water desalination and purification," *ACS Nano*, vol. 12, no. 1, pp. 829–835, 2018.
- [6] M. Ross, "Automobile fuel consumption and emissions: effects of vehicle and driving characteristics," *Annual Review of Energy and the Environment*, vol. 19, no. 1, pp. 75–112, 1994.
- [7] J. I. Hileman and R. W. Stratton, "Alternative jet fuel feasibility," *Transport Policy*, vol. 34, pp. 52–62, 2014.
- [8] H. Li, A. Riisager, S. Saravanamurugan et al., "Carbon-increasing catalytic strategies for upgrading biomass into energy-intensive fuels and chemicals," *ACS Catalysis*, vol. 8, no. 1, pp. 148–187, 2017.
- [9] F. D. Pileidis and M. M. Titirici, "Levulinic acid biorefineries: new challenges for efficient utilization of biomass," *ChemSusChem*, vol. 9, no. 6, pp. 562–582, 2016.

- [10] A. Bohre, B. Saha, and M. M. Abu-Omar, "Catalytic upgrading of 5-hydroxymethylfurfural to drop-in biofuels by solid base and bifunctional metal-acid catalysts," *ChemSusChem*, vol. 8, no. 23, pp. 4022–4029, 2015.
- [11] Y. Xu, J. Long, W. Zhao, H. Li, and S. Yang, "Efficient transfer hydrogenation of nitro compounds to amines enabled by mesoporous N-stabilized Co-Zn/C," *Frontiers in Chemistry*, vol. 7, p. 590, 2019.
- [12] S. Shinde, K. Deval, R. Chikate, and C. Rode, "Cascade synthesis of 5-(acetoxymethyl)furfural from carbohydrates over Sn-Mont catalyst," *ChemistrySelect*, vol. 3, no. 30, pp. 8770–8778, 2018.
- [13] N. Luo, T. Montini, J. Zhang et al., "Visible-light-driven coproduction of diesel precursors and hydrogen from lignocellulose-derived methylfurans," *Nature Energy*, vol. 4, no. 7, pp. 575–584, 2019.
- [14] Y. Xu, J. Long, J. He, and H. Li, "Alcohol-mediated reduction of biomass-derived furanic aldehydes via catalytic hydrogen transfer," *Current Organic Chemistry*, vol. 23, no. 20, pp. 2168–2179, 2019.
- [15] S. H. Shinde and C. V. Rode, "A two-phase system for the clean and high yield synthesis of furylmethane derivatives over $-SO_3H$ functionalized ionic liquids," *Green Chemistry*, vol. 19, no. 20, pp. 4804–4810, 2017.
- [16] R. Tripathi, U. Burke, A. K. Ramalingam et al., "Oxidation of 2-methylfuran and 2-methylfuran/n-heptane blends: an experimental and modeling study," *Combustion and Flame*, vol. 196, pp. 54–70, 2018.
- [17] I. Gandarias, S. García-Fernández, I. Obregón, I. Agirrezabal-Telleria, and P. L. Arias, "Production of 2-methylfuran from biomass through an integrated biorefinery approach," *Fuel Processing Technology*, vol. 178, pp. 336–343, 2018.
- [18] K. Alexandrino, C. Baena, Á. Millera, R. Bilbao, and M. U. Alzueta, "2-Methylfuran pyrolysis: gas-phase modelling and soot formation," *Combustion and Flame*, vol. 188, pp. 376–387, 2018.
- [19] B. Wang, Z. Wang, X. Bao et al., "Microscopic investigation of near-field spray characteristics of 2-methylfuran, ethanol and isoctane under flash boiling conditions," *Fuel*, vol. 215, pp. 142–152, 2018.
- [20] J. Xie, X. Zhang, Y. Liu et al., "Synthesis of high-density liquid fuel via Diels-Alder reaction of dicyclopentadiene and lignocellulose-derived 2-methylfuran," *Catalysis Today*, vol. 319, pp. 139–144, 2019.
- [21] H. Li, S. Saravanamurugan, S. Yang, and A. Riisager, "Catalytic alkylation of 2-methylfuran with formalin using supported acidic ionic liquids," *ACS Sustainable Chemistry & Engineering*, vol. 3, no. 12, pp. 3274–3280, 2015.
- [22] D. Jin, C. Fang, Y. Li et al., "Catalytic dimerization of bio-based 5-methylfurfuryl alcohol to bis(5-methylfuran-2-yl) methane with a solid acidic nanohybrid," *Current Nanoscience*, vol. 16, no. 2, pp. 235–245, 2020.
- [23] H. Li, Z. Gui, S. Yang, Z. Qi, S. Saravanamurugan, and A. Riisager, "Catalytic tandem reaction for the production of jet and diesel fuel range alkanes," *Energy Technology*, vol. 6, no. 6, pp. 1060–1066, 2018.
- [24] A. Corma, O. de la Torre, M. Renz, and N. Vollandier, "Production of high-quality diesel from biomass waste products," *Angewandte Chemie. International Edition*, vol. 123, no. 10, pp. 2423–2426, 2011.
- [25] S. Dutta, A. Bohre, W. Zheng et al., "Solventless C-C coupling of low carbon furanics to high carbon fuel precursors using an improved graphene oxide carbocatalyst," *ACS Catalysis*, vol. 7, no. 6, pp. 3905–3915, 2017.
- [26] Z. Wang, H. Li, W. Zhao, and S. Yang, "Low-temperature and solvent-free production of biomass-derived diesel-range C_{17} precursor via one-pot cascade acylation-alkylation over Sn^{4+} -montmorillonite," *Journal of Industrial and Engineering Chemistry*, vol. 66, pp. 325–332, 2018.
- [27] M. N. Gebresillase, R. Shavi, and J. G. Seo, "A comprehensive investigation of the condensation of furanic platform molecules to C_{14} – C_{15} fuel precursors over sulfonic acid functionalized silica supports," *Green Chemistry*, vol. 20, no. 22, pp. 5133–5146, 2018.
- [28] I. Weber, P. Friese, and M. Olzmann, "H-atom-forming reaction pathways in the pyrolysis of furan, 2-methylfuran, and 2, 5-dimethylfuran: a shock-tube and modeling study," *The Journal of Physical Chemistry. A*, vol. 122, no. 32, pp. 6500–6508, 2018.
- [29] A. R. K. Gollakota, N. Kishore, and S. Gu, "A review on hydrothermal liquefaction of biomass," *Renewable and Sustainable Energy Reviews*, vol. 81, pp. 1378–1392, 2018.
- [30] V. Heck, D. Gerten, W. Lucht, and A. Popp, "Biomass-based negative emissions difficult to reconcile with planetary boundaries," *Nature Climate Change*, vol. 8, no. 2, pp. 151–155, 2018.
- [31] M. Borghei, J. Lehtonen, L. Liu, and O. J. Rojas, "Advanced biomass-derived electrocatalysts for the oxygen reduction reaction," *Advanced Materials*, vol. 30, no. 24, p. 1703691, 2018.
- [32] S. V. Vassilev and C. G. Vassileva, "Water-soluble fractions of biomass and biomass ash and their significance for biofuel application," *Energy & Fuels*, vol. 33, no. 4, pp. 2763–2777, 2019.
- [33] M. Couturier, S. Ladevèze, G. Sulzenbacher et al., "Lytic xylan oxidases from wood-decay fungi unlock biomass degradation," *Nature Chemical Biology*, vol. 14, no. 3, pp. 306–310, 2018.
- [34] Y. Rodenas, R. Mariscal, J. L. G. Fierro, D. Martín Alonso, J. A. Dumesic, and M. López Granados, "Improving the production of maleic acid from biomass: TS-1 catalysed aqueous phase oxidation of furfural in the presence of γ -valerolactone," *Green Chemistry*, vol. 20, no. 12, pp. 2845–2856, 2018.
- [35] C. R. Correa and A. Kruse, "Supercritical water gasification of biomass for hydrogen production – Review," *The Journal of Supercritical Fluids*, vol. 133, pp. 573–590, 2018.
- [36] I. V. Kozhevnikov, "Catalysis by heteropoly acids and multi-component polyoxometalates in liquid-phase reactions," *Chemical Reviews*, vol. 98, no. 1, pp. 171–198, 1998.
- [37] H. Li, H. Wu, H. Zhang, Y. Su, S. Yang, and E. J. M. Hensen, "A facile direct route to N-(un)substituted lactams by cycloamination of oxocarboxylic acids without external hydrogen," *ChemSusChem*, vol. 12, no. 16, pp. 3778–3784, 2019.
- [38] Y. Li, L. Shuai, H. Kim et al., "An "ideal lignin" facilitates full biomass utilization," *Science Advances*, vol. 4, no. 9, p. eaa2968, 2018.
- [39] U. Tyagi, N. Anand, and D. Kumar, "Simultaneous pretreatment and hydrolysis of hardwood biomass species catalyzed by combination of modified activated carbon and ionic liquid in biphasic system," *Bioresource Technology*, vol. 289, pp. 121675–121675, 2019.
- [40] G. Wen, Q. Gu, Y. Liu et al., "Biomass-derived graphene-like carbon: efficient metal-free carbocatalysts for epoxidation,"

- Angewandte Chemie, International Edition*, vol. 57, no. 51, pp. 16898–16902, 2018.
- [41] R. Fang, P. Tian, X. Yang, R. Luque, and Y. Li, “Encapsulation of ultrafine metal-oxide nanoparticles within mesopores for biomass-derived catalytic applications,” *Chemical Science*, vol. 9, no. 7, pp. 1854–1859, 2018.
- [42] F. Chacón-Huete, C. Messina, F. Chen, L. Cuccia, X. Ottenwaelder, and P. Forgione, “Solvent-free mechanochemical oxidation and reduction of biomass-derived 5-hydroxymethyl furfural,” *Green Chemistry*, vol. 20, no. 23, pp. 5261–5265, 2018.
- [43] J. G. Hernández-Cortez, L. Martínez, L. Soto et al., “Liquid phase alkylation of benzene with dec-1-ene catalyzed on supported 12-tungstophosphoric acid,” *Catalysis Today*, vol. 150, no. 3–4, pp. 346–352, 2010.
- [44] H. Ilbeygi, I. Y. Kim, M. G. Kim et al., “Highly crystalline mesoporous phosphotungstic acid: a high-performance electrode material for energy-storage applications,” *Angewandte Chemie, International Edition*, vol. 58, no. 32, pp. 10849–10854, 2019.
- [45] P. Meng, H. Heng, Y. Sun, J. Huang, J. Yang, and X. Liu, “Positive effects of phosphotungstic acid on the in-situ solid-state polymerization and visible light photocatalytic activity of polyimide-based photocatalyst,” *Applied Catalysis B: Environmental*, vol. 226, pp. 487–498, 2018.
- [46] S. K. Bhatia, R. Gurav, T.-R. Choi et al., “Bioconversion of plant biomass hydrolysate into bioplastic (polyhydroxyalkanoates) using *Ralstonia eutropha* 5119,” *Bioresource Technology*, vol. 271, pp. 306–315, 2019.
- [47] C. Fang, Y. Li, Z. Yu, H. Li, and S. Yang, “Efficient catalytic upgrade of fructose to alkyl levulinates with phenylpyridine-phosphotungstate solid hybrids,” *Current Green Chemistry*, vol. 6, no. 1, pp. 44–52, 2019.
- [48] X. Wang, T. Lv, M. Wu et al., “Aluminum doped solid acid with suitable ratio of Brønsted and Lewis acid sites synthesized by electric-flocculation of phosphotungstic acid via hydrothermal treatment for producing 5-hydroxymethylfurfural from glucose,” *Appl. Catal. A: Gen.*, vol. 574, pp. 87–96, 2019.
- [49] F. Huang, Y. Su, Y. Tao, W. Sun, and W. Wang, “Preparation of 5-hydroxymethylfurfural from glucose catalyzed by silica-supported phosphotungstic acid heterogeneous catalyst,” *Fuel*, vol. 226, pp. 417–422, 2018.
- [50] Z. Wang, H. Li, C. Fang, W. Zhao, T. Yang, and S. Yang, “Simply assembly of acidic nanospheres for efficient production of 5-ethoxymethylfurfural from 5-hydroxymethylfurfural and fructose,” *Energy Technology*, vol. 5, no. 11, pp. 2046–2054, 2017.
- [51] C. Fang, Y. Li, W. Zhao et al., “Phosphotungstic acid heterogenized by assembly with pyridines for efficient catalytic conversion of fructose to methyl levulinate,” *RSC Advances*, vol. 8, no. 30, pp. 16585–16592, 2018.
- [52] T. CAI, M. YUE, X. WANG, Q. DENG, Z. PENG, and W. ZHOU, “Preparation, characterization, and photocatalytic performance of $\text{NdPW}_{12}\text{O}_{40}/\text{TiO}_2$ composite catalyst,” *Chinese Journal of Catalysis*, vol. 28, no. 1, pp. 10–16, 2007.
- [53] X. S. Wang, L. Li, J. Liang, Y. B. Huang, and R. Cao, “Boosting oxidative desulfurization of model and real gasoline over phosphotungstic acid encapsulated in metal-organic frameworks: the window size matters,” *ChemCatChem*, vol. 9, no. 6, pp. 971–979, 2017.
- [54] C. F. Oliveira, L. M. Dezaneti, F. A. C. Garcia et al., “Esterification of oleic acid with ethanol by 12-tungstophosphoric acid supported on zirconia,” *Applied Catalysis A: General*, vol. 372, no. 2, pp. 153–161, 2010.
- [55] X. Li and Y. Zhang, “The conversion of 5-hydroxymethyl furfural (HMF) to maleic anhydride with vanadium-based heterogeneous catalysts,” *Green Chemistry*, vol. 18, no. 3, pp. 643–647, 2016.
- [56] T. S. Wang, S. Bao, L. Xu, Z. R. Liu, and L. M. Duan, “The photodegradation performance of phosphotungstic acid/CdS composite materials to organic dyes,” *Applied Mechanics and Materials*, vol. 548–549, pp. 25–28, 2014.
- [57] S. H. Shinde and C. V. Rode, “An integrated production of diesel fuel precursors from carbohydrates and 2-methylfuran over Sn-mont catalyst,” *ChemistrySelect*, vol. 3, no. 15, pp. 4039–4046, 2018.

Review Article

Functionalized Metal-Organic Framework Catalysts for Sustainable Biomass Valorization

Xiaofang Liu , Zhigang Liu, and Rui Wang 

Guizhou Engineering Research Center for Fruit Processing, Food and Pharmaceutical Engineering Institute, Guiyang University, Guiyang 550005, China

Correspondence should be addressed to Rui Wang; wangrui060729@126.com

Received 9 August 2019; Revised 20 December 2019; Accepted 6 January 2020; Published 27 February 2020

Guest Editor: Song Yang

Copyright © 2020 Xiaofang Liu et al. This is an open access article distributed under the Creative Commons Attribution License, which permits unrestricted use, distribution, and reproduction in any medium, provided the original work is properly cited.

Currently, pristine and functionalized metal-organic frameworks (MOFs) are introduced in heterogeneous catalysis for biomass upgrading owing to the specific texture properties including regular higher-order structure, high specific surface area, and the precisely tailored diversity. The purpose of this review is to afford a comprehensive discussion of the most applications in biomass refinery. We highlight recently developed four types of MOFs like pristine MOFs and their composites, MOF-supported metal NPs, acid-functionalized MOFs, and biofunctionalized MOFs for production of green, sustainable, and industrially acceptable biomass-derived platform molecules: (1) upgrading of saccharides, (2) upgrading of furan derivatives, and (3) upgrading of other biobased compounds.

1. Introduction

Rapid population growth and enhanced living quality requirements led to an improvement in energy demand and fossil feedstocks containing coal, petroleum, and natural gas. Another mainstream of the current generation is the increasing motivation to protect the environment from greenhouse gas emissions aroused by the tremendous consumption of fossil fuels [1, 2]. This concern is an irritation for the researchers for renewable and replaces sustainable resources instead of non-renewable fossil-based fuels. Because biomass is a green, highly abundant, and carbon-natural process available, it is served as a promising and replacing one to be transformed through bio-refinery and catalytic valorization into an extensive series of value-added chemicals, which has a relatively low impact on the environment [3–11].

Various technologies including biological, thermal, and chemical procedures have been explored for biomass upgrading. Among those, chemical processes (e. g., dehydration, hydrolysis, esterification, alcoholysis, isomerization, and etherification) of biomass conversion have drawn

increasing researchers' attention, which resulting in petro-based products. While reaction rates, high yields of target molecules depend on catalysts.

Numerous heterogeneous catalysts for the efficient conversion of biomass feedstocks into platform molecules and high-energy fuels have been explored [12, 13]. Solid catalysts developed for biomass upgrading are commonly divided into four categories: (a) porous materials [14], (b) metal oxides [15–17], (c) immobilized metal nanoparticles, and (d) sulfonated materials [18, 19]. Among them, high specific surface areas, tunable acidity, porous nanostructures, and bifunctionality such as Brønsted-Lewis acidic, acidic-basic, and metal nanoparticle-acidic or basic play a pivotal role in efficient heterogeneous catalytic procedures. Generally, the biomass conversion processes are composed of a series of tandem reactions [20–24].

Metal-organic frameworks (MOFs), also identified as micro- and mesoporous coordination polymers (PCPs), are a class of crystalline porous materials produced by metal centers or metal-containing secondary building units (SBUs) and bi- or multimodal functional organic linkers [25, 26]. MOFs are of particular research topics for biomass valorization owing to the

proverbial texture properties such as changeable pore/cage size, high surface area, large cavity diameter and volume, the tunable diversity, and high hydrothermal stability [27]. In addition, the MOFs afford to functionalized anxious acid-base groups ($-\text{SO}_3\text{H}$, $-\text{NH}_2$, etc.), excellent support of active metal nanoparticles (Ru, Pt, Cu, etc.) on particular sites, and immobilization of high-efficient homogeneous catalyst (POMs, ILs, et al.). The obtained functionalized MOFs could be an arbitrary choice application in diverse catalytic strategies with the existence of synergistic active moieties (Figure 1).

Among more than 20,000 well-known MOFs, MIL (Material of Institut Lavoisier), consisting of rigid terephthalate organic linkers and trimeric octahedral metal-oxo clusters, possesses kinds of quasispherical mesoporous cages (20–35 Å), with 5–20 Å windows and large surface areas (2000–5900 m^2/g). UiO (UiO for University of Oslo), zirconium terephthalate, which has 3D microporous cubic pore system and relatively high stability ($\sim 500^\circ\text{C}$), is combined with large accessible pore volumes. ZIF (zeolitic imidazolate frameworks), having 3D structural feature with nanometre pore size and large Brunauer–Emmett–Teller (BET) surface area ($< 2000 \text{m}^2/\text{g}$), has been reported to act as a template/precursor to give porous carbon.

2. MOFs for Biomass Valorization

2.1. Pristine MOFs and Their Composites

2.1.1. Upgrading of Saccharides. Catalytic hydrolysis of carboxymethyl cellulose was investigated by MIL-53(Al) [28]. The HMF and total reducing sugar molar yielding high up to 40.3% and 54.2% were achieved with 200°C , 4 h, respectively. The aluminum-based MOF acted as a reuse catalyst for three cycles without obvious activity loss, and the HMF yield (40.3%) decreased to 38.4%, which was ascribed to MIL-53(Al) mass weightlessness in cleaning proceeds and plugging of active sites by unexpected byproducts.

The preparation of lactic acid and derivatives from carbohydrates are important processes in biomass valorization. Lactic acid is a worthy platform molecule for the development of degradable bioplastic manufacture and towards the preparation of multiple noticeable chemicals like acrylic acid, propylene glycol, 1,2-propanediol, poly(lactic acid) and linear esters (alkyl lactic acids). Two zeolitic imidazole frameworks (ZIFs) Zn-ZIF-8 and Co-ZIF-67 were synthesized and acted as a catalyst for the transformation of carbohydrates (sucrose, glucose, and fructose) to lactic acid derivatives for the first time [29]. The ZIFs processed by zeolite-type topology, 3D-porous rigid framework and high chemical and thermal stability are obtained facile, providing 42% methyl lactate using the prepared Zn-ZIF-8 for the ever-smaller crystal particles and higher content of Lewis acidic. Reusability studies indicated the reduction of methyl lactate yields from 34.8% to 27.2% after the fourth recycling catalyzed by ZIF-8, on account of active site absence and structural difference. Furthermore, the metal node effect of catalysts M-MOF-74 ($M = \text{Co}, \text{Ni}, \text{Mg}, \text{and Zn}$) on the performance of the transformation of carbohydrates to methyl lactate was studied [30]. Among these, it expressed

the optimal performance for 35% and 47% yields of the product based on glucose and sucrose under the optimal reaction conditions with 220°C and 6 h, respectively. Meanwhile, the Mg-MOF-74 catalyst exhibited excellent stability that could be reused three cycles without deactivation. Similarly, Huang et al. [31] revealed an efficient one-pot conversion of fructose to lactic acid via catalyst Fe-MOF. Lactic acid yielding high up to 32% was achieved with fructose as the substrate, benefitting from the particular porous feature of catalyst MIL-100(Fe), while relatively low yields of 18% and 20% lactic acid were found with other MOFs, such as Cu-BTC and MIL-100(Cr), respectively. Derived from hexose-based carbohydrates including glucose, sucrose, inulin, and cellobiose, moderate lactic acid yields were effectively converted over MIL-100(Fe). The existed pores or active sites blockage and the absence of partial active sites and the catalytic performance of MIL-100(Fe) evidently reduced after the fourth recycle. Modifying the regeneration method of catalyst MIL-100(Fe), lactic acid yield maintained 28% from fructose.

In another work, the possible mechanism accounting for the preparation of methyl lactate with glucose as the reactant was revealed. MIL-101(Cr) combined with activated fly ash complex was developed to be effectual for furfural synthesis over xylose dehydration [32]. Compared to the bare MOF, 71% and 80% high yield and selectivity of furfural were acquired at optimized reaction conditions; the excellent performance was retained after ten times continuous recycling. The synergistic action of Cr Lewis acidic and $-\text{OH}$ Brønsted acidic belonging to composite laid the foundations for application in other biomass valorization.

2.1.2. Upgrading of Furan Derivatives. The catalytic oxidation of HMF providing a series of great value platform molecule for chemical engineering industries includes 2,5-diformylfuran (DFF), 5-hydroxymethylfuran-2-carboxylic acid, 2,5-dimethyltetrahydrofuran, and 5-ethoxymethylfurfural. The conversion and selectivity of the aforementioned molecules can be adjusted by regulating catalyst active sites' constitutions and experiment conditions. Lucarelli et al. [33] verified the oxidation process of HMF-DFF over Ni-based MOFs including Ni(BDP), Ni(BPEB), and $\text{Ni}_3(\text{BTP})_2$, which were equipped with square planar and accessible metal centers. Among the base-free catalysts, $\text{Ni}_3(\text{BTP})_2$ exhibited the optimal catalytic activity, yielding 27% DFF under mild reaction conditions (120°C , 30 bar O_2 , in water). The satisfactory catalytic performance attributed to the accessibility of the metal centers, which depend on the crystal texture of the MOF. Following, an efficient MOF was applied in another conversion of one-pot two steps processes, which was investigated to prepare furilydenepropanenitrile derivatives, the key polymer basic entities [34]. The first oxidation procedure of HMF was explored by Fe-based MOFs (MIL-100(Fe), Cu-based MOF, Fe-HY zeolite, and Fe salts with 2,2,6,6-tetramethylpiperidine-1-oxide (TEMPO) acting as cocatalyst, NaNO_2 serving as an additive, and O_2 as the terminal oxidant. Post-treated by NH_4F , MIL-100(Fe) explained the highest catalytic activity, giving a full yield of DFF converted from HMF, which ascribe to the

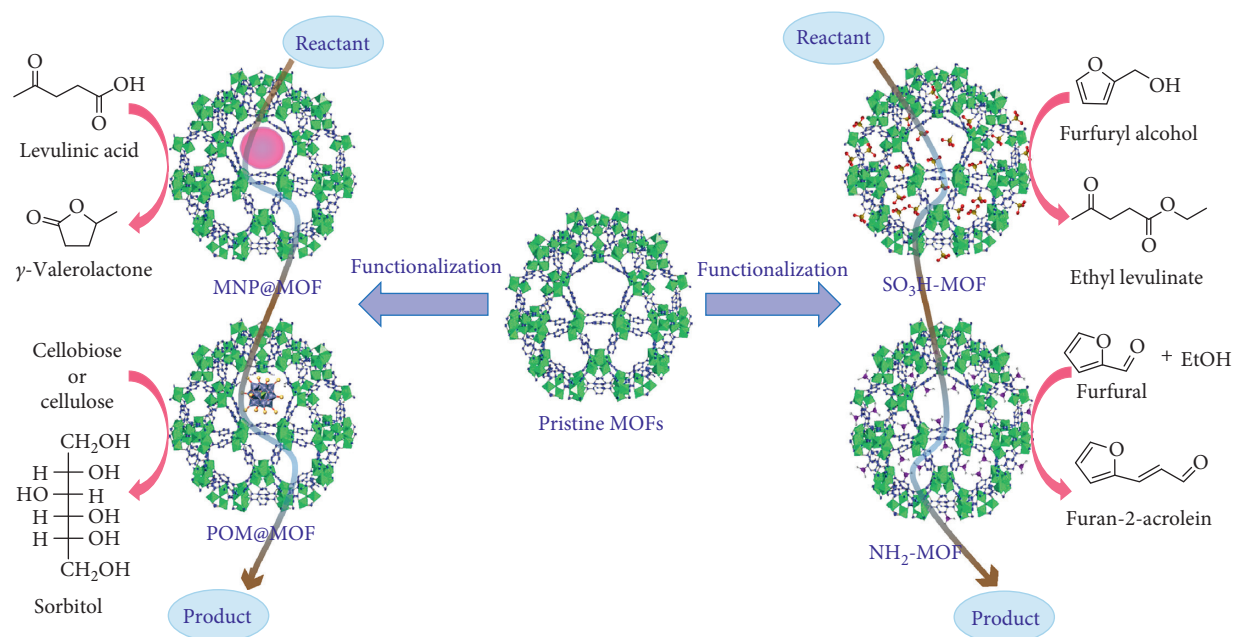


FIGURE 1: Application of MOFs for partial biomass upgrading.

existence of accessibility of Fe(III) active sites for reactants. The following Knoevenagel condensation step of DFF catalyzed by malononitrile or ethyl cyanoacetate was carried out under the basic medium.

Through aldol condensation, aldehydes and ketones react to provide high-value-added products from simple and inexpensive ones. On account of which, Kikhtyanin et al. [35] contrasted the catalytic effect of Lewis acidic MOFs (Cu-BTC, Fe-BTC) with zeolites including both Lewis acidity and Brønsted acidity to inquire the aldol condensation reaction of furfural with acetone. As demonstrated, acidic sites have the advantage to proceed aldol condensation rather than basic ones. It is worth noting that catalysts possessing weak Brønsted acidity, which are obtained by the mutual effect of Fe³⁺ with coordinated H₂O or the presence of structural defects, showed the best performance at 100°C.

The oxidative condensation reaction of furfural with alcohols-O₂ can promote double-carbon molecules to synthesize longer hydrocarbon chains acting as transport bio-fuels. In recent years, furfural reacting with alcohol to proceeding the aerobic oxidative condensation was explored by multiple Co-MOF catalysts [36]. Generally, two tactics were surveyed for the production of effective catalytic sites in MOFs: (1) removal of a coordinated small organic molecule or water molecules at 300°C, issuing in exposed and available metal active species; (2) thermolysis at 700°C, obtaining carbon-matrix nanometer and porous composites. Both types of Co-MOF exhibited satisfactory catalytic activity in the oxidative condensation with 84.9% and 99% furfural conversion and selectivity under optimal reaction conditions.

Except that, Zr-based MOFs (UiO-66 or UiO-66-NH₂), were further examined on the esterification reaction of levulinic acid with the amount of biomass-derived various alcohols [37]. The gained catalytic performances are

comparable to have published heterogeneous acidic catalysts' activities, and the data exhibit the excellent activity, thanks to the synthesis conditions, defect sites, and particle size in these MOFs.

2.1.3. Upgrading of Other Biobased Compounds. Because of the consumption of petrochemical energy, the development of transformation of biomass to biodiesel over esterification and transesterification reaction become an attractive topic. Larasati et al. [38] examined the catalytic performance of the synthesized Zr⁴⁺-BTC based MOF by the solvothermal and reflux method for the esterification of palmitic acid and ethanol. The solvothermal prepared MOF affords the maximum 69.2% palmitic acid conversion with 0.6% catalyst loading. In addition, Zr-MOFs, like UiO-66 and UiO-66-NH₂, are also inquired as heterogeneous acids for fatty acids with short-chain alcohols to carry out the esterification reaction [39]. With the optimized reaction condition, excellent outputs of fatty acid alkyl esters (94–99%) were provided over the superior UiO-66-NH₂, which was ascribed to cooperative acid-base catalytic properties. The investigation further proved that Zr-MOFs possess the potential to catalyze other biobased feedstock conversions.

2.2. MOF-Supported Metal NPs

2.2.1. Upgrading of Furan Derivatives. Implementing aerobic oxidative condensation with furfural combined alcohols acts as great important techniques for stabilizing furan derivatives and upgrading furan derivatives for desirable components for gasoline. Pt nanoparticles supported on MOFs like Pt@MOF-5, Pt@UiO-66, and Pt@UiO-66-NH₂ were prepared by the impregnation and gas-phase reduction process [40]. The catalytic performance was detected in the

oxidative process of furfural for furan-2-acrolein in the presence of O_2 . Among which, material Pt@MOF-5 exhibited the optimal efficiency as furfural converted up to 84.1% and furan-2-acrolein yielded 75.7% under 150°C, 4 h. Under the optimized reaction condition, Pt@MOF-5 demonstrated significant stability and five times reusability without any loss in furan-2-acrolein yields. Uniform dispersion of Pt nanoparticles proved the synergetic effect with the MOF-5 channel for superior catalytic performance.

In addition, for furfuryl alcohol which can be hydrogenated to form tetrahydrofurfuryl alcohol and can further polymerize, selective hydrogenation of readily produced furfural has drawn increasing attention. Yuan et al. studied the hydrogenation procedure via Ru nanoparticles immobilized on a range of Zr-MOFs [41]. Among the evaluated catalysts, such as Ru/UiO-66, Ru/UiO-67, Ru/Zr₆-NDC, MIL-140A, MIL-140B, and MIL-140C, Ru/UiO-66 provided the maximum yield with 94.9% furfuryl alcohol, which can reuse five consecutive times without obvious activity loss. Similarly, Hester et al. [42] explored the PtNP@UiO-67 application in the hydrogenation and oxidation of HMF, which are thermally stable consisting of Pt nanoparticles embedded in the UiO-67 channel. The results implied that PtNP@UiO-67 catalyst was more efficient for the hydrogenation than the oxidation of HMF with the same conditions.

To reduce the dependence on petroleum resources, γ -valerolactone (GVL) as the sustainable production from renewable biomass was identified as significant target chemicals. 5 wt.% Ru/MIL-101(Cr) catalyst afforded above 99% GVL yield with 100% conversion of levulinic acid compared to a Ru/zeolite catalyst at mild reaction conditions (70°C, 5 h, 1.0 MPa H_2 pressure) [43]. The higher catalytic performance is due to the synergistic effect between the MIL-101(Cr) supporter and the well-dispersed Ru sites.

2.2.2. Upgrading of Other Biobased Compounds. The oxidation of glycerol provides sustainable routes for value-added chemicals, such as polyglycerol, glyoxylic acid, and glycerolaldehyde [44]. Li et al. [45] studied M-NPs/Fe-MIL-101 ($M = Pd, Pd-Ce, Ce, \text{ and } Au$) for the production of dihydroxyacetone by adjusting the reaction time and metal types. Test results indicated that the longer reaction time better catalytic activity of the Pd-Ce NPs/Fe-MIL-101 for the glycerol oxidation to produce derivative dihydroxyacetone. Intriguingly, the modalism of Fe-MIL-101-NH₂ is slightly reliance on the preparation time, while the crystal structure maintained. With the MOF-supported metal-particles catalysts, bimetallic ones afforded higher yields of target compounds compared with the monometallic Pd-based MOF.

Furthermore, palladium nanocatalyst incorporated the hybrid support constituting the novel Pd/PRGO/Ce-MOF, among which the supports composed of Ce-MOF crystals and partially reduced graphene oxide (PRGO) nanosheets [46]. Results highlighted the developed 5 wt.% Pd/PRGO/Ce-MOF exhibited excellent catalytic performance for the transformation of vanillin to synthesize 2-methoxy-4-methylphenol by successive hydrogenation-deoxygenation

reactions. The desired performance is due to the reason of Pd nanoparticles' uniform dispersion on support and the existence of acidic active sites.

2.3. Acid-Functionalized MOFs

2.3.1. Upgrading of Saccharides. Utilization of renewable and abundant reserve resources like biomass caters to the development of sustainable production of chemicals. Biomass-derived saccharides (e.g., cellulose, sucrose, glucose, and fructose) can be catalyzed into bio-platform molecules, for instance, HMF was catalyzed and applied in medicine, fuel additives, and various fine chemicals which were applied to polymers and solvents [47, 48]. Generally, fructose bearing a five-membered ring can be easily transformed into HMF by dehydration reaction, while glucose with a more stable six-membered ring is the direct product of lignocellulosic biomass and is cost efficient; its conversion and application remain challenging. The transformation of glucose-HMF process carries out through two steps, I) the isomerization reaction of glucose over Lewis acid to fructose and II) the dehydration process for HMF catalyzed by Brønsted acid [49]. Considering the catalytic activity, the catalyst combined Brønsted and Lewis acidity would be superior over the separated ones.

In view of the situation, Oozeerally et al. [50] investigated the prominent stable and strong acidic UiO-66-MSBDC catalyst for the transformation of glucose-HMF, among which the catalyst was prepared via partially substituting the organic linker of UiO-66 by MSBDC. For the obtained catalyst constructed with Lewis (Zr^{4+}) and Brønsted ($-SO_3H$) acidities, the synergistic effect of the catalyst guaranteed prominent catalytic performance for the production of HMF in aqueous solution under optimized reaction condition.

Considering a more stable pyranose form of glucose reduces the efficiency of HMF yield; Oozeerally et al. [49] and Yabushita et al. [50] demonstrated PO_4/NU as an efficient catalyst for the production of HMF derived from glucose, which is synthesized by partial phosphate modification of Zr-MOF NU-1000 to provide strong acidic sites to accomplish the glucose-to-HMF conversion. Results verified the maximum yield of 64% HMF with 1 mM glucose concentration in water/2-propanol hybrid medium. The high yield and selectivity attributed to the reduced Lewis acidity combined Brønsted acidity, which are favorable for the glucose-fructose isomerization and the followed dehydration process.

Similarly, selective products of glucose catalyzed by nitro- or sulfo-modified functionalized MIL-101(Cr) catalysts and MOF derivatives were explored in depth [48]. Research has found that the MIL-101(Cr)- SO_3H catalyst afforded the highest yield (29%) of HMF derived from glucose with 24 h, which is the maximum value over MOF so far. The solvent effect was studied and it was revealed that the distribution of the products over MIL- SO_3H was different with sulfuric acid or Amberlyst-70 in pure THF or THF- H_2O . Furthermore, Su et al. developed a similar functionalized MOF, MIL-101(Cr)- SO_3H , possessing both

Lewis and Brønsted acidity, which was evaluated for glucose conversion to synthesize HMF with optimized reaction conditions and GVL-combined 10 wt.% water acted as the reaction medium [52]. The HMF yield reaching up to 45% with full conversion of glucose was achieved with Cr^{3+} centers as Lewis acid and $-\text{SO}_3\text{H}$ as the Brønsted one. The wonderful catalytic performance ascribed to the synergistic effect of Lewis and Brønsted acid and combined solvents, and the solvent effect was further proved by kinetic reactions, which revealed that the isomerization step obeyed second-order kinetics and GVL- H_2O decreased the E_a value from 114 to $100.9 \text{ KJ mol}^{-1}$.

With the same functionalized MOF- SO_3H , Chen et al. prepared various sulfonic acid-functionalized MOFs using the postsynthetic modification method of functionalized organic linkers by chlorosulfonic acid, realizing the fructose dehydration for HMF production (Figure 2). [53]. The grafting level of $-\text{SO}_3\text{H}$ groups affected the Brønsted acid density and the acidic strength of catalysts and further determined the output of the ultimate product HMF. The HMF yield reached up to 90% with the full conversion of fructose with the optimized MIL-101(Cr)- SO_3H (15.0%) catalyst, which is superior to the UiO-66 and MIL-53. About 55 KJ mol^{-1} activation energy was achieved through kinetic reaction, and at the same time, the fructose-HMF conversion process possibly followed the pseudo-first-order kinetics. Results showed that the product yields did not remain stable after five recycles, which indicated that the catalyst channel may accumulate oligomeric products derived from side reaction.

Followed, Hu et al. [54] directly synthesized the high stability and strong Brønsted acidity NUS-6, including two types of Zr and Hf clusters with modulated hydrothermal (MHT) approach. The novel catalysts NUS-6(Zr) and NUS-6(Hf) possessed high specific surface areas of 550 and $530 \text{ m}^2 \text{ g}^{-1}$, respectively, which increases the interaction sites between reactants and active acidic sites. As a consequence, the NUS-6(Hf) MOF exhibited the optimal HMF yield of 98% in the fructose dehydration process, which was also attributed to the strong Brønsted acidity and the appropriate pore size that suppressed secondary reactions.

Furthermore, the acidic adjustability played an increasing remarkable role in the catalytic conversion of biomass. A hybrid MOF-based solid acidic catalyst PVP-HNTs@UiO-66- SO_3H -x prepared with polyvinylpyrrolidone-modified halloysite nanotubes incorporated in a $-\text{SO}_3\text{H}$ group-functionalized UiO-66(Zr) revealed good catalytic property for fructose dehydration reaction with high HMF yield (92.4%) [55]. The acidic site density in the PVP-HNTs@UiO-66- SO_3H can be tuned by altering the dosage of support and $-\text{SO}_3\text{H}$ groups. The catalyst can be facilely and effectively reused for successive five cycles without obvious loss in its activity and stability.

2.3.2. Upgrading of Furan Derivatives. Research has shown that γ -valerolactone (GVL) can act as a plasticizer, fuel additive for gasoline, aviation kerosene that can reduce the dependence on the petrochemical energy, and can be further

converted to liquid long-chain hydrocarbon fuels for diesel. Considering this situation, Kuwahara et al. [56] developed an SO_3H -functionalized Zr-MOF (UiO-66-Sx) for the production of GVL through converted hydrogenation from levulinic acid and its corresponding esters. Owing to the strong connection of Brønsted acidic $-\text{SO}_3\text{H}$ groups and Lewis-basic $\text{Zr}_6\text{O}_4(\text{OH})_4$ clusters existed in the UiO-66 framework, the highest yield of GVL reaches up to 85% at 140°C . Meanwhile, UiO-66- S_{60} containing 60 mol% fraction of $-\text{SO}_3\text{H}$ maintained relatively high BET surface area although functionalization leads to the reduction of crystallinity and BET surface area.

In addition, among the various studies on biomass valorization, the preparations of alkyl levulinates have attracted much attention in recent years. The transformation of furfuryl alcohol to ethyl levulinate was investigated with the SO_3H -functionalized Cr-MOF MIL-101(Cr)- SO_3H in ethanol (Figure 3). [57] The as-prepared catalyst materials possessed special textural properties including high BET surface area, porous mesopore size, high hydrothermal/chemical stability, and increased approachability of $-\text{SO}_3\text{H}$ Brønsted acidic sites. By the reason of the aforementioned satisfying characteristics, the catalyst MIL-101(Cr)- SO_3H afforded good catalytic performance with a yield of 79.2% ethyl levulinate and 100% furfuryl alcohol conversion. Re-usability experiments further proved the material stability with a slight loss of activity was showed.

2.3.3. Upgrading of Other Biobased Compounds. Esters, the products of esterification, are widely applied for fragrances, lubricants, plasticizers, drugs, pharmaceuticals, and solvents. At the same time, dehydration of alcohol is a significant reaction to industrial development. Based on these, novel acid-functionalized MOF attracted numerous interests for the application in various areas. Hasan et al. [58] published the esterification reaction of oleic acid with MeOH to produce biodiesel using porous and strong acidic MIL-101(Cr)- SO_3H in order to improve process efficiency and energy conservation. Remarkably, the maximum yield of methyl oleate up to 93% was gained within only 20 min by microwave heating, which was superior compared to the conventional heating with 10 h, resulting in similar product yield.

For the sake of modification of vegetable oils in a friendly and environmentally pattern, the high catalytic activity and excellent stability $\text{Cs}_{2.5}\text{H}_{0.5}\text{PW}_{12}\text{O}_{40}$ @ UiO-66 were synthesized by facile solvothermal approach, which method encapsulated the Keggin-type $\text{Cs}_{2.5}\text{H}_{0.5}\text{PW}_{12}\text{O}_{40}$ heteropolyacid into microporous UiO-66 crystal with enhanced Lewis acidity [59]. Results demonstrated that functionalized MOF exhibited good catalytic activity for soybean oil proceeding the acidolysis reaction towards low-calorific lipids.

2.4. Bifunctionalized MOFs

2.4.1. Upgrading of Saccharides. For the purpose of understanding the effect between the acid and metal centers in the hydrothermal stable Ru-PTA/MIL-100(Cr) (PTA-phosphotungstic acid), Chen et al. [60] studied catalysts

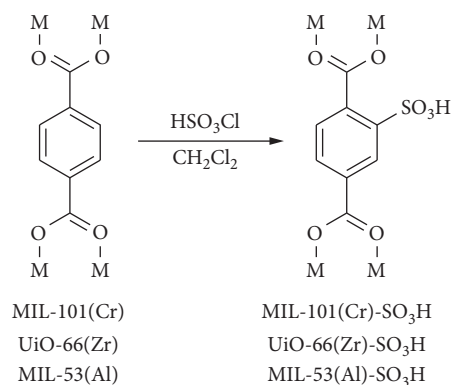


FIGURE 2: Preparation of MOF-SO₃H for the conversion of fructose into HMF.

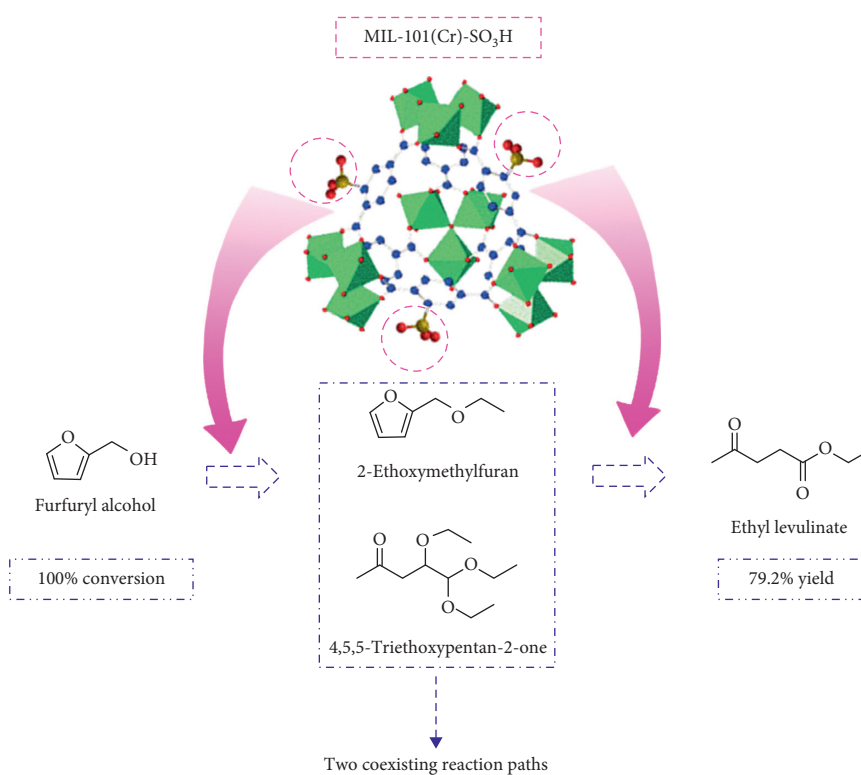


FIGURE 3: Possible mechanisms for the synthesis of ethyl levulinate from ethanolysis of furfuryl alcohol over MIL-101(Cr)-SO₃H.

during the conversion of cellulose and cellobiose for polyol preparation. Adjust the incorporated PTA dosage in MIL-100(Cr) to optimize the optimum amount of acidic sites (Figure 4). Under the optimal parameter, the Ru-PTA/MIL-100(Cr) catalyst supported 3.2 wt.% Ru and 16.7 wt.% PTA exhibited a high yield of 63.2% hexitols and 57.9% selectivity for sorbitol with 100% cellulose conversion. Meanwhile, yielding 97.1% hexitols combined 95.1% selectivity for sorbitol with full conversion of cellobiose. Uniform dispersion of metallic Ru NPs (<2 nm) played a pivotal part during the hydrogenation conversion, whereas acidic sites of PTA/MIL-100(Cr) are answerable for the hydrolysis course.

The efficient transformation of cellulose for the synthesis of polyols has attracted much attention owing to the polyols

acting as significant platform chemicals. With the similar catalysts, Wang et al. developed the metallic Ru nanoparticles embedded into NENU-3 (composing of PTA functionalized HKUST-1), applied in cellulose transformation to prepared ethylene glycol [61]. With the optimized parameters, 2.4 wt.% Ru and 34.8 wt.% PTA, the maximum ethylene glycol yield attained 50.2% under 4.0 MPa pressure and at 245°C for 4 h. The best catalytic activity attributed to the synergistic effect of acid sites and the well-dispersed Ru nanoparticles, which promoted hydrolysis and subsequent C-C bond fragmentation and hydrogenation reaction, respectively. Leaching of catalyst active species in the recycle reaction can be explained by partial decomposition of NENU-3, which further affects the decrease in product yields to a certain extent.

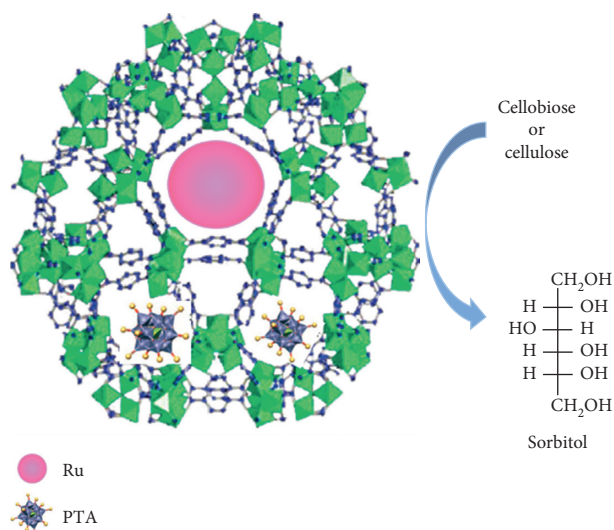


FIGURE 4: Metal-acid bifunctional catalyst Ru-PTA/MIL-100(Cr).

A one-pot hydrogenation conversion procedure of methyl levulinate into GVL was investigated with a bifunctional hybrid catalyst preparing by metallic Ru nanoparticles incorporated on functionalized UiO-66-SO₃H [62]. Under mild reaction conditions (0.5 MPa, 80°C, 4 h), 81% high yield of GVL was attained owing to the synergistic effect of Ru NPs and plenty of Brønsted acidic sites of catalysts that promoted the intermediates converted efficiently. Reusability experiments demonstrated the stability of the catalyst with five coherent times maintained no remarkable loss of activity, while the significantly decreased catalytic performance of two-stage processes further confirmed the indispensable role of -SO₃H groups.

A hybrid Pd/UiO-66@SGO (SGO-sulfonated graphene oxide) material was studied for the one-pot transformation of monosaccharides into 2,5-dimethylfuran [63], which was prepared by supporting the Pd nanoparticles on UiO-66@SGO. The abundant Brønsted acidity existing in UiO-66@SGO guaranteed the high yield of HMF, while the succeeding hydrogenation/hydrogenolysis for the product 2,5-dimethylfuran was catalyzed by uniform dispersed Pd nanoparticles. Direct conversion from fructose afforded the maximum 2,5-dimethylfuran yield of 70.5 mol% under the optimized reaction conditions, while surprisingly, glucose acted as the substrate provided 45.3% mol yield for 2,5-dimethylfuran.

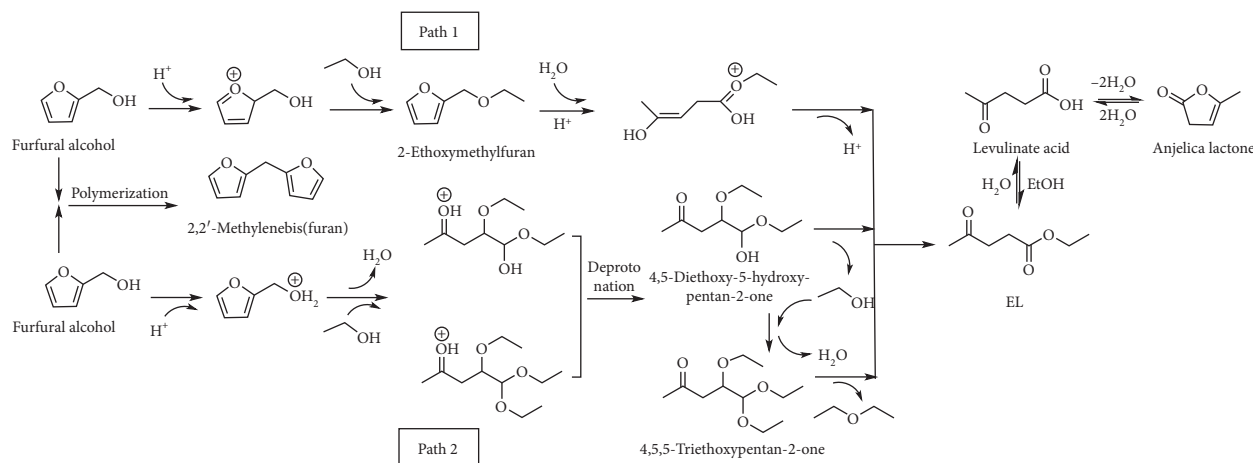
2.4.2. Upgrading of Furan Derivatives. Zhang et al. [64] introduced the ligand-based solid solution for MOF functionalization with the insertion of -SO₃H Brønsted acidic groups into the Cr-MOF and loading of Pd nanoparticles on MIL-101-SO₃H. The -SO₃H acidic density played a pivotal positive correlation role in the ring-open activity of γ -valerolactone and the succeeding hydrodeoxygenation to provided ethyl pentanoate, which was then catalyzed by the Pd NPs of bifunctional Pd/MIL-101-SO₃H to ethyl valerate (83% yield). Reusability experiments indicated a sudden reduction in target chemical yields from

83% to only 10% after the third recycle, owing to the aggregation of Pd NPs under enhanced reaction temperatures in acidic medium.

A bifunctional Pd/MIL-101(Al)-NH₂ was explored for the selective hydrogenation of HMF to produce 2,5-dihydroxymethyl-tetrahydrofuran (DHMTFH) [65]. The catalyst was prepared via direct anionic exchange procedure and then the reduction step was introduced for the Pd nanoparticles immobilized on MIL-101(Al)-NH₂. The existence of isolated amine groups of the catalyst guaranteed the constitution of well dispersion of Pd nanoparticles avoiding the aggregation of Pd NPs. With the explored catalyst, the conversion process HMF-DHMF (2,5-dihydroxymethyl-furan)-DHMTFH afforded a 96% high yield of DHMTFH and 100% conversion of HMF at only (30°C). The excellent catalytic activity partially ascribed to the hydrophilic nature of DHMF and the interaction of DHMF and MOF, which further promoted the transformation of DHMF to the target product. The investigation exploited the perspectives of functionalized Al-MOF-NH₂ for sustainable biomass valorization.

2.4.3. Upgrading of Other Biobased Compounds. As the ordinary component of lignin-derived bio-oil, vanillin was converted through hydrodeoxygenation reaction using bifunctional Pd/SO₃H-MIL-101(Cr), which was developed by immobilization of Pd nanoparticles on mesoporous functionalized Cr-MOF [66]. The existing Brønsted acidic groups -SO₃H of the MOF acted as the activator of the reactants guaranteeing the catalytic efficiency. Results showed that the 2 wt.% Pd/MIL-101(Cr)-SO₃H catalyst indicated excellent capability in the hydrodeoxygenation of vanillin for the product 2-methoxy-4-methylphenol. Meanwhile, the reusability of the catalyst proved the stability that can be continuously reused for no less than seven recycles without a decrease of catalytic effect. Comparable studies of the hydrodeoxygenation of vanillin were published with a similar catalyst Pd@NH₂-UiO-66, which was prepared by ultramicro Pd nanoparticles (1.5–2.5 nm) incorporated in a basic-functionalized MOF (NH₂-UiO-66) [67]. Until now, the maximum 100% yield of 2-methoxy-4-methylphenol was obtained higher than 2 wt.% Pd@NH₂-UiO-66 with mild reaction conditions as 0.5 MPa and 100°C for 60 min. The synergistic effect of uniform Pd sites and the NH₂-UiO-66 support played a critical role in the wonderful catalytic performance of Pd@NH₂-UiO-66.

The comparison study of Pd/UiO-66 and NH₂-functionalised Pd/UiO-66 catalysts was conducted for phenol hydrogenation to prepare cyclohexanol [68]. Interestingly, the introduction of NH₂ groups verified a destroyed crystalline structure in UiO-66, providing weak chemical interaction between Zr and Pd in prepared Pd-UiO-66-NH₂. Based on that, the Pd-UiO-66 catalyst exhibited preferable catalytic performances in phenol hydrogenation than Pd-UiO-66-NH₂ with complete conversion of phenol for only 2 h in 120°C. Chemical kinetic results exhibited that the activation energies with Pd-UiO-66 and Pd-UiO-66-NH₂ are 50.44 ± 3.20 and 43.11 ± 5.98 kJ/mol, respectively, which further proved the aforementioned conclusion.



SCHEME 1: Proposed mechanism for the transformation of furfuryl alcohol to ethyl levulinate in EtOH.

The presence of oxygen-containing C16-C18 fatty acids causes polymerization, weak oxidation stability, and low calorific value, even when cannot efficiently utilize the alga-derived bio-oil for transportation fuel. Considering this, Fang et al. [69] researched the facile conversion of palmitic acid to hexadecane catalyzed by the bifunctional PTA@PdCu@Fe^{III}-MOF-5, which was prepared by immobilizing phosphotungstic acid into the MOF structure. The explored catalyst demonstrates an enhanced acidity and efficiently facilitates palmitic acid for hexadecane with relatively high selectivity. The preferable catalytic activity was explained by its particular yolk-shell structural feature, increased acidity, and the superior supercritical fluid medium.

2.5. Determinant of MOF Catalytic Performance in Biomass Valorization. The multiplicity of metal centers and functional/nonfunctional organic ligands combined the chemical interactions grants MOFs to act as active catalysts, catalyst carriers, or catalyst precursors. Because of the stable SUB coordinated networks, MOFs possess adjustable pore size, high specific surface areas, and multiple topology structures compared to traditional heterogeneous solid catalysts.

Considering the conversion of biomass feedstocks which usually involves larger molecules, appropriate pore size, and morphologies which are needed to be serious-minded adjusted for the reactants, intermediates and productions efficiently diffuse towards catalytic active sites. For example, Li et al. [45] demonstrated that the morphology of Fe-MIL-101-NH₂ can be ameliorated by altering the preparation time, resulting in desired catalytic activities in glycerol oxidation.

The independent metal ions or clusters and functional/nonfunctional organic ligands can afford required acid-base properties. The unsaturated or defected metal centers in MOFs generally provide Lewis acidity. By the reason of Lewis acidic, MOFs can act as heterogeneous acid catalysts for glucose isomerization into fructose [50]. Owing to the necessity of Brønsted acid in various biomass-upgrading reactions, several feasible approaches have been explored to introduce Brønsted acidic functional sites onto specific sites of the MOFs [45, 70]. Up to now, the functionalization of MOFs

with Brønsted acid mainly including the post-synthetic modified method, [53] one-pot synthesis through organic ligands containing substituent groups [57] and active component supported on MOFs [60]. The functionalized MOFs integrate the superiorities of MOFs and encapsulated functional active sites facilitating cascade catalytic conversion for efficient biomass valorization (Scheme 1).

The rigid coordination textural properties of frameworks are fatal determinants used as catalyst supports to synthesize highly stable heterogeneous catalysts. The easily regulated porous textures of MOFs supply strategies for the incorporation of catalytic metal NPs, avoiding agglomeration and enhancing catalytic performance [40, 71].

Furthermore, MOFs have also been employed as matrixes for the production of carbon matrixes over pyrolysis procedure for supporting metal catalysts [72–75]. The obtained carbon templates can further work as a high S_{BET} and stability carrier, which bore the generated metal nanoparticles, forming novel and well-dispersed active site catalysts. Wang et al. [73], tailoring the MOF-templated strategy, published an efficient bimetallic CuCo/C catalyst for the furfural conversion with the maximum 96.4% yield of furfuryl alcohol.

3. Conclusions and Perspectives

Taking the global warming impact into consideration, the sustainable and renewable resources such as biomass have become the hot research topic in the 21st century. With appropriate approaches (biological, thermal, or chemical processes), biomass can be derived into various value-added chemicals and fuels.

Addressing challenges in MOF preparation and application include concerns of availability, cost, toxicity, safety, and environmental impact, which are critical to evaluate the introduction of MOF materials for biomass upgrading. The exploitation of multifunctional solid catalysts with an abundance of acidic, basic, or redox-active sites is significant for performing superior reaction efficiency, notably in tandem biomass procedures. Several promising approaches investigated for the fixation of acid-base and redox

functional groups on specific sites of the abovementioned materials were argued at great length. Eventually, the succeeding impacts of functionalization on one-pot tandem procedures and other procedures that generally generated in biorefineries were thoroughly argued. More interesting research endeavors are therefore needed to develop novel functionalized solid catalysts, with multiple active sites and particular morphologies.

Although enormous procedures have been accomplished upon the investigation of effective functionalized heterogeneous catalysts for biomass upgrading, further enhancements are still essential on account of continuable and renewable manufacturing. There are challenges needed to be faced towards MOF-based catalyst handy applied in biomass valorization. For instance, (i) the fertile preparation method for cost-efficient MOFs as one-pot synthesis precesses; (ii) more stable MOFs and active sites; and (iii) effective analysis of structure-function relationships. Hence, in the future investigation, we would focus on minimizing catalyst production costs, improving production yields and hydrothermal stability, tailoring the selectivity towards a target product, and enhancing efficient reusability.

Conflicts of Interest

The authors declare that there are no conflicts of interest regarding the publication of this paper.

Acknowledgments

This work was financially supported by the Basic Research Program of Guizhou Province ([2019]1009), the Joint Science and Technology Funds of the Youth Growth S&T Personnel Foundation of Guizhou Education Department (no. KY [2018]292), and the Special Funding of Guiyang Science and Technology Bureau and Guiyang University (GYU-KYZ [2019~2020] PT07-01).

References

- [1] W. Schutyser, T. Renders, S. Van den Bosch, S.-F. Koelewijn, G. T. Beckham, and B. F. Sels, "Chemicals from lignin: an interplay of lignocellulose fractionation, depolymerisation, and upgrading," *Chemical Society Reviews*, vol. 47, no. 3, pp. 852–908, 2018.
- [2] B. Malleshham, P. Sudarsanam, G. Raju, and B. M. Reddy, "Design of highly efficient Mo and W-promoted SnO₂ solid acids for heterogeneous catalysis: acetalization of bio-glycerol," *Green Chemistry*, vol. 15, no. 2, pp. 478–489, 2013.
- [3] X. Zhang, L. Chen, Y. Li et al., "Palladium NPs supported on sulfonic acid functionalized metal-organic frameworks as catalysts for biomass cascade reactions," *Dalton Transactions*, vol. 48, no. 17, pp. 5515–5519, 2019.
- [4] T. Guo, M. Qiu, and X. Qi, "Selective conversion of biomass-derived levulinic acid to ethyl levulinate catalyzed by metal organic framework (MOF)-supported polyoxometalates," *Applied Catalysis A: General*, vol. 572, pp. 168–175, 2019.
- [5] S. Dostagir, M. Awasthi, A. Kumar et al., "Selective catalysis for room-temperature hydrogenation of biomass-derived compounds over supported NiPd catalysts in water," *ACS Sustainable Chemistry & Engineering*, vol. 7, no. 10, pp. 9352–9359, 2019.
- [6] L. T. Mika, E. Cséfalvay, and Á. Németh, "Catalytic conversion of carbohydrates to initial platform chemicals: chemistry and sustainability," *Chemical Reviews*, vol. 118, no. 2, pp. 505–613, 2018.
- [7] S. Van de Vyver, J. Geboers, P. A. Jacobs, and B. F. Sels, "Recent advances in the catalytic conversion of cellulose," *ChemCatChem*, vol. 3, no. 1, pp. 82–94, 2011.
- [8] J. A. Geboers, S. Van de Vyver, R. Ooms, B. Op De Beeck, P. A. Jacobs, and B. F. Sels, "Chemocatalytic conversion of cellulose: opportunities, advances and pitfalls," *Catalysis Science & Technology*, vol. 1, no. 5, pp. 714–726, 2011.
- [9] D. M. Alonso, J. Q. Bond, and J. A. Dumesic, "Catalytic conversion of biomass to biofuels," *Green Chemistry*, vol. 12, no. 9, pp. 1493–1513, 2010.
- [10] P. S. Reddy, P. Sudarsanam, B. Malleshham, G. Raju, and B. M. Reddy, "Acetalisation of glycerol with acetone over zirconia and promoted zirconia catalysts under mild reaction conditions," *Journal of Industrial and Engineering Chemistry*, vol. 17, no. 3, pp. 377–381, 2011.
- [11] S. Santoro, F. Ferlin, L. Luciani, L. Ackermann, and L. Vaccaro, "Biomass-derived solvents as effective media for cross-coupling reactions and C-H functionalization processes," *Green Chemistry*, vol. 19, no. 7, pp. 1601–1612, 2017.
- [12] H. Zhang, H. Li, C. Xu, and S. Yang, "Heterogeneously Chemo/enzyme-functionalized porous polymeric catalysts of high-performance for efficient biodiesel production," *ACS Catalysis*, vol. 9, no. 12, pp. 10990–11029, 2019.
- [13] H. Zhang, H. Li, Y. Hu, K. T. Venkateswara Rao, C. Xu, and S. Yang, "Advances in production of bio-based ester fuels with heterogeneous bifunctional catalysts," *Renewable and Sustainable Energy Reviews*, vol. 114, p. 109296, 2019.
- [14] S. Zhang, J. Zhang, Y. Zhang, and Y. Deng, "Nanoconfined ionic liquids," *Chemical Reviews*, vol. 117, no. 10, pp. 6755–6833, 2017.
- [15] H. Li, Q. Zhang, X. Liu et al., "Immobilizing Cr³⁺ with SO₃H-functionalized solid polymeric ionic liquids as efficient and reusable catalysts for selective transformation of carbohydrates into 5-hydroxymethylfurfural," *Bioresource Technology*, vol. 144, pp. 21–27, 2013.
- [16] P. Sudarsanam, B. Hillary, M. H. Amin, S. B. A. Hamid, and S. K. Bhargava, "Structure-activity relationships of nanoscale MnO_x/CeO₂ heterostructured catalysts for selective oxidation of amines under eco-friendly conditions," *Applied Catalysis B: Environmental*, vol. 185, pp. 213–224, 2016.
- [17] B. Hillary, P. Sudarsanam, M. H. Amin, and S. K. Bhargava, "Nanoscale cobalt-manganese oxide catalyst supported on shape-controlled cerium oxide: effect of nanointerface configuration on structural, redox, and catalytic properties," *Langmuir*, vol. 33, no. 8, pp. 1743–1750, 2017.
- [18] M. Besson, P. Gallezot, and C. Pinel, "Conversion of biomass into chemicals over metal catalysts," *Chemical Reviews*, vol. 114, no. 3, pp. 1827–1870, 2014.
- [19] M. Hara, K. Nakajima, and K. Kamata, "Recent progress in the development of solid catalysts for biomass conversion into high value-added chemicals," *Science Technology Advanced Materials*, vol. 16, Article ID 034903, 2015.
- [20] I. Fechete, Y. Wang, and J. C. Védrine, "The past, present and future of heterogeneous catalysis," *Catalysis Today*, vol. 189, no. 1, pp. 2–27, 2012.
- [21] P. Ferrini and R. Rinaldi, "Catalytic biorefining of plant biomass to non-pyrolytic lignin bio-oil and carbohydrates through hydrogen transfer reactions," *Angewandte Chemie International Edition*, vol. 53, no. 33, pp. 8634–8639, 2014.
- [22] Y.-D. Chiang, S. Dutta, C.-T. Chen et al., "Functionalized Fe₃O₄@Silica core-shell nanoparticles as microalgae

- harvester and catalyst for biodiesel production,” *ChemSusChem*, vol. 8, no. 5, pp. 789–794, 2015.
- [23] H. Li, C. Wang, Y. Xu et al., “Heterogeneous (de)chlorination-enabled control of reactivity in liquid-phase synthesis of furanic biofuel from cellulosic feedstock,” *Green Chemistry*, vol. 22, pp. 637–645, 2020.
- [24] H. Li, H. Guo, Y. Su et al., “N-formyl-stabilizing quasi-catalytic species afford rapid and selective solvent-free amination of biomass-derived feedstocks,” *Nature Communications*, vol. 10, p. 699, 2019.
- [25] A. Herbst and C. Janiak, “MOF catalysts in biomass upgrading towards value-added fine chemicals,” *CrystEngComm*, vol. 19, no. 29, pp. 4092–4117, 2017.
- [26] O. Fleker, A. Borenstein, R. Lavi, L. Benisvy, S. Ruthstein, and D. Aurbach, “Preparation and properties of metal organic framework/activated carbon composite materials,” *Langmuir*, vol. 32, no. 19, pp. 4935–4944, 2016.
- [27] Y.-X. Zhou, Y.-Z. Chen, Y. Hu, G. Huang, S.-H. Yu, and H.-L. Jiang, “MIL-101-SO₃H: a highly efficient brønsted acid catalyst for heterogeneous alcoholysis of epoxides under ambient conditions,” *Chemistry—A European Journal*, vol. 20, no. 46, pp. 14976–14980, 2014.
- [28] G. Zi, Z. Yan, Y. Wang et al., “Catalytic hydrothermal conversion of carboxymethyl cellulose to value-added chemicals over metal-organic framework MIL-53(Al),” *Carbohydrate Polymers*, vol. 115, pp. 146–151, 2015.
- [29] B. Murillo, B. Zornoza, O. de la Iglesia, C. Téllez, and J. Coronas, “Chemocatalysis of sugars to produce lactic acid derivatives on zeolitic imidazolate frameworks,” *Journal of Catalysis*, vol. 334, pp. 60–67, 2016.
- [30] X. Lu, L. Wang, and X. Lu, “Catalytic conversion of sugars to methyl lactate over Mg-MOF-74 in near-critical methanol solutions,” *Catalysis Communications*, vol. 110, pp. 23–27, 2018.
- [31] S. Huang, K.-L. Yang, X.-F. Liu, H. Pan, H. Zhang, and S. Yang, “MIL-100(Fe)-catalyzed efficient conversion of hexoses to lactic acid,” *RSC Advances*, vol. 7, no. 10, pp. 5621–5627, 2017.
- [32] A. Chatterjee, X. Hu, and F. L.-Y. Lam, “Catalytic activity of an economically sustainable fly-ash-metal-organic-framework composite towards biomass valorization,” *Catalysis Today*, vol. 314, pp. 137–146, 2018.
- [33] C. Lucarelli, S. Galli, A. Maspero et al., “Adsorbent-adsorbate interactions in the oxidation of HMF catalyzed by Ni-based mofs: a drift and FT-IR insight,” *The Journal of Physical Chemistry C*, vol. 120, no. 28, pp. 15310–15321, 2016.
- [34] A. Rapeyko, K. S. Arias, M. J. Climent, A. Corma, and S. Iborra, “Polymers from biomass: one pot two-step synthesis of furilydenepropanenitrile derivatives with MIL-100(Fe) catalyst,” *Catalysis Science & Technology*, vol. 7, no. 14, pp. 3008–3016, 2017.
- [35] O. Kikhtyanin, D. Kubička, and J. Čejka, “Toward understanding of the role of Lewis acidity in aldol condensation of acetone and furfural using MOF and zeolite catalysts,” *Catalysis Today*, vol. 243, pp. 158–162, 2015.
- [36] L. Ning, S. Liao, X. Liu, L. Yu, X. Zhuang, and X. Tong, “Selective transformation of renewable furfural catalyzed by diverse active species derived from 2D co-based metal-organic frameworks,” *Journal of Catalysis*, vol. 352, pp. 480–490, 2017.
- [37] F. G. Cirujano, A. Corma, and F. X. Llabrés i Xamena, “Conversion of levulinic acid into chemicals: synthesis of biomass derived levulinate esters over Zr-containing MOFs,” *Chemical Engineering Science*, vol. 124, pp. 52–60, 2015.
- [38] I. Larasati, D. Winarni, F. R. Putri, Q. A. Hanif, and W. W. Lestari, “Synthesis of metal-organic frameworks based on Zr⁴⁺ and benzene 1,3,5-tricarboxylate linker as heterogeneous catalyst in the esterification reaction of palmitic acid,” *IOP Conference Series: Materials Science and Engineering*, vol. 214, Article ID 012006, 2017.
- [39] F. G. Cirujano, A. Corma, and F. X. Llabrés i Xamena, “Zirconium-containing metal organic frameworks as solid acid catalysts for the esterification of free fatty acids: synthesis of biodiesel and other compounds of interest,” *Catalysis Today*, vol. 257, pp. 213–220, 2015.
- [40] L. Ning, S. Liao, H. Cui, L. Yu, and X. Tong, “Selective conversion of renewable furfural with ethanol to produce furan-2-acrolein mediated by Pt@MOF-5,” *ACS Sustainable Chemistry & Engineering*, vol. 6, no. 1, pp. 135–142, 2018.
- [41] Q. Yuan, D. Zhang, L. V. Haandel et al., “Selective liquid phase hydrogenation of furfural to furfuryl alcohol by Ru/Zr-MOFs,” *Journal of Molecular Catalysis A: Chemical*, vol. 406, pp. 58–64, 2015.
- [42] P. Hester, S. Xu, W. Liang et al., “On thermal stability and catalytic reactivity of Zr-based metal-organic framework (UiO-67) encapsulated Pt catalysts,” *Journal of Catalysis*, vol. 340, pp. 85–94, 2016.
- [43] Y. Guo, Y. Li, J. Chen, and L. Chen, “Hydrogenation of levulinic acid into γ -valerolactone over ruthenium catalysts supported on metal-organic frameworks in aqueous medium,” *Catalysis Letters*, vol. 146, no. 10, pp. 2041–2052, 2016.
- [44] S. B. A. Hamid, N. Basiron, W. A. Yehye, P. Sudarsanam, and S. K. Bhargava, “Nanoscale Pd-based catalysts for selective oxidation of glycerol with molecular oxygen: structure-activity correlations,” *Polyhedron*, vol. 120, pp. 124–133, 2016.
- [45] X. Li, A. K. Tjiptoputro, J. Ding, J. M. Xue, and Y. Zhu, “Pd-Ce nanoparticles supported on functional Fe-MIL-101-NH 2: an efficient catalyst for selective glycerol oxidation,” *Catalysis Today*, vol. 279, pp. 77–83, 2017.
- [46] A. A. Ibrahim, A. Lin, F. Zhang, K. M. AbouZeid, and M. S. El-Shall, “Palladium nanoparticles supported on a metal-organic framework-partially reduced graphene oxide hybrid for the catalytic hydrodeoxygenation of vanillin as a model for biofuel upgrade reactions,” *ChemCatChem*, vol. 9, no. 3, pp. 469–480, 2017.
- [47] R.-J. van Putten, J. C. van der Waal, E. de Jong, C. B. Rasrendra, H. J. Heeres, and J. G. de Vries, “Hydroxymethylfurfural, a versatile platform chemical made from renewable resources,” *Chemical Reviews*, vol. 113, no. 3, pp. 1499–1597, 2013.
- [48] Z. Xue, M.-G. Ma, Z. Li, and T. Mu, “Advances in the conversion of glucose and cellulose to 5-hydroxymethylfurfural over heterogeneous catalysts,” *RSC Advances*, vol. 6, no. 101, pp. 98874–98892, 2016.
- [49] R. Oozeerally, D. L. Burnett, T. W. Chamberlain, R. I. Walton, and V. Degirmenci, “Exceptionally efficient and recyclable heterogeneous metal-organic framework catalyst for glucose isomerization in water,” *ChemCatChem*, vol. 10, no. 4, pp. 706–709, 2018.
- [50] M. Yabushita, P. Li, T. Islamoglu et al., “Selective metal-organic framework catalysis of glucose to 5-hydroxymethylfurfural using phosphate-modified NU-1000,” *Industrial & Engineering Chemistry Research*, vol. 56, no. 25, pp. 7141–7148, 2017.
- [51] A. Herbst and C. Janiak, “Selective glucose conversion to 5-hydroxymethylfurfural (5-HMF) instead of levulinic acid with MIL-101Cr MOF-derivatives,” *New Journal of Chemistry*, vol. 40, no. 9, pp. 7958–7967, 2016.
- [52] Y. Su, G. Chang, Z. Zhang et al., “Catalytic dehydration of glucose to 5-hydroxymethylfurfural with a bifunctional metal-organic framework,” *AIChE Journal*, vol. 62, no. 12, pp. 4403–4417, 2016.

- [53] J. Chen, K. Li, L. Chen, R. Liu, X. Huang, and D. Ye, "Conversion of fructose into 5-hydroxymethylfurfural catalyzed by recyclable sulfonic acid-functionalized metal-organic frameworks," *Green Chemistry*, vol. 16, no. 5, pp. 2490–2499, 2014.
- [54] Z. Hu, Y. Peng, Y. Gao et al., "Direct synthesis of hierarchically porous metal-organic frameworks with high stability and strong brønsted acidity: the decisive role of hafnium in efficient and selective fructose dehydration," *Chemistry of Materials*, vol. 28, no. 8, pp. 2659–2667, 2016.
- [55] M. Liu, Y. Zhang, E. Zhu et al., "Facile synthesis of halloysite nanotubes-supported acidic metal-organic frameworks with tunable acidity for efficient fructose dehydration to 5-hydroxymethylfurfural," *Chemistryselect*, vol. 2, no. 32, pp. 10413–10419, 2017.
- [56] Y. Kuwahara, H. Kango, and H. Yamashita, "Catalytic transfer hydrogenation of biomass-derived levulinic acid and its esters to γ -valerolactone over sulfonic acid-functionalized UiO-66," *ACS Sustainable Chemistry & Engineering*, vol. 5, no. 1, pp. 1141–1152, 2017.
- [57] X.-F. Liu, H. Li, H. Zhang et al., "Efficient conversion of furfuryl alcohol to ethyl levulinate with sulfonic acid-functionalized MIL-101(Cr)," *RSC Advances*, vol. 6, no. 93, pp. 90232–90238, 2016.
- [58] Z. Hasan, J. W. Jun, and S. H. Jhung, "Sulfonic acid-functionalized MIL-101(Cr): an efficient catalyst for esterification of oleic acid and vapor-phase dehydration of butanol," *Chemical Engineering Journal*, vol. 278, pp. 265–271, 2015.
- [59] W. Xie, X. Yang, and P. Hu, "Cs₂.5H_{0.5}PW₁₂O₄₀ encapsulated in metal-organic framework UiO-66 as heterogeneous catalysts for acidolysis of soybean oil," *Catalysis Letters*, vol. 147, no. 11, pp. 2772–2782, 2017.
- [60] J. Chen, S. Wang, J. Huang, L. Chen, L. Ma, and X. Huang, "Conversion of cellulose and cellobiose into sorbitol catalyzed by ruthenium supported on a polyoxometalate/metal-organic framework hybrid," *ChemSusChem*, vol. 6, no. 8, pp. 1545–1555, 2013.
- [61] S. Wang, J. Chen, and L. Chen, "Selective conversion of cellulose into ethylene glycol over metal-organic framework-derived multifunctional catalysts," *Catalysis Letters*, vol. 144, no. 10, pp. 1728–1734, 2014.
- [62] Z. Lin, X. Cai, Y. Fu, W. Zhu, and F. Zhang, "Cascade catalytic hydrogenation-cyclization of methyl levulinate to form γ -valerolactone over Ru nanoparticles supported on a sulfonic acid-functionalized UiO-66 catalyst," *RSC Advances*, vol. 7, no. 70, pp. 44082–44088, 2017.
- [63] R. Insyani, D. Verma, S. M. Kim, and J. Kim, "Direct one-pot conversion of monosaccharides into high-yield 2,5-dimethylfuran over a multifunctional Pd/Zr-based metal-organic framework@sulfonated graphene oxide catalyst," *Green Chemistry*, vol. 19, no. 11, pp. 2482–2490, 2017.
- [64] D. Zhang, F. Ye, Y. Guan, Y. Wang, and E. J. M. Hensen, "Hydrogenation of γ -valerolactone in ethanol over Pd nanoparticles supported on sulfonic acid functionalized MIL-101," *RSC Advances*, vol. 4, no. 74, pp. 39558–39564, 2014.
- [65] J. Chen, R. Liu, Y. Guo, L. Chen, and H. Gao, "Selective hydrogenation of biomass-based 5-hydroxymethylfurfural over catalyst of palladium immobilized on amine-functionalized metal-organic frameworks," *ACS Catalysis*, vol. 5, no. 2, pp. 722–733, 2015.
- [66] F. Zhang, Y. Jin, Y. Fu et al., "Palladium nanoparticles incorporated within sulfonic acid-functionalized MIL-101(Cr) for efficient catalytic conversion of vanillin," *Journal of Materials Chemistry A*, vol. 3, no. 33, pp. 17008–17015, 2015.
- [67] F. Zhang, S. Zheng, Q. Xiao et al., "Synergetic catalysis of palladium nanoparticles encaged within amine-functionalized UiO-66 in the hydrodeoxygenation of vanillin in water," *Green Chemistry*, vol. 18, no. 9, pp. 2900–2908, 2016.
- [68] Q. Guan, B. Wang, X. Chai, J. Liu, J. Gu, and P. Ning, "Comparison of Pd-UiO-66 and Pd-UiO-66-NH₂ catalysts performance for phenol hydrogenation in aqueous medium," *Fuel*, vol. 205, pp. 130–141, 2017.
- [69] X. Fang, Y. Shi, K. Wu, J. Liang, Y. Wu, and M. Yang, "Upgrading of palmitic acid over MOF catalysts in supercritical fluid of *n*-hexane," *RSC Advances*, vol. 7, no. 64, pp. 40581–40590, 2017.
- [70] J. Jiang and O. M. Yaghi, "Brønsted acidity in metal-organic frameworks," *Chemical Reviews*, vol. 115, no. 14, pp. 6966–6997, 2015.
- [71] V. Pascanu, A. Bermejo Gómez, C. Ayats et al., "Double-supported silica-metal-organic framework palladium nanocatalyst for the aerobic oxidation of alcohols under batch and continuous flow regimes," *ACS Catalysis*, vol. 5, no. 2, pp. 472–479, 2015.
- [72] T. B. Čelič, M. Grilc, B. Likozar, and N. N. Tušar, "In situ generation of Ni nanoparticles from metal-organic framework precursors and their use for biomass hydrodeoxygenation," *ChemSusChem*, vol. 8, pp. 1703–1710, 2015.
- [73] Y. Wang, Y. Miao, S. Li, L. Gao, and G. Xiao, "Metal-organic frameworks derived bimetallic Cu-Co catalyst for efficient and selective hydrogenation of biomass-derived furfural to furfuryl alcohol," *Molecular Catalysis*, vol. 436, pp. 128–137, 2017.
- [74] Y. Wang, S. Sang, W. Zhu, L. Gao, and G. Xiao, "CuNi@C catalysts with high activity derived from metal-organic frameworks precursor for conversion of furfural to cyclopentanone," *Chemical Engineering Journal*, vol. 299, pp. 104–111, 2016.
- [75] P. Sudarsanam, R. Zhong, S. Van den Bosch, S. M. Coman, V. I. Parvulescu, and B. F. Sels, "Functionalised heterogeneous catalysts for sustainable biomass valorisation," *Chemical Society Reviews*, vol. 47, no. 22, pp. 8349–8402, 2018.

Review Article

Progress of Catalytic Valorization of Bio-Glycerol with Urea into Glycerol Carbonate as a Monomer for Polymeric Materials

Heng Zhang ^{1,2}, Hu Li ¹, Anping Wang ¹, Chunbao (Charles) Xu ² and Song Yang ¹

¹State Key Laboratory Breeding Base of Green Pesticide & Agricultural Bioengineering, Key Laboratory of Green Pesticide & Agricultural Bioengineering, Ministry of Education, State-Local Joint Laboratory for Comprehensive Utilization of Biomass, Center for Research & Development of Fine Chemicals, Guizhou University, Guiyang, Guizhou 550025, China

²Institute for Chemicals and Fuels from Alternative Resources (ICFAR), Department of Chemical and Biochemical Engineering, Western University, London, Ontario N6A 5B9, Canada

Correspondence should be addressed to Hu Li; hli13@gzu.edu.cn, Chunbao (Charles) Xu; cxu6@uwo.ca, and Song Yang; jhxx.msm@gmail.com

Received 8 August 2019; Accepted 20 November 2019; Published 29 January 2020

Academic Editor: Leonard D. Tijing

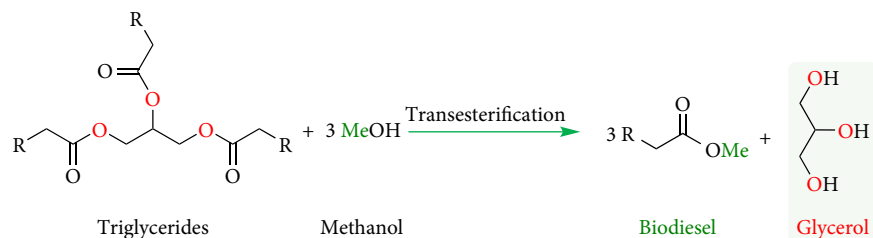
Copyright © 2020 Heng Zhang et al. This is an open access article distributed under the Creative Commons Attribution License, which permits unrestricted use, distribution, and reproduction in any medium, provided the original work is properly cited.

Versatile polymers with highly adjustable characteristics and a broad range of applications are possibly developed owing to the contemporary industrial polymerization techniques. However, industrial production of large amounts of chemicals and polymers heavily depends on petroleum resources which are dwindling and unsustainable. Of particular interest is to utilize sustainable and green resources for the manufacture of polymeric materials. The efficient transformation of bio-glycerol to the relevant functional derivatives are being widely investigated owing to the increasing demand for enhancing the value of glycerol manufactured by biodiesel and oleochemical industries. With respect to glycerol-based polymer chemistry and technology, considering the economy and environmental benefits, using effective catalysts for the selective transformation of bio-glycerol and urea into glycerol carbonate (GC) as a polymer monomer is of great significance. In this review, recent studies on GC synthesis involving the catalysts such as zinc, magnesium, tungsten, ionic liquid-based catalysts, reaction conditions, and possible pathways are primarily described. Some critical issues and challenges with respect to the rational development of heterogeneous catalytic materials like well-balanced acid-base sites are also illustrated.

1. Introduction

Modern life depends on polymers, from materials applied in the manufacture of clothing, houses, cars, and airplanes to those demonstrating complex adhibitions in medicine, diagnostics, and electronics [1–4]. A vast majority of polymers have been contributing greatly to our better daily life of enhanced quality and cleaner living environments, for instance, as materials capable of purifying water or as polymers bearing the better fuel economy in aerospace utilizations. Nonetheless, most of these polymers are supplied by the traditional petrochemicals. It is reported that merely 6% of the oils furnished globally are used to produce polymers, but the raw resources and their end-of-life options will arouse the important environmental issues [5]. Since there is no panacea for these sophisticated environmental concerns, one

alternative is to exploit more “sustainable” polymers. Research has been focusing basically on developing the renewable feed-stocks to substitute fossil raw sources and on opening-up the end-of-life options that can provide materials that are feasible in recycling or biodegradation [6, 7]. As polymers are derived from sustainable biomass resources, they are generally deemed to be bioderived. It should be recognized that with respect to the concept of biodegradation, some petrochemical-derived polymers are also biodegradable, while some bioderived polymers will not biodegrade [8]. Generally, two procedures are used to prepare sustainable polymers: decreasing the environmental influence of traditional manufacture, such as by employing biomass materials for the manufacture of known monomers or polymers like polyethylene terephthalate and polyethylene; and preparing the novel, and “sustainable” structures like polylactide from renewable resources that are applied

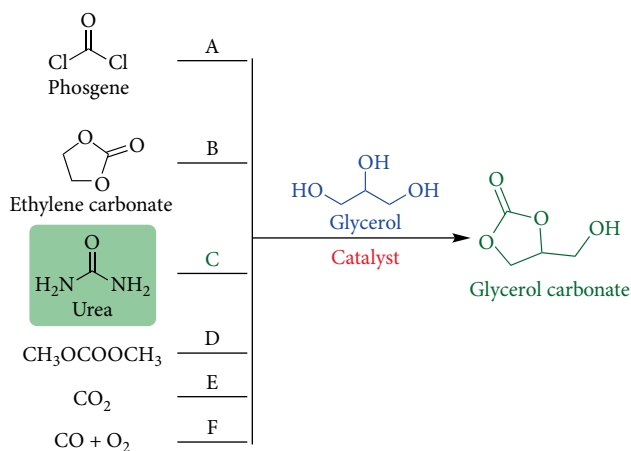


SCHEME 1: Catalytic transesterification of triglycerides to biodiesel and glycerol.

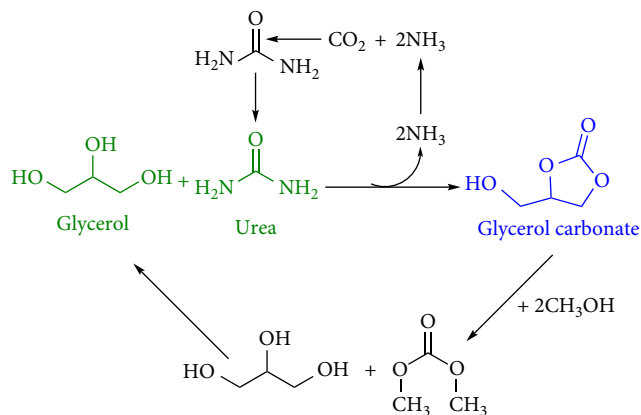
increasingly for preparing polymers [9, 10]. Specifically, the vital monomers including carbon dioxide, terpenes, vegetable oils, and carbohydrates are being applied in manufacturing various sustainable materials and products, such as elastomers, plastics, hydrogels, flexible electronics, resins, engineering polymers, and composites [11, 12]. There are large opportunities to apply such sustainable polymers for the manufacture of both high-value fuels and chemicals, and for basic applications like packaging. It is worth noting that effective catalysis is usually demanded to generate monomers, to facilitate selective polymerizations and to enable recycling or upcycling of waste materials [13–15].

The increasing demands of biofuels and fuel additives, among which biodiesel has caused a considerable surplus of glycerol to the market that will create new threats in terms of their sustainable exploitation [16–19]. Stoichiometrically (Scheme 1), for the transesterification of triglycerides with methanol into biodiesel and glycerol, each tonne of biodiesel along with 100 kg of by-product crude glycerol are simultaneously generated [20, 21]. It is important to recognize that the surplus of glycerol will not only arouse the serious disposal issues but also bring about the negative impact on the economy of the biodiesel industry. Therefore, with respect to the biodiesel process, the demand to use such a glycerol fraction by an economical approach is highly desirable [22–25]. A vast majority of means for the incorporation of by-product glycerol into the various branches of industry usually require costly and complicated purification courses. Among the possibilities, glycerol related polymer chemistry and technology has been bringing about increasing concerns because of the diversity of polymer constitutions and architectures available. This branch of industry is one of the largest glycerol consumers after food, pharmaceutical, and personal care applications sectors, and possibly the largest branch with no requirement of complex purification of glycerol during the biodiesel manufacture process [26, 27].

Glycerol carbonate (4-hydroxymethyl-2-oxo-1,3-dioxolane, GC), a very versatile chemical compound, is a colorless protic polar liquid having the merits of nontoxic, low evaporation rate, low flammability, and high boiling point [28, 29]. It is of great industrial interest to develop the novel approaches to produce GC from glycerol since GC demonstrates the large potential ability in numerous applications, such as reactive protic solvent, surfactants, and pharmaceuticals. More importantly, GC can also serve as the vital building block to prepare polymers, such as polycarbonates, polyglycerol esters, hyperbranched polyols, and nonisocyanate polyurethanes [30, 31].

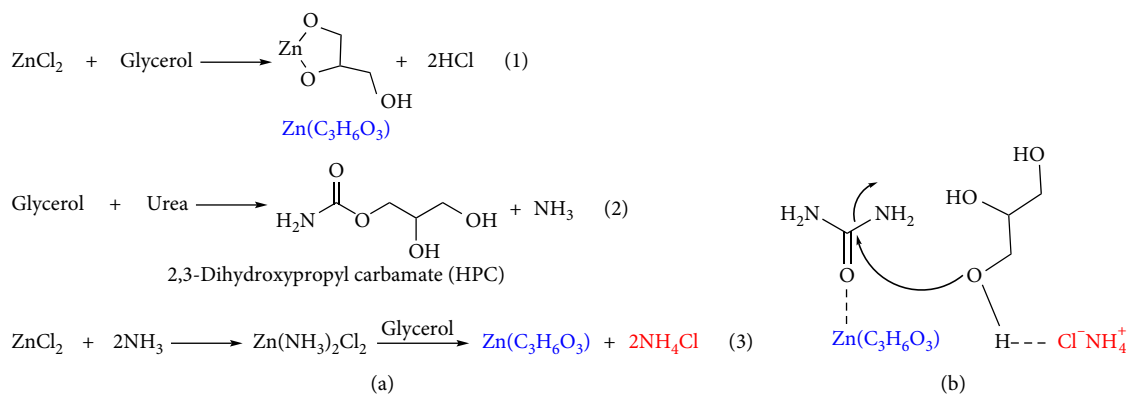


SCHEME 2: Synthetic routes to glycerol carbonate.



SCHEME 3: The glycerolysis of glycerol with urea into glycerol carbonate.

Thus far, some promising manners have been reported for GC manufacture from glycerol, as depicted in Scheme 2: (A) the reaction of glycerol with phosgene; (B) the transesterification of dialkyl carbonates with glycerol; (C) the glycerolysis of urea; (D) the transesterification of ethylene carbonate with glycerol; (E) the direct carboxylation with CO₂; and (F) the oxidative carbonylation of glycerol with CO and O₂ [32, 33]. Nonetheless, upon using ethylene carbonate, GC will be hard to acquire since the by-product ethylene glycol is very difficult to be separated. Moreover, the important environmentally friendly issues should also be considered because the carcinogenic,



SCHEME 4: (a) Reaction routes for the synthesis of $\text{Zn}(\text{C}_3\text{H}_6\text{O}_3)$; (b) Activation of urea and glycerol by $\text{Zn}(\text{C}_3\text{H}_6\text{O}_3)$ and NH_4Cl , respectively.

acutely toxic, and highly flammable substance, oxirane is utilized to prepare ethylene carbonate [34, 35]. Considering the sustainable development, the application of toxic reagents including asphosgene or CO to make GC is also certainly not preferable [36]. In addition, some other attempts to synthesize GC directly using glycerol and CO_2 under a supercritical reaction condition usually exhibit the low product yields (i.e., zeolites, 8% yield) [37]. Satisfactorily, in comparison with the methods mentioned above, the glycerolysis of urea can be deemed as a relatively green process to produce GC. The main advantages of glycerolysis of urea are that both glycerol and urea are readily available, cheap, and nontoxic, and this simple procedure can be conducted without using any solvent along with the high selectivity and GC yield under mild reaction conditions [38, 39]. It is noteworthy that the GC production from glycerol and urea is currently drawing a mass of attention from a sustainable chemistry perspective: (a) utilizing and reducing the undesirable CO_2 via the chemical transformation, (b) using the biodiesel by-product glycerol, and (c) producing a value-added chemical GC with versatile practical applications [40, 41]. More importantly, as illustrated in Scheme 3, urea is an easily available and cheap substrate, while the coproduct ammonia, can be cycled back into urea manufacture, rendering the protocol quite atom economical [42].

Therefore, this review is dedicated to the state-of-the-art accomplishments made in the efficient transformation of bio-glycerol and urea into GC. The emphasis would be given to the catalytic performance of the relevant catalysts such as zinc, magnesium, tungsten, ionic liquid-based catalysts, and waste-derived materials, reaction conditions, and possible pathways. In addition, how to modify the reaction conditions that will influence the related activities and selectivity to GC is also depicted.

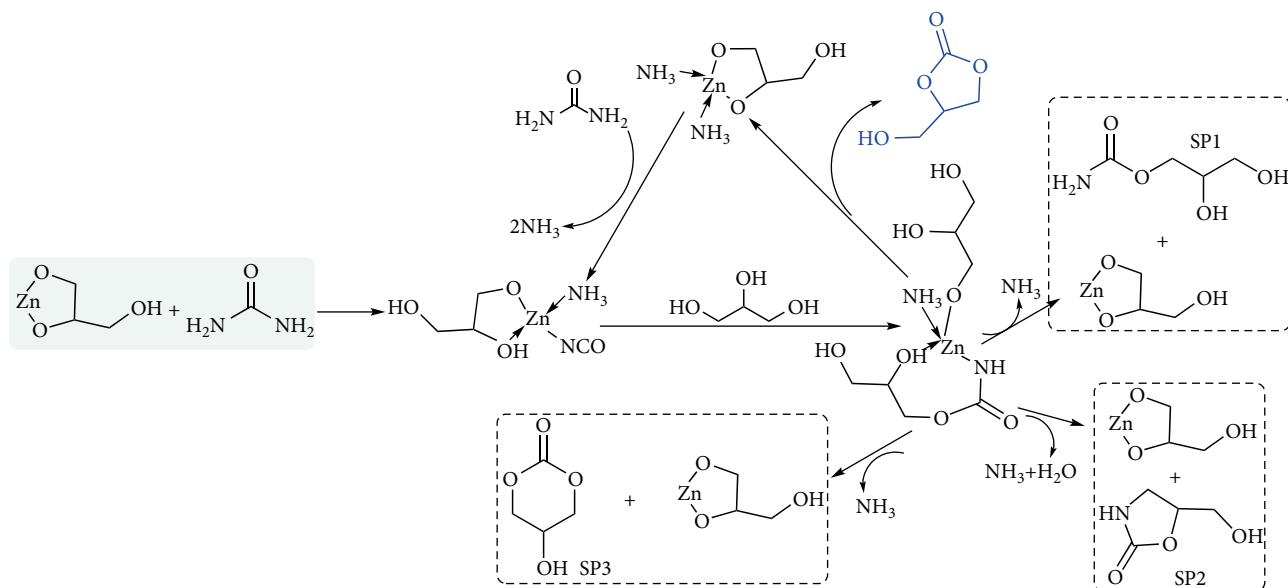
2. Catalysts for Glycerol Carbonate Synthesis from Glycerol and Urea

2.1. Reaction with Zinc-Based Catalyst. As depicted in Table 1, zinc-based catalysts demonstrate a lot of important results for GC synthesis. Zinc-catalyzed (homogeneous ZnCl_2 , ZnBr_2 , ZnI_2 , ZnF_2 , $\text{Zn}(\text{NO}_3)_2 \cdot 6\text{H}_2\text{O}$, and $\text{Zn}(\text{OAc})_2 \cdot 2\text{H}_2\text{O}$) synthesis of GC using glycerol and urea as substrates, was

systematically evaluated with medium to excellent GC yields. Of the zinc-based catalysts measured, ZnCl_2 demonstrated the highest catalytic activity, giving a high GC yield of 80.2% with 99.7% selectivity at 150°C in 2 h along with the urea/glycerol and ZnCl_2 /glycerol molar ratios of 1 and 0.02, respectively [43]. As shown in Scheme 4(a), according to the spectroscopic and elemental analyses, $\text{Zn}(\text{NH}_3)_2\text{Cl}_2$ was produced firstly by the reaction of ZnCl_2 with NH_3 , followed by reacting with glycerol to transform into zinc glycerolate, $\text{Zn}(\text{C}_3\text{H}_6\text{O}_3)$, and NH_4Cl . However, the catalytic performance of the sole $\text{Zn}(\text{C}_3\text{H}_6\text{O}_3)$ was determined to be considerably inferior to that of ZnCl_2 . Upon combining the employment of NH_4Cl , the activity could be greatly enhanced, indicating that the key catalytic active sites for glycerolysis of glycerol with urea were $\text{Zn}(\text{C}_3\text{H}_6\text{O}_3)$ and NH_4Cl together. As depicted in Scheme 4(b), NH_4Cl functioned to activate glycerol whereas $\text{Zn}(\text{C}_3\text{H}_6\text{O}_3)$ played the role in activating urea.

The homogeneous catalysts, polymeric glycerolate complexes of zinc (ZMG) and cobalt (CMG) containing a coordinated isocyanate ligand were successfully developed for the production of GC from the mixtures of glycerol and urea [44]. By analyzing the parameters of reaction temperature, time, and glycerol to urea molar ratios, the optimized reaction conditions for achieving a high GC yield of 83% were 5 wt% ZMG catalyst dosage referred to glycerol at 140°C for 7 h, and glycerol to urea molar ratio of 1:1.5. More importantly, as illustrated in Scheme 5, the proposed reaction mechanism shows that the polymeric glycerolate structure firstly breaks down by the reaction with urea, affording the vital intermediate complex involving a coordinated isocyanate complex. Then, the rearrangement of intermediate isocyanate ligand would generate a carbamate derivative which in turn could reversibly be replaced through cyclizing glycerol into GC. Meanwhile, this would also regenerate the metal monoglycerolate catalyst and the release of ammonia gas under vacuum conditions, accordingly.

By a coprecipitation manner at room temperature, zinc-aluminum hydrotalcite-like composite (Zn-Al-SO_4), comprising sulfate anion with a molar ratio of 3, was developed and employed for preparing GC in one-pot [45]. To determine the optimal parameters, the effects of reaction temperature, time, the molar ratio of glycerol to urea, and dosage of catalyst were investigated in detail. It was found that the synthesis of

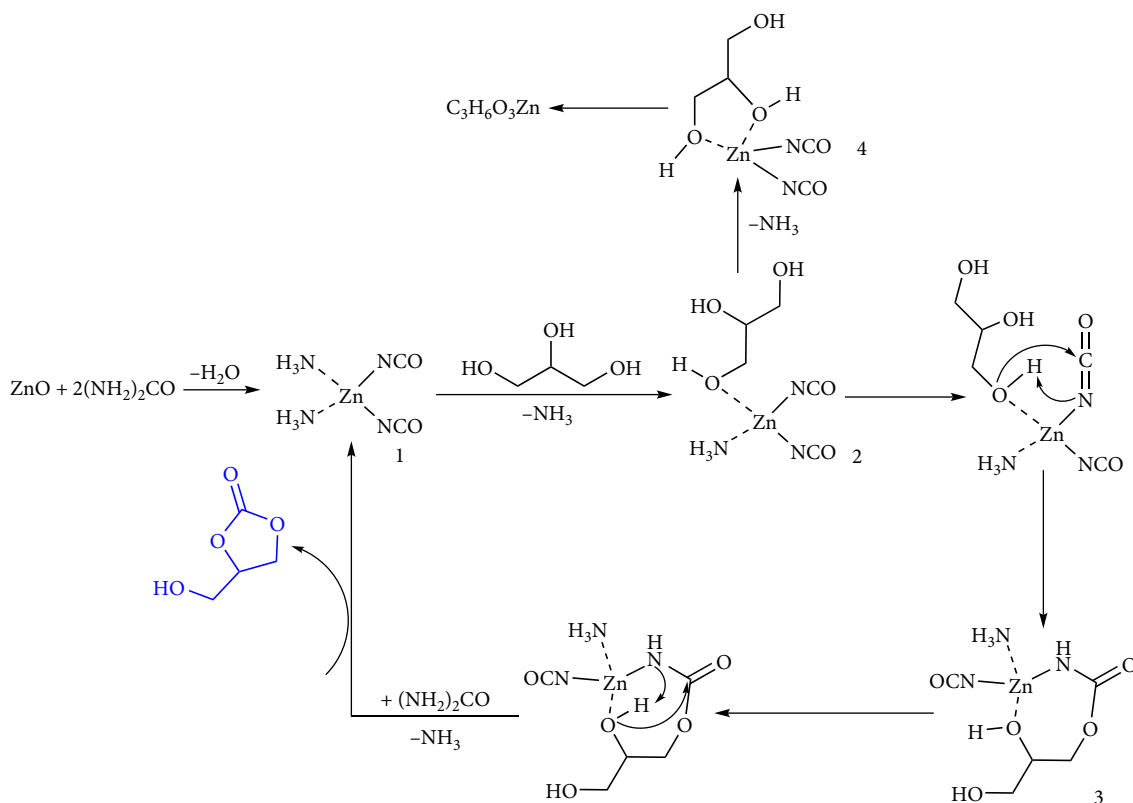


SCHEME 5: Reaction mechanism of glycerolysis of glycerol and urea using ZMG catalyst.

GC could be better conducted using the heterogeneous catalysts bearing an appropriate acidity. Accordingly, the maximum GC yield (92.8%) was determined at 140°C for 4 h using the Zn-Al-SO₄ catalysts with an amount ratio of 3.5 wt%, and 5 wt% stoichiometric excess of urea. Furthermore, the as-prepared catalytic material was found to be insoluble in both the reactants and GC product, wherein enables Zn-Al-SO₄ catalysts to substitute the difficult commercial ZnO or ZnSO₄ catalysts of nonreusable property, to some extent. Interestingly, by deeply investigating the Zn-containing solid catalysts (zinc oxide, smectite, hydrotalcite) along with several inorganic zinc salts for GC synthesis from glycerol and urea proceeded under solvent-free reaction conditions at 130°C, the homogeneous but not heterogeneous catalytic behavior was discovered [46]. The constituent Zn species was found to be dissolved into the liquid phase even for the solid catalysts because of the action of both glycerol and urea, and the GC yield was determined to be correlated with the amount of zinc species leached into the liquid phase with a single relationship. As depicted in Scheme 6, based on the consequences of the reactions carried out under different reaction conditions and the detection of the liquid phase after the reaction by Fourier transform infrared spectroscopy (FT-IR), the possibly active Zn species were determined to be a complex of a Zn atom coordinated with N=C=O. In fact, derived from this study, the dissolved Zn species were the active sites for the glycerolysis of glycerol and urea, which have the same structure irrespective of the parent solid catalysts employed.

To further develop the environmentally friendly catalytic protocols for GC synthesis from glycerol and urea, heterogeneous catalysts of environmental value synthesized by an important preparation stratagem should be considered first and foremost. Motivated by the residue-free and solvent-free synthetic manner that can fabricate the hierarchical nano-scaled catalyst dispersed on microparticles [47–51], the hierarchical nano-scaled Co₃O₄/ZnO composites wherein CoO

(40–50 nm) were hierarchically dispersed on the ZnO microscale particles (0.2–1 μm) were synthesized by a very fast, easy and eco-friendly (no solvent, no surfactant, no residue) dry nanodispersion procedure. Importantly, this room-temperature-prepared material could bring about a clear interaction between Co₃O₄ and ZnO oxides, endowing an excellent catalytic activity (69% conversion and close to 100% selectivity) in the transformation of sustainable resources as the glycerolysis of glycerol with urea at mild condition (140°C for 4 h) [52]. More importantly, Raman spectroscopy evidenced the essence of the interphase oxides reaction whereas the formation of the spinel phase, ZnCo₂O₄, upon thermal treated at a high temperature of 400°C was the active species. A novel porous ZnO was manufactured by the calcination method using Zn glycerolate platelets as raw materials which were derived from a glycerol approach, and was used for GC production via glycerol carbonylation with urea [53]. Interestingly, the as-prepared catalyst displayed a porous and irregular morphology along with a proper acid-base property, thus affording the highest GC yield of 85.97% under the optimized reaction conditions of 5.0 wt% catalyst amount, 1:1.5 molar ratio of glycerol to urea at 140°C within 6 h. Interestingly, in contrast to [46], the porous ZnO was also found to maintain its original catalytic performance during 5 recycles, indicating its active, recyclable, and environmentally friendly nature in industrial settings. Zn-Al mixed oxides were synthesized through the coprecipitation or the hydrothermal manner and were employed for GC production by glycerolysis of glycerol with urea [54]. According to the physicochemical property investigated, the coprecipitation-prepared Zn-Al mixed-oxides exhibited the better catalytic performance for GC synthesis than that of the hydrothermal-prepared ones. However, Shin et al. made three important contributions to ZnAl mixed oxides used in synthesizing GC from glycerol and urea, especially focusing on the detailed structure-function relationships [55–57]. ZnO and ZnAl mixed oxides (ZnAlO) were

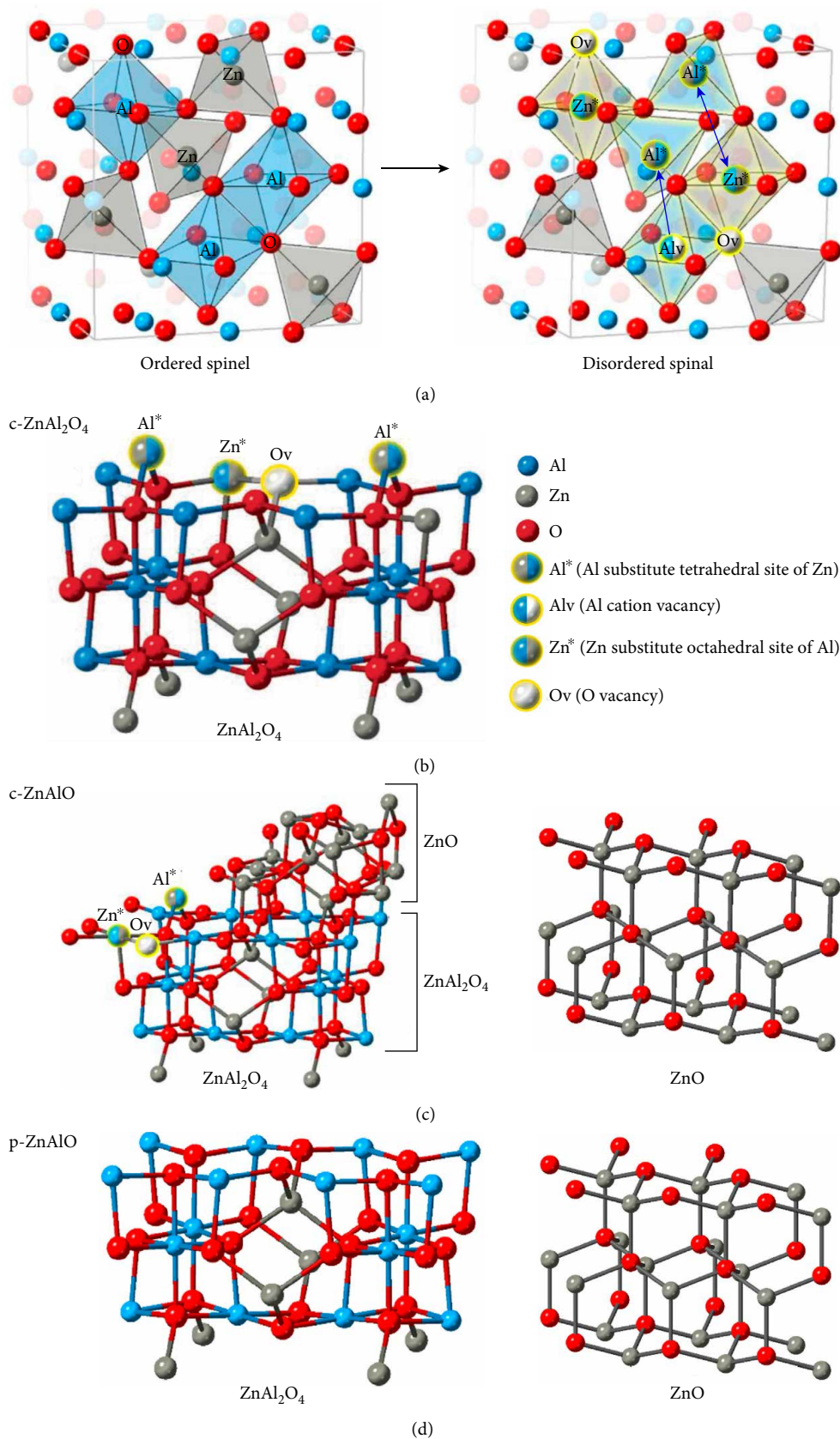


SCHEME 6: The possible reaction mechanism for GC synthesis from glycerol and urea using Zn-containing catalyst.

developed and used in glycerol carbonylation with urea, aiming to investigate the Zn-phase-dependent catalysis in detail [56]. It was found that the ZnAlO catalyst showed higher selectivity and yield of GC than those of ZnO catalyst. In detail, due to the reaction between Zn NCO complex and glycerol, the formed zinc glycerolate (ZnGly) in the solid phase lowered the GC selectivity accordingly. Alternatively, by using the ZnAlO catalyst, the Zn isocyanate (NCO) complexes formed were dominant up to 2 h in both liquid and solid phases. For recent research, they continued to investigate the effect of the disordered ZnAl₂O₄ spinel structure on GC production from glycerol and urea using pure ZnAl₂O₄ (c-ZnAl₂O₄), ZnAl mixed oxides (c-ZnAlO) synthesized by a citrate complex manner, and ZnAl physically mixed oxides (p-ZnAlO) [57]. As demonstrated in detail in Scheme 7, the disordered bulk ZnAl₂O₄ phase could generate the disordered sites on the catalysts surface: Zn²⁺ cations were substituted by Al³⁺ cations at the tetrahedral sites, and the surface oxygen vacancy corresponding to the Zn²⁺ cations substituting for Al³⁺ cations at the octahedral sites. Accordingly, the disordered sites of AlO₄ and oxygen vacancy of the partially inverted ZnAl₂O₄ spinel structure produced high surface acidity for c-ZnAlO and c-ZnAl₂O₄. c-ZnAlO showed the best catalytic activity because of the higher ability to absorb the liquid Zn NCO complexes. Based on these reports, the solid Zn NCO complex was determined to primarily generate GC, whereas the liquid Zn NCO complex generated both GC and ZnGly.

It is worth mentioning that the acid–base nature of heterogeneous catalytic materials and their surface areas play a

decisive role in GC production efficiency [58, 59]. With respect to this, the novel zinc–tin composite oxide was prepared using three different means including coprecipitation, solid-state, and evaporation methods, and investigated in producing GC [60]. According to the relevant characterization techniques, three components of Zn₂SnO₄, ZnO, and SnO₂ were determined as the main composite oxides. Upon testing in the selective transformation of glycerol and urea into GC, Zn–Sn mixed oxides synthesized by the coprecipitation manner (ZnSn–CoPre) performed better when compared to the others. Basically, the superior excellent catalytic performance of ZnSn–CoPre should be principally attributed to the existence of higher contents of acid and base active sites. Accordingly, the Zn/Sn molar ratio of 2:1 calcined at 600°C showed a high 96.0% glycerol conversion and 99.6% selectivity towards GC at 155°C for 4 h. More importantly, the negligible marginal decrease in catalytic activity was also found when recycled for four times. Moreover, it is anticipated that the combinations of porous structures and metal oxides could potentially endow a better catalytic activity [33, 61]. Interestingly, by using an ingenious heterometallic metal-organic framework (MOF)-templated preparation method of chemical transformation at 350°C, the highly porous nanocage composite consisting well-joined Co₃O₄ and ZnO nanocrystal was triumphantly manufactured and used for GC synthesis from glycerol and urea [62]. Consequently, the as-prepared Co₅₀Zn₅₀-350 catalyst showed a significantly improved catalytic activity in terms of the high yield of GC over 85.2% and 91% GC selectivity, which were superior to those of most solid catalysts. The excellent catalyst



SCHEME 7: Lattice structure of (a) ordered and disordered spinel ZnAl₂O₄ phase, (b) c-ZnAl₂O₄, (c) c-ZnAlO, and (d) p-ZnAlO [57]. Reproduced from Ref. [57] with permission, Copyright 2019 Elsevier.

TABLE 1: Catalytic glycerolysis of urea to GC using zinc-based catalyst.

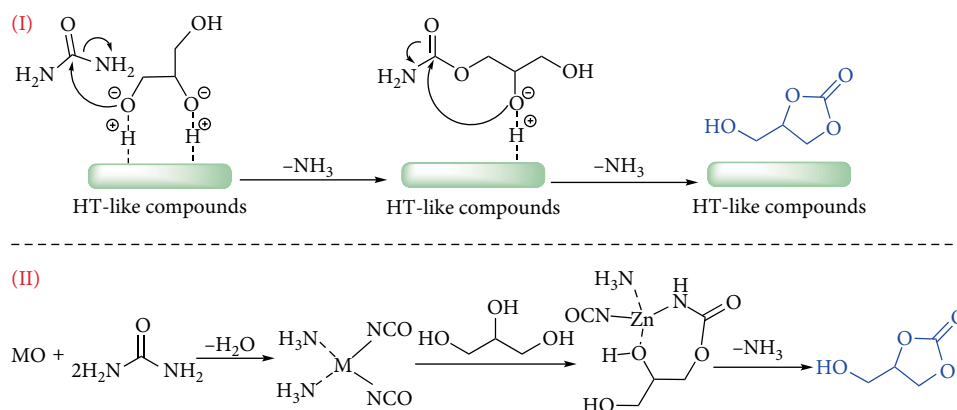
Entry	Catalyst	Acid amount (mmol/g)	Base amount (mmol/g)	Reaction conditions	Yield of GC (%)	Ref.
1	ZnCl ₂	- ^a	- ^a	150°C, 2 h	80.2	[43]
2	ZMG	- ^a	- ^a	140°C, 7 h	83	[44]
3	Zn-Al-SO ₄	1.58	- ^a	140°C, 4 h	92.8	[45]
4	HT(Zn/Al)	- ^a	- ^a	130°C, 3 h	65.6	[46]
5	Co ₃ O ₄ /ZnO	- ^a	- ^a	140°C, 4 h	69	[52]
6	Porous ZnO	Integrated area, 5414	Integrated area, 4042	140°C, 6 h	85.97	[53]
7	Zn-Al-O	3.43	2.76	160°C, 5 h	82.4	[54]
8	Zn ₆ Al ₄	0.342	0.274	140°C, 3 h	73	[55]
9	ZnAlO	0.375	0.383	140°C, 3 h	68	[56]
10	ZnAl ₂ O ₄	0.687	0.287	140°C, 3 h	58	[57]
11	ZnSn-CoPre	0.268	0.061	155°C, 4 h	95.6	[60]
12	Co ₅₀ Zn ₅₀ -350	- ^a	- ^a	150°C, 3 h	85.2	[62]
13	Zn/MCM-41(im)	0.02054	1.61776	145°C, 5 h	73.5	[63]
14	5% Zn/MCM-41	0.5254	0.6177	140°C, 5 h	83	[64]
15	Zn-HY-3	2.64	- ^a	150°C, 3 h	93	[65]
16	Zn ₁ TPA	2.677	- ^a	140°C, 4 h	68.8	[66]
17	ZnSO ₄	- ^a	- ^a	150°C, 100 min, micro-wave irradiation (600 W)	93.7	[81]

^aNot reported.

performance should be attributed to (a) the abundant active species and remarkable mass transfer of the substrates afforded by the as-synthesized nanocages containing massive pores and (2) the more efficient catalytic roles derived from the establishment of Co₃O₄/ZnO hetero-interfaces. Unfortunately, the relevant recyclability was not presented.

As mentioned above, the immobilization of active zinc sites onto porous carriers is of significance for achieving high GC yield. With regard to this, Zn impregnated onto mesoporous MCM-41 support catalyst, Zn/MCM-41(im), was successfully developed and investigated the acid-base sites' roles on GC yield in detail [63]. Thanks to its high surface area of 692 m² g⁻¹, well-dispersed ZnO phase onto the mesoporous framework of MCM-41, and good balanced acid (which activates urea molecules, 0.020 mmol g⁻¹) with basic sites (which activates the glycerol, 1.61 mmol g⁻¹), 75% glycerol conversion and 98% selectivity of GC were determined. Similarly, immobilizing ZnO catalyst onto the different acid carriers (MCM-41, SBA-15, SiO₂, Al₂O₃, ZrO₂, and s-ZrO₂) (5% Zn/MCM-41, 83% GC yield at 140°C in 5 h) [64], Zn-exchanged zeolites including Zn-MOR, Zn-ZSM-5, Zn-beta, and Zn-FAU (Zn-HY-3, 93% GC yield at 150°C for 3 h) [65], activated red mud-supported Zn/Al oxide catalysts (50% Zn/Al-ARM, 58.1% GC yield at 140°C within 5 h) were also reported for efficient transformation of glycerol and urea into GC with relative good yields. Zinc exchanged heteropoly tungstate (Zn_xTPA) catalysts were successfully developed and evaluated for selective carbonylation of glycerol with urea to manufacture GC [66]. It was determined that the catalytic performance of Zn_xTPA was mainly decided by the exchangeable Zn²⁺ ions that were loaded in the secondary structure of heteropoly tungstate. Exchange of protons of TPA with Zn²⁺ ions could generate acid Lewis and Bronsted sites, simultaneously. Under the reaction temperature of 140°C and reaction time of 4 h, 68.8% GC yield was achieved by using Zn₁TPA catalyst.

Normally, the glycerolysis of urea has to be operated under a vacuum condition or a sweeping gas to eliminate the by-product ammonia, to shift the chemical equilibrium towards the products [67]. Moreover, to our knowledge, previous works on the glycerolysis of urea have been performed in batch operation making it difficult to be applied to industrial-scale [40, 68, 69]. Therefore, it is of high importance to develop a new procedure to prepare GC through the carbonylation of glycerol with urea at atmospheric pressure and continuous operation. With the aim of reducing the by-product NH₃ that shifts the thermodynamic chemical equilibrium, the combing of the reaction and separation units in a single reactive distillation column process was developed accordingly [70]. Through this promising process of reactive distillation, the optimal design and operating variables for GC production were no rectifying stage, 3 reactive stage, 3 stripping stages, reflux ratio of 2, and reboiler heat duty of 15 kW for each glycerol and urea feed flow rate of 100 mol/h, giving a high 90.0% GC yield and 100% purity of GC. Moreover, compared to the traditional *in vacuo* manner, reactive distillation improved the glycerol conversion of 29.1% and saved in energy consumption by 37.1%, accordingly. Importantly, the interesting microwave irradiation technology has been developed and employed in various procedures, like chemical reaction [71, 72], material synthesis [73], nanotechnology [74] and biochemical processes [75, 76]. It is noteworthy that microwave would improve the product yield and shorten the reaction time in producing carbonates from CO₂ and epoxide [77], NaHCO₃ and olefins [78], CO and diols [79], and polycarbonates from open-ring polymerization of trimethylene carbonate [80]. Han et al. performed important research in the synthesis of GC from glycerol and urea with and without the microwave irradiation condition [81]. By using ZnSO₄ as the catalyst, the glycerolysis reaction could efficiently proceed with the assistance of microwave, and the high GC yield reached



SCHEME 8: Proposed mechanism for GC production from glycerol and urea using HT.

TABLE 2: Catalytic glycerolysis of urea to GC using magnesium-based catalyst.

Entry	Catalyst	Acid amount (mmol/g)	Base amount (mmol/g)	Reaction conditions	Yield of GC (%)	Ref.
1	MgO	- ^a	- ^a	140°C, 5 h	70 ^b	[82]
2	Combustion synthesized MgO	0.69	0.73	150 °C, 6 h	71	[91]
3	2.5 wt% Au-MgO	- ^a	- ^a	150°C, 4 h	73	[95]
4	Au-Pd-MgO	- ^a	- ^a	150°C, 4 h	67	[96]
5	HT(Mg/Zn/Al)	- ^a	- ^a	130°C, 3 h	83.7	[97]
6	Mg-Al-Zr	0.119	0.261	140°C, 3 h	87.8	[98]

^aNot reported. ^bGlycerol conversion.

93.7%. It could be believed that this green and effective process will show a promising prospect in GC production application.

2.2. Reaction with Magnesium-Based Catalyst. As shown in Table 2, magnesium-based catalysts also perform well in GC production from glycerol and urea. Three catalysts involving ZnO/Zeolite, PbO/Zeolite, and MgO were investigated for biodiesel synthesis from *Jatropha* oil, and the highest biodiesel yield using ZnO/zeolite reached 93.8 %. However, for the utilization of biodiesel byproduct glycerol, MgO as a catalyst was found to perform better than ZnO for the production of GC via urea-glycerol [82]. Nearly 70% glycerol conversion for MgO at 140°C within 5 h could be presented, which was higher than that of ZnO with 60% glycerol conversion. Generally, various protocols for the manufacture of nanocrystalline metal oxides such as inert gas condensation, laser ablation, chemical vapor deposition, sputtering, molecular beam epitaxy, coprecipitation [83], sol-gel process [84], thermal decomposition of nitrates and carbonates [85], and combustion synthesis [86–90] have been reported. Particularly, combustion synthesis was proven to improve the activity, shape selectivity, and to generate more active sites for acid and base catalysts. An eco-friendly manner has been reported in the selective conversion of glycerol and urea to GC using MgO that was prepared by the combustion method with glycerol as fuel [91]. Up to 71% glycerol conversion with 100% selectivity was determined by using the as-prepared MgO catalyst at 150°C for 6 h. In addition, the recoverable and reusable characters of the MgO catalyst during the consecutive reactions could also be found.

Gold (Au) has attracted great attention because of its catalytic activity serving as the homogeneous and heterogeneous catalysis [92]. Especially, gold was proven to perform well in the selective oxidize glycerol to glyceric acid in aqueous solution [93], and selective solvent-free oxidation of alcohols [94]. More importantly, gold could also serve as an active Lewis acidic catalyst upon being suitably immobilized on the advisable oxides. Therefore, it is of great interest to design the supported gold catalyst for GC synthesis from glycerol and urea. By using a simple impregnation method, the Au immobilized on the supports of titania, carbon, niobium oxide, zinc oxide, and magnesium oxide was successfully developed and tested in GC synthesis [95]. It was reported that the most active catalyst was the 2.5 wt% Au deposited on MgO followed by calcined at 400°C, showing 73% yield of GC at 150°C which were superior to that of homogenous zinc sulfate salts. As evidenced in this report, the promotion of the intramolecular cyclization of the carbamate intermediate to generate GC was the key role. More importantly, the catalyst could maintain its catalytic reactivity even after 10 recycles. After this research, bimetallic gold and palladium nanoparticles were further supported on MgO and utilized as the efficient catalytic material in promoting the synthesis of GC using urea and glycerol as feedstocks [96]. Through both of the sol immobilization and impregnation manners, high dispersions of the vibrant metals could be obtained. Interestingly, the MgO partly underwent transformations into magnesium carbonate upon reaction since the little impact on reactivity was found.

The Mg-Al hydrotalcite catalyst was investigated in GC production, and the hydrotalcite-like compounds containing Mg, Zn, and Al metals showed an excellent catalytic performance [97]. Consequently, 89.8% conversion of glycerol and 93.2% selectivity for GC were presented under 130°C for 3 h by using HT(Mg/Zn/Al) catalyst. Furthermore, the proposed reaction mechanism realized with two routes promoted by hydrotalcite-like compounds is depicted in Scheme 8. As reported in this research, Route I was deemed as the possible heterogeneous mechanism. Firstly, a bidentate ligand was formed through the coordination of glycerol with HT *via* hydrogen bond, wherein the oxygen atoms would be activated. The oxygen of the primary alcohol attacked the carbonyl carbon of urea that might generate NH₃. Afterward, the oxygen of the secondary hydroxyl group further attacked the carbonyl carbon through the intramolecular transesterification, which is supported because of the stable five-member cycle structure. The second NH₃ was also produced and GC would be detached from the surface of HT. Route II should be a plausible homogeneous mechanism. Initially, the metal complex was generated, wherein the two NH₃ from urea were weakly coordinated. Then, one of the coordinated NH₃ was exchanged with glycerol, leading to the intermediate to which glycerol interacted with the metal centers by their oxygen. Followed by this, the interacting hydroxyl groups of glycerol captured the adjacent isocyanate groups. Finally, the coordinated carbamate groups would be converted into GC by intracyclization, releasing NH₃ and the catalytic active ingredients. After that, a sequence of Mg-Al hydrotalcite-like (HTL) catalysts doped with Zr bearing the mesoporous structures upon under heat treatment were also developed and employed for GC production from glycerol and urea [98]. As a result, the well-balanced surface acid and base active sites of the catalyst with $Zr^{4+}:(Al^{3+} + Zr^{4+}) = 0.3$ demonstrated the highest 87.8% yield of GC at 140°C within 3 h.

2.3. Reaction with Tungsten-Based Catalyst. In Table 3, tungsten-based catalysts also show interesting works regarding GC synthesis. A series of tungsten (W)-tin (Sn) mixed oxides with varied mole ratios were synthesized using the coprecipitation process and evaluated for GC production from glycerol and urea [99]. Sn-W catalyst with a 2:1 molar ratio calcined at 500°C showed the best catalytic performance in terms of 52% of glycerol conversion with >95% GC selectivity. Similarly, different WO₃ contents supported on SnO₂ catalytic materials were prepared and employed for GC synthesis [100]. *In situ* Raman technology revealed the existence of isolated monomers and polymeric species of WO₃. Accordingly, the glycerol conversion and selectivity were found to be depended on the well-dispersed amorphous WO₃ which in turn was related to the acidity of the catalysts. The catalyst with 5 wt% WO₃ on SnO₂ calcined at 500°C for 4 h brought about the high dispersions of larger contents of strong acid active sites, giving 85.4% selectivity towards GC at 140°C in 4 h. Following up these valuable studies, tungsten oxide species supported on titania catalysts (100% selectivity for GC, 140°C in 4 h) [101], silicotungstates impregnated into MCM-41 (77% selectivity for GC, 150°C in 8 h) [102], silicotungstates anchored to large

pore zeolite H β (75% selectivity for GC, 150°C in 8 h) [103] were also developed for GC synthesis with authentic and acceptable results.

Early transition metals formed in the metal-oxygen clusters of their highest oxidation state, also known as polyoxometalates (HPA), are a group of important inorganic compounds showing large potential application prospects in catalysis [104–106]. Due to their compelling features of strong Brønsted acidity, multistage redox activity, and remarkable thermal and hydrolytic stability, polyoxometalates have been applied in acid and oxidation catalysis. In addition, the catalytic properties can be tuned by proton exchange of the HPA with various metal or alkali ions. For instance, the proton exchange of tungstophosphoric acid with Cs⁺ generated a strong acid in comparison with the pristine acid [107]. In a similar manner, exchanging the protons of the HPA with Sn²⁺ and Al³⁺ resulted in the Lewis acidic sites [108–110]. In this context, samarium-exchanged heteropoly tungstate catalyst (Sm_xTPA) was designed and used for GC synthesis, aiming to enhance the acidity thereby increasing GC yield accordingly [111]. The activity of the catalysts was determined to depend on the Lewis and Brønsted acidity that came from the Sm contents, and the partially exchanged Sm_xTPA catalysts exhibited the best performance, due to the higher amounts of Lewis acid sites. As illustrated in Scheme 9, the plausible reaction mechanism using Sm_xTPA catalysts was also proposed by the authors. In short, Lewis and Brønsted acidic sites activated the carbonyl group of urea, the conjugate base, and the hydroxyl group of the glycerol. Cs-exchanged heteropolyacid catalysts functionalized with Sn, Sn-CsPW (83% GC selectivity, 140°C) [112], tantalum exchanged tungstophosphoric acid catalysts (100% GC selectivity, 140°C) [113] were also developed for GC synthesis from glycerol and urea.

2.4. Reaction with Functional Ionic Liquid. Using ionic liquids (ILs) as catalysts to produce GC via urea-glycerol is also presented in Table 4. Acidic, basic, and neutral ILs were adopted as the catalysts for GC production through glycerolysis of glycerol with urea [114]. Interestingly, neutral ILs were determined to perform best while acid and base ILs exhibited the poor activity. The well-balanced acid–base properties of the neutral ILs that were derived from the synergistic effect of the cations and anions, were treated as the key role in obtaining high GC yield. The positively charged cation activated urea by attracting the electronegative oxygen of the carbonyl group of urea, which was similar to that of Lewis acid site. On the other hand, the negatively charged anion attracted the proton of glycerol at the same time. Moreover, the IL catalysts could be recycled and reused at least 5 times without significant activity decrease. Nonetheless, the obvious difficulty in separation and recovery will limit ILs to be applied on a large scale [115]. Of particular interest is to immobilize ILs through heterogenization of ILs onto suitable solid supports like organic polymers and inorganic materials [116, 117]. By the reaction of imidazole with alkoxyated Merrifield peptide resin (MPR), ILs incorporated on the MPR catalysts MPR-ILs were successfully developed [118]. MPR-ILs with longer alkyl chains and fewer sterically hindered counteranions demonstrated better catalytic performance in GC synthesis, giving 80.9%

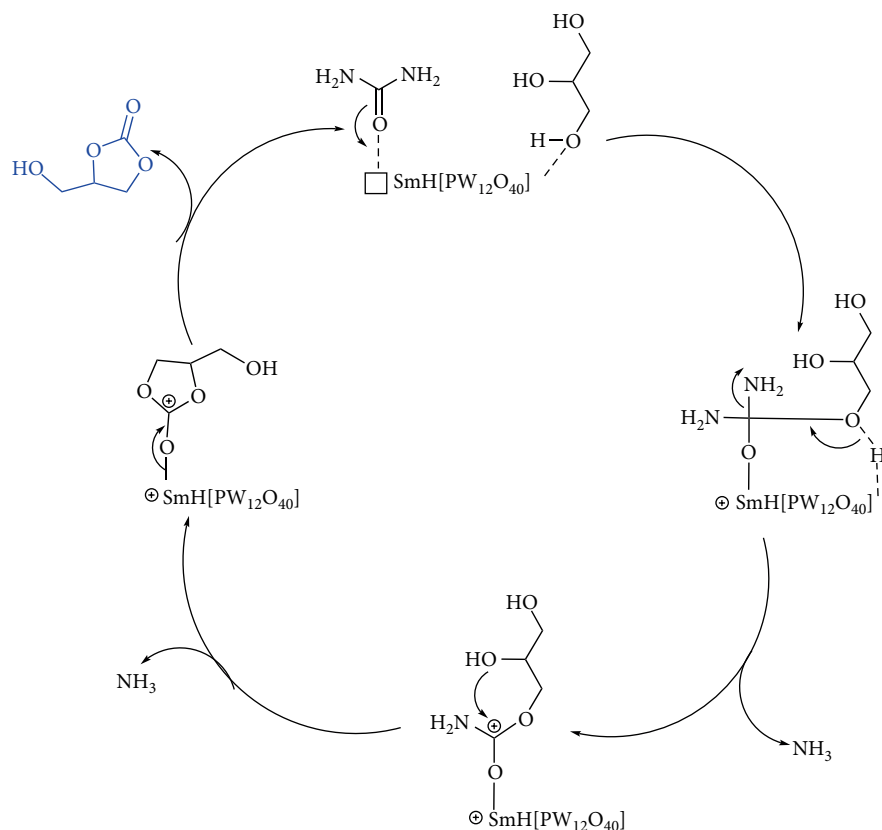
SCHEME 9: Proposed reaction mechanism using Sm_xTPA catalyst.

TABLE 3: Catalytic glycerolysis of urea to GC using tungsten-based catalyst.

Entry	Catalyst	Acid amount (mmol/g)	Base amount (mmol/g)	Reaction conditions	Yield of GC (%)	Ref.
1	SW21	0.472	- ^a	140°C, 4 h	49.4	[99]
2	5 wt% WO ₃ -SnO ₂	0.271	- ^a	140°C, 4 h	85.4 ^b	[100]
3	15% WO ₃ /TiO ₂	0.554	- ^a	140°C, 4 h	73	[101]
4	30% SiW ₁₂ /MCM-41	3.4	- ^a	150°C, 8 h	77 ^b	[102]
5	SiW-Hβ	3.5	- ^a	150°C, 8 h	75 ^b	[103]
6	Sm _{0.66} TPA	1.726	- ^a	140°C, 4 h	85 ^b	[111]
7	Sn-CsPW	528	- ^a	140°C, 4 h	85 ^b	[112]
8	Ta _{0.4} TPA	0.128	- ^a	140°C, 4 h	100 ^b	[113]

^aNot reported. ^bGC selectivity.

selectivity of GC at 140°C for 3 h. High temperature, high degree of vacuum and the addition of co-catalyst of ZnO could improve the GC selectivity to 100%.

As depicted in Scheme 10, the Zn-containing ILS immobilized on the polymeric support polystyrene (PS) PS-(Im)₂ZnBr₂, was successfully developed and employed for GC production [119]. PS-(Im)₂ZnBr₂ was prepared through two steps: (1) bis[1-(2-hydroxyethyl)imidazolium]zinc bromide (HEIm)₂ZnBr₂ was synthesized via metal insertion; (2) the (HEIm)₂ZnBr₂ was incorporated into MPR by alkoxylation. Under the reaction temperature of 140°C for 6 h, 72.3% selectivity of GC was achieved using (HEIm)₂ZnBr₂ catalyst because of its well-balanced acid-base properties. In addition, the as-synthesized catalyst could be reused for 4

times with 70.1% selectivity of GC. Various quaternary ammonium salts (QX) ILS supported onto montmorillonite clay (Q-MMT) were manufactured through the ion-exchange method between the tetra-alkyl ammonium salts and ions in the clay interlayer [120]. By the detailed investigations, the Q-MMTs were found to perform well in the selective synthesis of GC from glycerol and urea, showing 80% selectivity of GC at 145°C within 3 h. More importantly, Q-MMT could be easily reused during 4 recycles without any significant activity decrease. Similar to [119], polystyrene immobilized with different kinds (Cu, Mg, Zn) of metal-containing imidazolium salt [PS-(Im)₂MX₂] catalysts were prepared and used for GC production [121]. Among different metal-containing PS-(Im)₂MBr₂ catalytic materials, the yield of GC increased

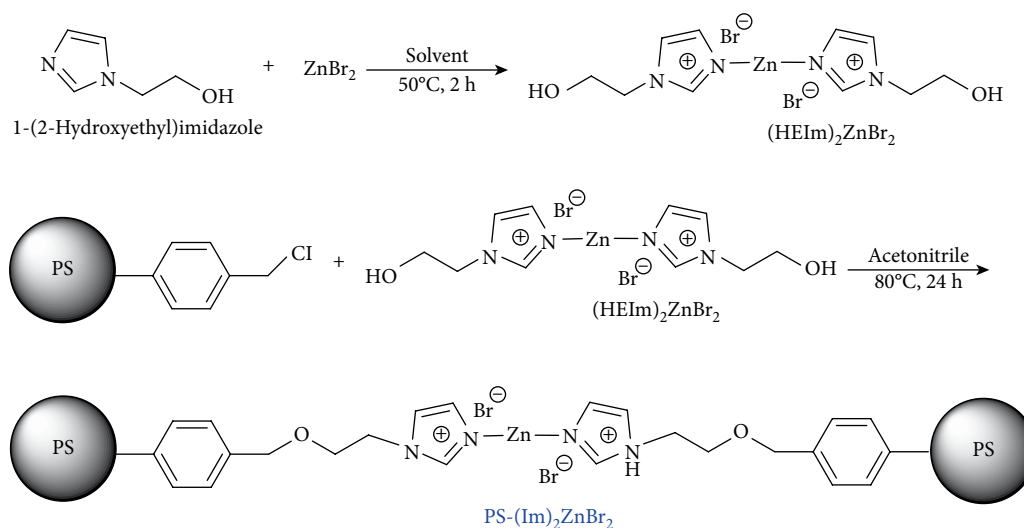
SCHEME 10: The synthetic route for PS-(Im)₂ZnBr₂.

TABLE 4: Catalytic glycerolysis of urea to GC using ILS-based catalyst.

Entry	Catalyst	Acid amount (mmol/g)	Base amount (mmol/g)	Reaction conditions	Yield of GC (%)	Ref.
1	MPR[pmim][Cl] + ZnO	- ^a	- ^a	140°C, 3 h	78.6	[118]
2	PS-(Im) ₂ ZnBr ₂	0.165	0.66	140°C, 6 h	72.3 ^b	[119]
3	Q-MMTs	- ^a	0.97	145°C, 3 h	80 ^b	[120]
4	[PS-(Im) ₂ MX ₂]	6.01	6.67	140°C, 6 h	60.3	[121]

^aNot reported. ^bGC selectivity.

TABLE 5: Catalytic glycerolysis of urea to GC with other catalysts.

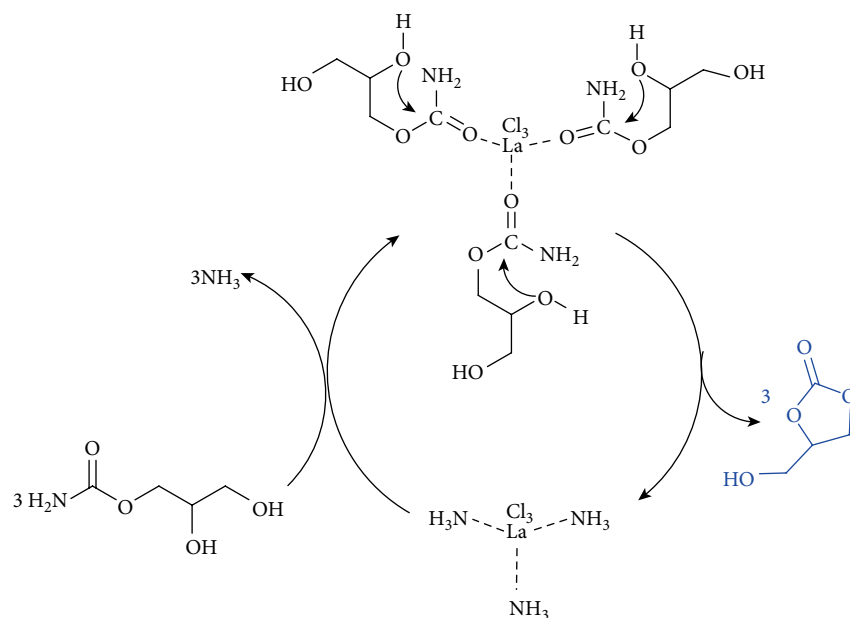
Entry	Catalyst	Acid amount (mmol/g)	Base amount (mmol/g)	Reaction conditions	Yield of GC (%)	Ref
1	La ₂ O ₃	- ^a	0.108	140°C, 1 h	90	[124]
2	La ₂ Cu _{0.5} Fe _{0.5} O ₄	Qualitatively, not quantitatively	Qualitatively, not quantitatively	150°C, 4 h	81.9 ^b	[125]
3	Cu ¹ Mn	Qualitatively, not quantitatively	Qualitatively, not quantitatively	140°C, 6 h	99.1 ^b	[126]
4	AlCaMO	Qualitatively, not quantitatively	Qualitatively, not quantitatively	145°C, 5 h	88 ^b	[68]
5	γ-Zirconium phosphate	1.49	0.18	135°C, 3 h	100 ^b	[127]
6	Waste boiler ash	- ^a	7.1	150°C, 4 h	84.3	[128]
7	Gypsum-based catalyst	0.12	- ^a	150°C, 4 h	83.6	[129]

^aNot reported. ^bGC selectivity.

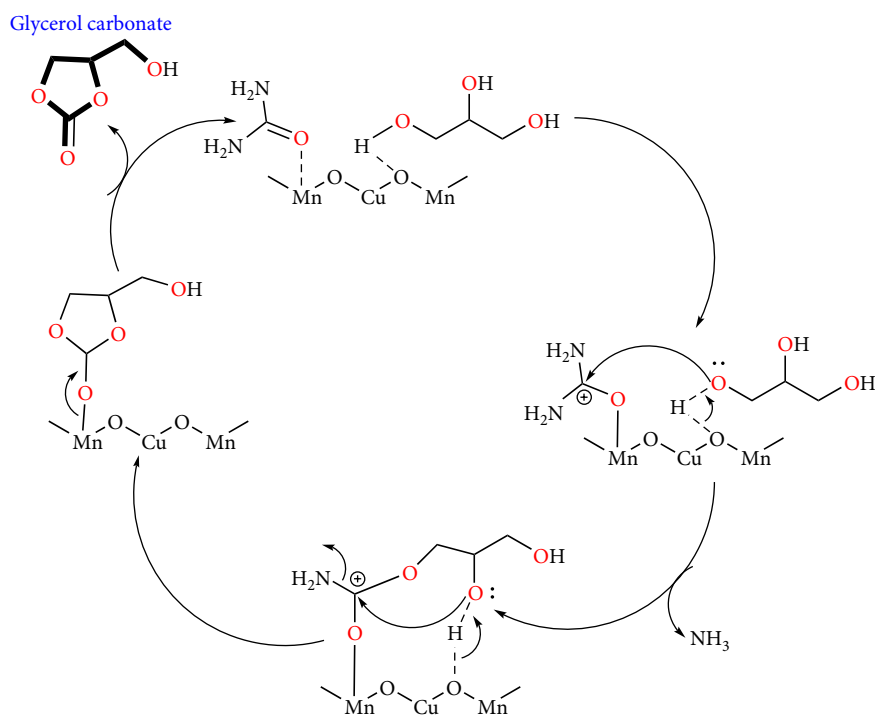
Cu < Mg < Zn, which follows the order of acid-base balance of the catalysts wherein Zn-containing catalyst presented better acid/base ratio than those of Mg and Cu.

2.5. Reaction with Other Catalysts. In addition to the catalytic materials mentioned above, some other catalysts illustrated in Table 5 also demonstrate good results for GC production. Commercial polymeric cation resin Amberlyst-15 was used for GC synthesis from urea and glycerol with 62.76% glycerol conversion at 120°C for 5 h [122]. Three lanthanum

(La) based catalysts were also developed in the synthesis of GC, including LaCl₃ [123], La₂O₃ [124], and La₂Cu_{0.5}Fe_{0.5}O₄ [125]. For LaCl₃ catalyzed glycerolysis, the key reaction mechanism is illustrated in Scheme 11. Three oxygen atoms of the carbonyl group of the 2,3-dihydroxypropyl carbamate (HPC) coordinated with La³⁺ of LaCl₃; the electrons of C–N groups redistributed wherein the proton transferred onto the carbon atom leading to the carbocation and nitrogen anion and favoring the intramolecular nucleophilic attack of adjoining hydroxyl group. Consequently, there was the



SCHEME 11: The proposed reaction mechanism for GC synthesis from HPC over LaCl_3 .



SCHEME 12: The possible reaction mechanism for the synthesis of GC by Cu-Mn composites.

important bond between the electrophilic carbonyl carbon of complex and the lone pair of electrons of oxygen of the hydroxyl group. Meanwhile, the hydrogen protons broke away from the hydroxyl groups united with the amino groups leaving from the formed complexes. At last, the final product GC was generated by the broke of C-N bond and the new formation of C-O bond, while the corresponding complex $\text{La}(\text{NH}_3)_3\text{Cl}_3$ could be also regenerated. In addition, due to

the strong nucleophilicity of HPC and the release of NH_3 , the catalytic circulation was finished accompanied by the substitution of NH_3 molecules with HPC.

Cu-Mn composite oxides prepared by coprecipitation method (99.1% GC selectivity, 140°C for 6 h) [126], Al/Ca-mixed oxide (AlCaMO) derived from hydrotalcite (88% GC selectivity, 145°C for 5 h) [68], γ -zirconium phosphate (100% GC selectivity, 135°C for 3 h) [127], waste boiler

ash (90.1% GC selectivity, 150°C for 4 h) [128], and gypsum-based catalyst (90.1% GC selectivity, 150°C for 4 h) [129] were developed for GC manufacture. For the GC production catalyzed by Cu–Mn composites (Scheme 12), $\text{Cu}_{1.4}\text{Mn}_{1.6}\text{O}_4$ crystal phase was determined as the active species in glycerolysis. It was reported that this phase can efficiently afford acid sites of Mn^{4+} and lattice oxygen O^{2-} base sites, and the presence of the $\text{Mn}^{4+}\text{--O}^{2-}$ Lewis acid-base pairs would facilitate the transformation of glycerol and urea into GC, consequently.

3. Conclusion

The effective production of glycerol carbonate (GC) has been arousing great attention because of its importance in lessening excessive glycerol in biodiesel process as well as its potential industrial application prospect, especially in the polymer area. Selective catalytic valorization of glycerol with urea by carbonylation into GC has been shown to be the most promising in terms of the reactants available and reaction environmental benefits. Although the sole acidic or basic site can exhibit some reactivity for glycerolysis of urea, the achievement of high conversion and high selectivity of GC using recyclable heterogeneous catalysts remains a great challenge. On the one hand, the strong interaction between urea and acid sites will lead to the deactivation of active sites for further procedures. On the other hand, the undesirable reactions like decarbonylation and 2-HPC dehydration can be accelerated by the base and the GC selectivity will decrease due to the overmuch amounts of basic sites. Consequently, the catalysts with the appropriate balance of active acidic and basic sites will be favorable for the synthesis of GC from glycerol and urea. Moreover, the energetical development of heterogeneous catalysts of high-performance for this process demonstrates the powerful and significant strategic and environmental benefits.

It is noteworthy that the catalytic activity of catalysts can be considerably improved by the rationale regulating their compositions and surface structures. As anticipated, the joint application of pore formation such as well-defined ordered channel frameworks and catalytic active species combinations would potentially enable the promising environmentally friendly catalysts. In addition, insightful reaction mechanisms and structure-property understanding will also help us to design the appropriate catalysts for GC manufacture from glycerol and urea. Finally, the proper employment of the relevant auxiliaries to boost catalytic activity and product selectivities, such as heating modes of microwave irradiation and reactive distillation replacing the traditional in vacuo system are also suggested.

Conflicts of Interest

The authors have no conflicting interests to declare.

Acknowledgments

This work was financially supported by the Natural Science Foundation of China (21576059, 21666008, 21908033), Chinese Scholarship Council (CSC, No. 201706670012), Fok Ying Tong Education Foundation (161030), and Guizhou Science & Technology Foundation ([2018]1037).

References

- [1] Y. Zhu, C. Romain, and C. K. Williams, "Sustainable polymers from renewable resources," *Nature*, vol. 540, no. 7633, pp. 354–362, 2016.
- [2] H. Zhang, Y. Hu, L. Qi, J. He, H. Li, and S. Yang, "Chemocatalytic production of lactates from biomass-derived sugars," *International Journal of Chemical Engineering*, vol. 2018, Article ID 7617685, 18 pages, 2018.
- [3] X. Yao, H. Liu, and C. Li, "Development of eco-friendly soy meal adhesives enhanced by ethylene glycol diglycidyl ether," *Advances in Polymer Technology*, vol. 2019, Article ID 8697047, 7 pages, 2019.
- [4] Q. Yu, Y. Wang, X. Cao et al., "One-step formation of chondrocytes through direct reprogramming via polysaccharide-based gene delivery," *Advances in Polymer Technology*, vol. 2019, Article ID 7632873, 12 pages, 2019.
- [5] J. R. Jambeck, R. Geyer, C. Wilcox et al., "Plastic waste inputs from land into the ocean," *Science*, vol. 347, no. 6223, pp. 768–771, 2015.
- [6] H. Zhang, H. Pan, and S. Yang, "Upgrading of cellulose to biofuels and chemicals with acidic nanocatalysts," *Current Nanoscience*, vol. 13, no. 5, pp. 513–527, 2017.
- [7] H. Zhang, H. Li, H. Pan et al., "Magnetically recyclable acidic polymeric ionic liquids decorated with hydrophobic regulators as highly efficient and stable catalysts for biodiesel production," *Applied Energy*, vol. 223, pp. 416–429, 2018.
- [8] J. C. Philp, A. Bartsev, R. J. Ritchie, M. A. Baucher, and K. Guy, "Bioplastics science from a policy vantage point," *New Biotechnology*, vol. 30, no. 6, pp. 635–646, 2013.
- [9] F. Ferdosian, Y. Zhang, Z. Yuan, M. Anderson, and C. C. Xu, "Curing kinetics and mechanical properties of bio-based epoxy composites comprising lignin-based epoxy resins," *European Polymer Journal*, vol. 82, pp. 153–165, 2016.
- [10] B. Li, S. Feng, H. Niasar et al., "Preparation and characterization of bark-derived phenol formaldehyde foams," *RSC Advances*, vol. 6, no. 47, pp. 40975–40981, 2016.
- [11] H. Zhang and M. W. Grinstaff, "Recent advances in glycerol polymers: chemistry and biomedical applications," *Macromolecular Rapid Communications*, vol. 35, no. 22, pp. 1906–1924, 2014.
- [12] C. H. C. Zhou, J. N. Beltramini, Y. X. Fan, and G. M. Lu, "Chemoselective catalytic conversion of glycerol as a biorenewable source to valuable commodity chemicals," *Chemical Society Reviews*, vol. 37, no. 3, pp. 527–549, 2008.
- [13] H. Pan, X. Liu, H. Zhang, K. Yang, S. Huang, and S. Yang, "Multi- SO_3H functionalized mesoporous polymeric acid catalyst for biodiesel production and fructose-to-biodiesel

- additive conversion,” *Renewable Energy*, vol. 107, pp. 245–252, 2017.
- [14] H. Zhang, H. Li, H. Pan, A. Wang, C. C. Xu, and S. Yang, “Magnetically recyclable basic polymeric ionic liquids for efficient transesterification of *Firmiana platanifolia* L.f. oil into biodiesel,” *Energy Conversion and Management*, vol. 153, pp. 462–472, 2017.
- [15] H. Li, Z. Fang, R. L. Smith Jr, and S. Yang, “Efficient valorization of biomass to biofuels with bifunctional solid catalytic materials,” *Progress in Energy and Combustion Science*, vol. 55, pp. 98–194, 2016.
- [16] H. Zhang, H. Li, Y. Hu, K. T. V. Rao, C. C. Xu, and S. Yang, “Advances in production of bio-based ester fuels with heterogeneous bifunctional catalysts,” *Renewable and Sustainable Energy Reviews*, vol. 114, p. 109296, 2019.
- [17] K. L. Yang, S. Huang, H. Pan, H. Zhang, X. F. Liu, and S. Yang, “Polyoxometalate-MgF₂ hybrids as heterogeneous solid acid catalysts for efficient biodiesel production,” *RSC Advances*, vol. 7, no. 53, pp. 33335–33343, 2017.
- [18] H. Zhang, H. Li, C. Xu, and S. Yang, “Heterogeneously chemo/enzyme-functionalized porous polymeric catalysts of high-performance for efficient biodiesel production,” *ACS Catalysis*, vol. 9, pp. 10990–11029, 2019.
- [19] A. Wang, H. Li, H. Zhang, H. Pan, and S. Yang, “Efficient catalytic production of biodiesel with acid-base bifunctional rod-like Ca-B oxides by the sol-gel approach,” *Materials*, vol. 12, no. 1, p. 83, 2019.
- [20] C. H. Zhou, H. Zhao, D. S. Tong, L. M. Wu, and W. H. Yu, “Recent advances in catalytic conversion of glycerol,” *Catalysis Reviews*, vol. 55, no. 4, pp. 369–453, 2013.
- [21] H. Pan, H. Li, H. Zhang, A. Wang, D. Jin, and S. Yang, “Effective production of biodiesel from nonedible oil using facile synthesis of imidazolium salts-based Brønsted-Lewis solid acid and co-solvent,” *Energy Conversion and Management*, vol. 166, pp. 534–544, 2018.
- [22] M. Sulewski and W. Urbaniak, “Utilization of biodiesel by-products,” *Czysta Energia*, vol. 2011, no. 6, pp. 27–28, 2011.
- [23] W. J. Choi, “Glycerol-based biorefinery for fuels and chemicals,” *Recent Patents on Biotechnology*, vol. 2, no. 3, pp. 173–180, 2008.
- [24] Y. Wu, X. Song, F. Cai, and G. Xiao, “Synthesis of glycerol carbonate from glycerol and diethyl carbonate over Ce-NiO catalyst: the role of multiphase Ni,” *Journal of Alloys and Compounds*, vol. 720, pp. 360–368, 2017.
- [25] Y. Wu, X. Song, J. Zhang et al., “Synthesis of glycerol carbonate from glycerol and diethyl carbonate over CeO₂-CdO catalyst: the role of Ce⁴⁺ doped into CdO lattice,” *Journal of the Taiwan Institute of Chemical Engineers*, vol. 87, pp. 131–139, 2018.
- [26] M. R. Monteiro, C. L. Kugelmeier, R. S. Pinheiro, M. O. Batalha, and A. da Silva César, “Glycerol from biodiesel production: technological paths for sustainability,” *Renewable and Sustainable Energy Reviews*, vol. 88, pp. 109–122, 2018.
- [27] A. Cornejo, I. Barrio, M. Campoy, J. Lázaro, and B. Navarrete, “Oxygenated fuel additives from glycerol valorization. Main production pathways and effects on fuel properties and engine performance: a critical review,” *Renewable and Sustainable Energy Reviews*, vol. 79, pp. 1400–1413, 2017.
- [28] N. T. Nguyen and Y. Demirel, “A novel biodiesel and glycerol carbonate production plant,” *International Journal of Chemical Reactor Engineering*, vol. 9, no. 1, 2011.
- [29] U. Nda-Umar, I. Ramli, Y. Taufiq-Yap, and E. Muhamad, “An overview of recent research in the conversion of glycerol into biofuels, fuel additives and other bio-based chemicals,” *Catalysts*, vol. 9, no. 1, p. 15, 2019.
- [30] A. Dibenedetto, A. Angelini, M. Aresta, J. Ethiraj, C. Fragale, and F. Nocito, “Converting wastes into added value products: from glycerol to glycerol carbonate, glycidol and epichlorohydrin using environmentally friendly synthetic routes,” *Tetrahedron*, vol. 67, no. 6, pp. 1308–1313, 2011.
- [31] A. Wang, H. Li, H. Pan et al., “Efficient and green production of biodiesel catalyzed by recyclable biomass-derived magnetic acids,” *Fuel Processing Technology*, vol. 181, pp. 259–267, 2018.
- [32] G. Rokicki, P. Rakoczy, P. Parzuchowski, and M. Sobiecki, “Hyperbranched aliphatic polyethers obtained from environmentally benign monomer: glycerol carbonate,” *Green Chemistry*, vol. 7, no. 7, pp. 529–539, 2005.
- [33] H. Pan, H. Li, H. Zhang, A. Wang, and S. Yang, “Acidic ionic liquid-functionalized mesoporous melamine-formaldehyde polymer as heterogeneous catalyst for biodiesel production,” *Fuel*, vol. 239, pp. 886–895, 2019.
- [34] J. Hu, Y. Gu, Z. Guan et al., “An efficient palladium catalyst system for the oxidative carbonylation of glycerol to glycerol carbonate,” *ChemSusChem*, vol. 4, no. 12, pp. 1767–1772, 2011.
- [35] J. Hu, J. Li, Y. Gu et al., “Oxidative carbonylation of glycerol to glycerol carbonate catalyzed by PdCl₂(phen)/KI,” *Applied Catalysis A: General*, vol. 386, no. 1–2, pp. 188–193, 2010.
- [36] J. George, Y. Patel, S. M. Pillai, and P. Munshi, “Methanol assisted selective formation of 1, 2-glycerol carbonate from glycerol and carbon dioxide using “Bu₂SnO as a catalyst,” *Journal of Molecular Catalysis A: Chemical*, vol. 304, no. 1–2, pp. 1–7, 2009.
- [37] C. Vieville, J. Yoo, S. Pelet, and Z. Mouloungui, “Synthesis of glycerol carbonate by direct carbonation of glycerol in supercritical CO₂ in the presence of zeolites and ion exchange resins,” *Catalysis Letters*, vol. 56, no. 4, pp. 245–247, 1998.
- [38] Y. Hu, B. Zhou, and C. Wang, “Inert C-H bond transformations enabled by organometallic manganese catalysis,” *Accounts of Chemical Research*, vol. 51, no. 3, pp. 816–827, 2018.
- [39] J. He, H. Li, S. Saravanamurugan, and S. Yang, “Catalytic upgrading of biomass-derived sugars with acidic nanoporous materials: structural role in carbon-chain length variation,” *ChemSusChem*, vol. 12, no. 2, pp. 347–378, 2019.
- [40] A. Behr, J. Eilting, K. Irawadi, J. Leschinski, and F. Lindner, “Improved utilisation of renewable resources: new important derivatives of glycerol,” *Green Chemistry*, vol. 10, no. 1, pp. 13–30, 2008.
- [41] M. Pagliaro, R. Ciriminna, H. Kimura, M. Rossi, and C. Della Pina, “From glycerol to value-added products,” *Angewandte Chemie International Edition*, vol. 46, no. 24, pp. 4434–4440, 2007.
- [42] T. Sakakura, J. C. Choi, and H. Yasuda, “Transformation of carbon dioxide,” *Chemical Reviews*, vol. 107, no. 6, pp. 2365–2387, 2007.
- [43] J. H. Park, J. S. Choi, S. K. Woo et al., “Isolation and characterization of intermediate catalytic species in the Zn-catalyzed glycerolysis of urea,” *Applied Catalysis A: General*, vol. 433, pp. 35–40, 2012.
- [44] T. W. Turney, A. Patti, W. Gates, U. Shaheen, and S. Kulasegaram, “Formation of glycerol carbonate from glycerol and urea catalysed by metal monoglycerolates,” *Green Chemistry*, vol. 15, no. 7, pp. 1925–1931, 2013.

- [45] E. E. Oprescu, E. Stepan, P. Rosca, A. Radu, and C. E. Enascuta, "Synthesis of glycerol carbonate over hydrotalcite catalyst," *Revista de Chimie*, vol. 63, pp. 621–625, 2012.
- [46] S. Fujita, Y. Yamanishi, and M. Arai, "Synthesis of glycerol carbonate from glycerol and urea using zinc-containing solid catalysts: a homogeneous reaction," *Journal of Catalysis*, vol. 297, pp. 137–141, 2013.
- [47] M. S. Martín-González, M. A. García, I. Lorite et al., "A solid-state electrochemical reaction as the origin of magnetism at oxide nanoparticle interfaces," *Journal of the Electrochemical Society*, vol. 157, no. 3, pp. E31–E35, 2010.
- [48] A. Brinkman, M. Huijben, M. van Zalk et al., "Magnetic effects at the interface between nonmagnetic oxides," *Nature Materials*, vol. 6, no. 7, pp. 493–496, 2007.
- [49] F. Bruno, J. Garcia-Barriocanal, M. Torija et al., "Effects of interface states on the transport properties of all-oxide $\text{La}_{0.8}\text{Sr}_{0.2}\text{CoO}_3/\text{SrTi}_{0.99}\text{Nb}_{0.01}\text{O}_3$ *p-n* heterojunctions," *Applied Physics Letters*, vol. 92, no. 8, p. 082106, 2008.
- [50] A. Quesada, M. A. Garcia, M. Andrés et al., "Ferromagnetism in bulk Co-Zn-O," *Journal of Applied Physics*, vol. 100, no. 11, p. 113909, 2006.
- [51] M. S. Martín-González, J. F. Fernández, F. Rubio-Marcos et al., "Insights into the room temperature magnetism of ZnO/ Co_3O_4 mixtures," *Journal of Applied Physics*, vol. 103, no. 8, p. 083905, 2008.
- [52] F. Rubio-Marcos, V. Calvino-Casilda, M. Banares, and J. Fernandez, "Novel hierarchical $\text{Co}_3\text{O}_4/\text{ZnO}$ mixtures by dry nanodispersion and their catalytic application in the carbonylation of glycerol," *Journal of Catalysis*, vol. 275, no. 2, pp. 288–293, 2010.
- [53] P. Zhang, L. Liu, M. Fan, Y. Dong, and P. Jiang, "The value-added utilization of glycerol for the synthesis of glycerol carbonate catalyzed with a novel porous ZnO catalyst," *RSC Advances*, vol. 6, no. 80, pp. 76223–76230, 2016.
- [54] Y. B. Ryu, J. S. Kim, K. H. Kim, Y. Kim, and M. S. Lee, "Synthesis of Zn/Al mixed-oxide catalyst for carbonylation of glycerol with urea," *Research on Chemical Intermediates*, vol. 42, no. 1, pp. 83–93, 2016.
- [55] H. Nguyen-Phu, C. Park, and E. W. Shin, "Dual catalysis over ZnAl mixed oxides in the glycerolysis of urea: homogeneous and heterogeneous reaction routes," *Applied Catalysis A: General*, vol. 552, pp. 1–10, 2018.
- [56] H. Nguyen-Phu and E. W. Shin, "Investigating time-dependent Zn species over Zn-based catalysts in glycerol carbonylation with urea and their roles in the reaction mechanism," *Applied Catalysis A: General*, vol. 561, pp. 28–40, 2018.
- [57] H. Nguyen-Phu and E. W. Shin, "Disordered structure of ZnAl_2O_4 phase and the formation of a Zn NCO complex in ZnAl mixed oxide catalysts for glycerol carbonylation with urea," *Journal of Catalysis*, vol. 373, pp. 147–160, 2019.
- [58] H. Li, X. Jiao, L. Li et al., "Synthesis of glycerol carbonate by direct carbonylation of glycerol with CO_2 over solid catalysts derived from Zn/Al/La and Zn/Al/La/M (M = Li, Mg, and Zr) hydrotalcites," *Catalysis Science & Technology*, vol. 5, no. 2, pp. 989–1005, 2015.
- [59] F. Rubio-Marcos, V. Calvino-Casilda, M. A. Banares, and J. F. Fernandez, "Control of the interphases formation degree in $\text{Co}_3\text{O}_4/\text{ZnO}$ catalysts," *ChemCatChem*, vol. 5, no. 6, pp. 1431–1440, 2013.
- [60] P. Manjunathan, R. Ravishankar, and G. V. Shanbhag, "Novel bifunctional Zn-Sn composite oxide catalyst for the selective synthesis of glycerol carbonate by carbonylation of glycerol with urea," *ChemCatChem*, vol. 8, no. 3, pp. 631–639, 2016.
- [61] X. Liu, H. Zhang, F. Chang, S. Huang, K. Yang, and S. Yang, "Catalytic transformations of organic compounds and biomass derivatives with functionalized metal-organic frameworks," *Current Organic Chemistry*, vol. 20, no. 7, pp. 761–776, 2016.
- [62] Y. Lü, Y. Jiang, Q. Zhou et al., "Heterometallic metal-organic framework-templated synthesis of porous $\text{Co}_3\text{O}_4/\text{ZnO}$ nanocage catalysts for the carbonylation of glycerol," *Journal of Solid State Chemistry*, vol. 256, pp. 93–100, 2017.
- [63] S. Kondawar, A. Potdar, and C. Rode, "Solvent-free carbonylation of glycerol with urea using metal loaded MCM-41 catalysts," *RSC Advances*, vol. 5, no. 21, pp. 16452–16460, 2015.
- [64] S. Kondawar, R. Mane, A. Vasishtha, S. More, S. Dhengale, and C. Rode, "Carbonylation of glycerol with urea to glycerol carbonate over supported Zn catalysts," *Applied Petrochemical Research*, vol. 7, no. 1, pp. 41–53, 2017.
- [65] V. S. Marakatti and A. B. Halgeri, "Metal ion-exchanged zeolites as highly active solid acid catalysts for the green synthesis of glycerol carbonate from glycerol," *RSC Advances*, vol. 5, no. 19, pp. 14286–14293, 2015.
- [66] K. Jagadeeswaraiyah, C. R. Kumar, P. S. Prasad, and N. Lingaiah, "Incorporation of Zn^{2+} ions into the secondary structure of heteropoly tungstate: catalytic efficiency for synthesis of glycerol carbonate from glycerol and urea," *Catalysis Science & Technology*, vol. 4, no. 9, pp. 2969–2977, 2014.
- [67] J. Li and T. Wang, "Coupling reaction and azeotropic distillation for the synthesis of glycerol carbonate from glycerol and dimethyl carbonate," *Chemical Engineering and Processing: Process Intensification*, vol. 49, no. 5, pp. 530–535, 2010.
- [68] M. J. Climent, A. Corma, P. De Frutos et al., "Chemicals from biomass: synthesis of glycerol carbonate by transesterification and carbonylation with urea with hydrotalcite catalysts. The role of acid–base pairs," *Journal of Catalysis*, vol. 269, no. 1, pp. 140–149, 2010.
- [69] C. Buchaly, P. Kreis, and A. Górak, "Hybrid separation processes—Combination of reactive distillation with membrane separation," *Chemical Engineering and Processing: Process Intensification*, vol. 46, no. 9, pp. 790–799, 2007.
- [70] N. Lertlukkanasuk, S. Phiyalaninmat, W. Kiatkittipong, A. Arpornwichanop, F. Aiouache, and S. Assabumrungrat, "Reactive distillation for synthesis of glycerol carbonate via glycerolysis of urea," *Chemical Engineering and Processing: Process Intensification*, vol. 70, pp. 103–109, 2013.
- [71] J. D. Moseley and C. O. Kappe, "A critical assessment of the greenness and energy efficiency of microwave-assisted organic synthesis," *Green Chemistry*, vol. 13, no. 4, pp. 794–806, 2011.
- [72] N. Kaur, "Applications of microwaves in the synthesis of polycyclic six-membered N, N-heterocycles," *Synthetic Communications*, vol. 45, no. 14, pp. 1599–1631, 2015.
- [73] N. A. Khan and S. H. Jhung, "Synthesis of metal-organic frameworks (MOFs) with microwave or ultrasound: rapid reaction, phase-selectivity, and size reduction," *Coordination Chemistry Reviews*, vol. 285, pp. 11–23, 2015.
- [74] M. G. Ma, J. F. Zhu, Y. J. Zhu, and R. C. Sun, "The microwave-assisted ionic-liquid method: a promising methodology in nanomaterials," *Chemistry—An Asian Journal*, vol. 9, no. 9, pp. 2378–2391, 2014.

- [75] D. D. Young, J. Nichols, R. M. Kelly, and A. Deiters, "Microwave activation of enzymatic catalysis," *Journal of the American Chemical Society*, vol. 130, no. 31, pp. 10048–10049, 2008.
- [76] W. Xiao, X. Zhang, X. Wang, W. Niu, and L. Han, "Rapid liquefaction of corn stover with microwave heating," *BioResources*, vol. 10, no. 3, pp. 4038–4047, 2015.
- [77] J. Tharun, G. Mathai, A. C. Kathalikkattil, R. Roshan, J. Y. Kwak, and D. W. Park, "Microwave-assisted synthesis of cyclic carbonates by a formic acid/KI catalytic system," *Green Chemistry*, vol. 15, no. 6, pp. 1673–1677, 2013.
- [78] X. Yang, J. Wu, X. Mao, T. F. Jamison, and T. A. Hatton, "Microwave assisted synthesis of cyclic carbonates from olefins with sodium bicarbonates as the C1 source," *Chemical Communications*, vol. 50, no. 24, pp. 3245–3248, 2014.
- [79] D. M. Pearson, N. R. Conley, and R. M. Waymouth, "Palladium-catalyzed carbonylation of diols to cyclic carbonates," *Advanced Synthesis & Catalysis*, vol. 353, no. 16, pp. 3007–3013, 2011.
- [80] L. Liao, C. Zhang, and S. Gong, "Rapid synthesis of poly(trimethylene carbonate) by microwave-assisted ring-opening polymerization," *European Polymer Journal*, vol. 43, no. 10, pp. 4289–4296, 2007.
- [81] L. Zhang, Z. Zhang, C. Wu et al., "Microwave assisted synthesis of glycerol carbonate from glycerol and urea," *Pure and Applied Chemistry*, vol. 90, no. 1, pp. 1–6, 2018.
- [82] D. Singh, A. Ganesh, and S. Mahajani, "Heterogeneous catalysis for biodiesel synthesis and valorization of glycerol," *Clean Technologies and Environmental Policy*, vol. 17, no. 4, pp. 1103–1110, 2015.
- [83] T. Lopez, P. Bosch, E. Ramos et al., "Synthesis and characterization of sol-gel hydrotalcites. Structure and texture," *Langmuir*, vol. 12, no. 1, pp. 189–192, 1996.
- [84] T. Yamaguchi, Y. Wang, M. Komatsu, and M. Ookawa, "Preparation of new solid bases derived from supported metal nitrates and carbonates," *Catalysis Surveys from Japan*, vol. 5, no. 2, pp. 81–89, 2002.
- [85] V. Montouillout, D. Massiot, A. Douy, and J. P. Coutures, "Characterization of MgAl₂O₄ precursor powders prepared by aqueous route," *Journal of the American Ceramic Society*, vol. 82, no. 12, pp. 3299–3304, 1999.
- [86] A. G. Merzhanov, "The chemistry of self-propagating high-temperature synthesis," *Journal of Materials Chemistry*, vol. 14, no. 12, pp. 1779–1786, 2004.
- [87] K. C. Patil, S. T. Aruna, and T. Mimani, "Combustion synthesis: an update," *Current Opinion in Solid State and Materials Science*, vol. 6, no. 6, pp. 507–512, 2002.
- [88] K. Deshpande, A. Mukasyan, and A. Varma, "Direct synthesis of iron oxide nanopowders by the combustion approach: reaction mechanism and properties," *Chemistry of Materials*, vol. 16, no. 24, pp. 4896–4904, 2004.
- [89] K. C. Patil, S. T. Aruna, and S. Ekambaram, "Combustion synthesis," *Current Opinion in Solid State and Materials Science*, vol. 2, no. 2, pp. 158–165, 1997.
- [90] G. D. Yadav, N. P. Ajgaonkar, and A. Varma, "Preparation of highly superacidic sulfated zirconia via combustion synthesis and its application in Pechmann condensation of resorcinol with ethyl acetoacetate," *Journal of Catalysis*, vol. 292, pp. 99–110, 2012.
- [91] G. P. Fernandes and G. D. Yadav, "Selective glycerolysis of urea to glycerol carbonate using combustion synthesized magnesium oxide as catalyst," *Catalysis Today*, vol. 309, pp. 153–160, 2018.
- [92] A. S. K. Hashmi and G. J. Hutchings, "Gold catalysis," *Angewandte Chemie International Edition*, vol. 45, no. 47, pp. 7896–7936, 2006.
- [93] F. Porta and L. Prati, "Selective oxidation of glycerol to sodium glycerate with gold-on-carbon catalyst: an insight into reaction selectivity," *Journal of Catalysis*, vol. 224, no. 2, pp. 397–403, 2004.
- [94] N. Dimitratos, J. A. Lopez-Sanchez, D. Morgan, A. Carley, L. Prati, and G. J. Hutchings, "Solvent free liquid phase oxidation of benzyl alcohol using Au supported catalysts prepared using a sol immobilization technique," *Catalysis Today*, vol. 122, no. 3-4, pp. 317–324, 2007.
- [95] C. Hammond, J. A. Lopez-Sanchez, M. H. Ab Rahim et al., "Synthesis of glycerol carbonate from glycerol and urea with gold-based catalysts," *Dalton Transactions*, vol. 40, no. 15, pp. 3927–3937, 2011.
- [96] M. H. Ab Rahim, Q. He, J. A. Lopez-Sanchez et al., "Gold, palladium and gold-palladium supported nanoparticles for the synthesis of glycerol carbonate from glycerol and urea," *Catalysis Science & Technology*, vol. 2, no. 9, pp. 1914–1924, 2012.
- [97] Y. Sun, X. Tong, Z. Wu, J. Liu, Y. Yan, and S. Xue, "A sustainable preparation of glycerol carbonate from glycerol and urea catalyzed by hydrotalcite-like solid catalysts," *Energy Technology*, vol. 2, no. 3, pp. 263–268, 2014.
- [98] D. Wang, X. Zhang, X. Cong, S. Liu, and D. Zhou, "Influence of Zr on the performance of Mg-Al catalysts via hydrotalcite-like precursors for the synthesis of glycerol carbonate from urea and glycerol," *Applied Catalysis A: General*, vol. 555, pp. 36–46, 2018.
- [99] K. Jagadeeswaraiyah, C. R. Kumar, P. S. Prasad, S. Loridant, and N. Lingaiah, "Synthesis of glycerol carbonate from glycerol and urea over tin-tungsten mixed oxide catalysts," *Applied Catalysis A: General*, vol. 469, pp. 165–172, 2014.
- [100] M. Srinivas, G. Raveendra, G. Parameswaram, P. S. Prasad, S. Loridant, and N. Lingaiah, "Understanding the surface and structural characteristics of tungsten oxide supported on tin oxide catalysts for the conversion of glycerol," *Journal of Chemical Sciences*, vol. 127, no. 5, pp. 897–908, 2015.
- [101] K. Jagadeeswaraiyah, C. R. Kumar, A. Rajashekar, A. Srivani, and N. Lingaiah, "The role of tungsten oxide species supported on titania catalysts for the synthesis of glycerol carbonate from glycerol and urea," *Catalysis Letters*, vol. 146, no. 3, pp. 692–700, 2016.
- [102] N. Narkhede and A. Patel, "Facile synthesis of glycerol carbonate via glycerolysis of urea catalysed by silicotungstates impregnated into MCM-41," *RSC Advances*, vol. 5, no. 65, pp. 52801–52808, 2015.
- [103] N. Narkhede and A. Patel, "Sustainable valorisation of glycerol via acetalization as well as carboxylation reactions over silicotungstates anchored to zeolite H β ," *Applied Catalysis A: General*, vol. 515, pp. 154–163, 2016.
- [104] I. V. Kozhevnikov, "Catalysis by heteropoly acids and multicomponent polyoxometalates in liquid-phase reactions," *Chemical Reviews*, vol. 98, no. 1, pp. 171–198, 1998.
- [105] N. Mizuno and M. Misono, "Heterogeneous catalysis," *Chemical Reviews*, vol. 98, no. 1, pp. 199–218, 1998.
- [106] E. F. Kozhevnikova, E. G. Derouane, and I. V. Kozhevnikov, "Heteropoly acid as a novel efficient catalyst for Fries rearrangement," *Chemical Communications*, vol. 11, pp. 1178–1179, 2002.
- [107] A. Corma, A. Martinez, and C. Martinez, "Acidic Cs⁺, NH₄⁺, and K⁺ salts of 12-tungstophosphoric acid as solid catalysts for

- isobutane/2-butene alkylation,” *Journal of Catalysis*, vol. 164, no. 2, pp. 422–432, 1996.
- [108] C. R. Kumar, K. V. Rao, P. S. Prasad, and N. Lingaiah, “Tin exchanged heteropoly tungstate: an efficient catalyst for benzylation of arenes with benzyl alcohol,” *Journal of Molecular Catalysis A: Chemical*, vol. 337, no. 1–2, pp. 17–24, 2011.
- [109] C. R. Kumar, P. S. Prasad, and N. Lingaiah, “Aluminium exchanged heteropoly tungstate supported on titania catalysts: the generation of Lewis acidity and its role for benzylation reaction,” *Journal of Molecular Catalysis A: Chemical*, vol. 350, no. 1–2, pp. 83–90, 2011.
- [110] K. M. Reddy, N. S. Babu, P. S. Prasad, and N. Lingaiah, “Aluminium-exchanged tungstophosphoric acid: an efficient catalyst for intermolecular hydroarylation of vinyl arenes,” *Catalysis Communications*, vol. 9, no. 15, pp. 2525–2531, 2008.
- [111] C. R. Kumar, K. Jagadeeswaraiyah, P. S. Prasad, and N. Lingaiah, “Samarium-exchanged heteropoly tungstate: an efficient solid acid catalyst for the synthesis of glycerol carbonate from glycerol and benzylation of anisole,” *ChemCatChem*, vol. 4, no. 9, pp. 1360–1367, 2012.
- [112] A. Srikanth, B. Viswanadham, V. P. Kumar, N. R. Anipindi, and K. V. Chary, “Synthesis and characterization of Cs-exchanged heteropolyacid catalysts functionalized with Sn for carbonolysis of glycerol to glycerol carbonate,” *Applied Petrochemical Research*, vol. 6, no. 2, pp. 145–153, 2016.
- [113] M. S. Babu, A. Srivani, G. Parameswaram, G. Veerabhadram, and N. Lingaiah, “Understanding the role of tantalum in heteropoly tungstate catalysts for the synthesis of glycerol carbonate from glycerol and urea,” *Catalysis Letters*, vol. 145, no. 9, pp. 1784–1791, 2015.
- [114] J. Chen, C. Wang, B. Dong et al., “Ionic liquids as eco-friendly catalysts for converting glycerol and urea into high value-added glycerol carbonate,” *Chinese Journal of Catalysis*, vol. 36, no. 3, pp. 336–343, 2015.
- [115] H. Zhang, H. Li, H. Pan et al., “Efficient production of biodiesel with promising fuel properties from *Koelreuteria integrifoliola* oil using a magnetically recyclable acidic ionic liquid,” *Energy Conversion and Management*, vol. 138, pp. 45–53, 2017.
- [116] M. Valkenberg, C. DeCastro, and W. Hölderich, “Immobilisation of ionic liquids on solid supports,” *Green Chemistry*, vol. 4, no. 2, pp. 88–93, 2002.
- [117] C. P. Mehnert, R. A. Cook, N. C. Dispenziere, and M. Afeworki, “Supported ionic liquid catalysis—A new concept for homogeneous hydroformylation catalysis,” *Journal of the American Chemical Society*, vol. 124, no. 44, pp. 12932–12933, 2002.
- [118] D. W. Kim, M. S. Park, M. Selvaraj, G. A. Park, S. D. Lee, and D. W. Park, “Catalytic performance of polymer-supported ionic liquids in the synthesis of glycerol carbonate from glycerol and urea,” *Research on Chemical Intermediates*, vol. 37, no. 9, pp. 1305–1312, 2011.
- [119] D. W. Kim, M. J. Kim, K. Roshith, M. I. Kim, J. Y. Kwak, and D. W. Park, “Comparative catalytic activity of supported ZnBr₂-containing ionic liquid catalysts for preparation of glycerol carbonate by glycerolysis of urea,” *Korean Journal of Chemical Engineering*, vol. 31, no. 6, pp. 972–980, 2014.
- [120] S. D. Lee, M. S. Park, D. W. Kim, I. Kim, and D. W. Park, “Catalytic performance of ion-exchanged montmorillonite with quaternary ammonium salts for the glycerolysis of urea,” *Catalysis Today*, vol. 232, pp. 127–133, 2014.
- [121] D. W. Kim, K. A. Park, M. J. Kim, D. H. Kang, J. G. Yang, and D. W. Park, “Synthesis of glycerol carbonate from urea and glycerol using polymer-supported metal containing ionic liquid catalysts,” *Applied Catalysis A: General*, vol. 473, pp. 31–40, 2014.
- [122] R. I. D. Suyatmo, H. Sulistyono, and W. B. Sediawan, “The synthesis of glycerol carbonate from biodiesel by product glycerol and urea over amberlyst 15,” *Jurnal Bahan Alam Terbarukan*, vol. 6, no. 2, pp. 143–149, 2017.
- [123] D. Wang, X. Zhang, C. Liu, and T. Cheng, “Synthesis of glycerol carbonate from glycerol and urea over lanthanum compounds,” *Reaction Kinetics, Mechanisms and Catalysis*, vol. 115, no. 2, pp. 597–609, 2015.
- [124] L. Wang, Y. Ma, Y. Wang, S. Liu, and Y. Deng, “Efficient synthesis of glycerol carbonate from glycerol and urea with lanthanum oxide as a solid base catalyst,” *Catalysis Communications*, vol. 12, no. 15, pp. 1458–1462, 2011.
- [125] J. Zhang and D. He, “Lanthanum-based mixed oxides for the synthesis of glycerol carbonate from glycerol and urea,” *Reaction Kinetics, Mechanisms and Catalysis*, vol. 113, no. 2, pp. 375–392, 2014.
- [126] W. Luo, L. Sun, Y. Yang et al., “Cu–Mn composite oxides: highly efficient and reusable acid–base catalysts for the carbonylation reaction of glycerol with urea,” *Catalysis Science & Technology*, vol. 8, no. 24, pp. 6468–6477, 2018.
- [127] M. Aresta, A. Dibenedetto, F. Nocito, and C. Ferragina, “Valorization of bio-glycerol: new catalytic materials for the synthesis of glycerol carbonate via glycerolysis of urea,” *Journal of Catalysis*, vol. 268, no. 1, pp. 106–114, 2009.
- [128] V. P. Indran, N. A. S. Zuhaimi, M. A. Deraman et al., “An accelerated route of glycerol carbonate formation from glycerol using waste boiler ash as catalyst,” *RSC Advances*, vol. 4, no. 48, pp. 25257–25267, 2014.
- [129] N. A. S. Zuhaimi, V. P. Indran, M. A. Deraman et al., “Reusable gypsum based catalyst for synthesis of glycerol carbonate from glycerol and urea,” *Applied Catalysis A: General*, vol. 502, pp. 312–319, 2015.

Research Article

Adsorption of Chelerythrine from *Toddalia asiatica* (L.) Lam. by ZSM-5

Yunlong Liu , Jie Guo , Zhuobing Xiao , Dazhao Peng , and Ke Song 

Key Laboratory of Forest Chemical Engineering of Hunan Province, Jishou University, Zhang Jiajie 427000, China

Correspondence should be addressed to Ke Song; kesong@jsu.edu.cn

Received 1 October 2019; Revised 25 November 2019; Accepted 27 November 2019; Published 3 January 2020

Guest Editor: Song Yang

Copyright © 2020 Yunlong Liu et al. This is an open access article distributed under the Creative Commons Attribution License, which permits unrestricted use, distribution, and reproduction in any medium, provided the original work is properly cited.

Separation and purification of active components from biomass by inorganic materials during the pretreatment process of hydrothermal conversion are studied in this work. The batch experiment results show that an initial solution pH of 6 favors chelerythrine adsorption, and the optimum adsorbent dosage is 2.0 g. The adsorption mechanism of ZSM-5 for chelerythrine is investigated by adsorption kinetics, isotherm adsorption models, and thermodynamics analysis. The results show that the kinetics data fit the pseudo-second-order model well ($R^2 = 0.9991$), and the intraparticle diffusion model has 3 diffusion stages, preliminarily indicating that chemisorption plays a major role in the adsorption process, and the sorption mechanism includes intraparticle, external, and boundary diffusion. The adsorption isotherms agree well with the Langmuir model, indicating the occurrence of monolayer molecular adsorption during the adsorption process. Meanwhile, the maximum adsorption capacity is 2.327, 2.072, and 1.877 mg/g at different temperatures (288 K, 298 K, and 308 K), respectively. The thermodynamic data demonstrate that the adsorption process is exothermic and spontaneous in nature. These observed results clearly confirm that ZSM-5 has potential superior properties for the enrichment and purification of alkaloids during the pretreatment of biomass.

1. Introduction

Biomass, as a renewable carbohydrate found in nature, is a promising alternative to petroleum resources for the production of fuels, carbon-based chemicals, and materials [1, 2]. The pretreatment process of biomass before transformation is particularly important owing to the presence of various active components (e.g., flavonoids and alkaloids) in biomass. Therefore, isolating and purifying the active components from the pretreatment process of biomass are of great significance. In particular, Chelerythrine (CHE) is a common alkaloid that is found in the pretreatment process of *Toddalia asiatica* (L.) Lam., *Celandine*, *Macleaya cordata*, et al. As shown in Figure 1, the molecular formula and molecular weight of CHE are $C_{21}H_{18}NO_4^+$ and 348.37, respectively [3]. CHE has been widely used as an insecticide because it is harmful to the nerves and heart as well as it may cause paralysis, cardio-inhibitory activity, and even death. Moreover, CHE has shown favorable anti-inflammatory, antitumor, and antiplaque activity, as well as SH-enzyme inhibition [4–6]. The extraction of CHE from renewable

biomass has received considerable attentions. Especially, *Toddalia asiatica* (L.) Lam. represents a better starting material to access CHE since *Toddalia asiatica* (L.) Lam. is easily available in nature and contains high amount of CHE. Therefore, it is very interesting to sustainably obtain CHE from *Toddalia asiatica* (L.) Lam. Furthermore, the residue after extraction can be used as a raw material for the production of value-added chemicals and biofuels, which enables the full utilization of *Toddalia asiatica* (L.) Lam. to be possible.

Many approaches, including resin adsorption [3, 7] and column chromatography [8–10], have been proposed to separate CHE from organic extracts. Although the two methods can achieve favorable CHE separation, the pretreatment and regeneration of the resin are complex and consume large quantities of reagents. Moreover, the high requirements for chromatographic equipment are not conducive to industrial applications. Therefore, developing a suitable carrier that is efficient and environmentally friendly for the enrichment and purification of alkaloids is necessary.

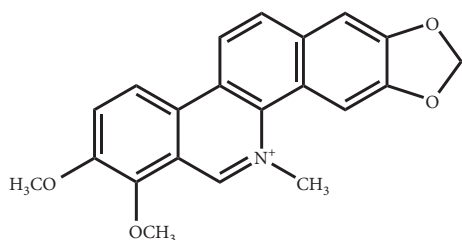


FIGURE 1: The molecular structure of chelerythrine.

Zeolite molecular sieves, as aluminosilicate crystals, are widely used in ion exchange [11], gas adsorption [12–14], and catalysis [15, 16] due to their regular structure, high surface area, and large inner pores. Since zeolites have holes connected by a plurality of pore canal structures with the same diameter, organic molecules with smaller size than the pore diameter can be adsorbed, while molecules with larger size than the pore diameter can be excluded, and then the organics can be separated. ZSM-5 is a typical representative of zeolite molecular sieves. It contains two types of channels: straight cylindrical channels with an oval cross section (channel size of 0.54 nm \times 0.56 nm) and Z-shaped channels with an approximately circular cross section (channel size of 0.52 nm \times 0.58 nm). Catalytic active centers and strong acid sites of ZSM-5 are concentrated at the intersections of the two channels [17–19]. In addition to its unique structural properties, the regeneration process of ZSM-5 is simple (calcinations in air for 4 h at the temperature of 873 K). Because of its mature technology and outstanding performance, ZSM-5 is widely used in the petrochemical industry [20], fine chemicals [21], environmental protection [22], and adsorption [23, 24].

The abundant acid sites and hydroxyl groups of ZSM-5 are expected to be obviously beneficial for adsorbing the target product. It is envisioned that ZSM-5 can efficiently purify target compounds from plant extracts on account of its unique structure. However, there are few reports on the application of molecular sieves in the field of separation and purification of plant active ingredients. Therefore, the adsorption of lycorine and galantamine by ZSM-5 molecular sieves from *Lycoris radiata* Herb. was reported in our previous study [24]; the results showed that the adsorption and desorption performance of lycorine and galantamine by molecular sieves was superior to those obtained using resin, which indicates that the application of molecular sieves in the separation and purification of active components from medicinal herb ingredients is promising. Therefore, to clarify the adsorption performance and mechanism of ZSM-5 towards active ingredients from plants, an alkaloid (CHE) was selected for use as a target and ZSM-5 was selected as an adsorbent. Batch experiments were used to study the optimal adsorption dose and initial solution pH. The adsorption kinetics, isotherms, and thermodynamics were investigated to explore the adsorption performance and mechanism of CHE on ZSM-5, and the technology described in this work is expected to be applied to isolate and purify the active ingredients from the pretreatment process of biomass.

2. Materials and Methods

2.1. Chemicals and Apparatus. Rhizomes of *Toddalia asiatica* (L.) Lam. were obtained from the planting base in Zhangjiajie. ZSM-5 (Na-type: Si/Al = 25, pore size 0.54 nm, surface area 380 m²/g, and pore volume more than 0.21 cm³/g) was purchased from Shanghai Saint Chemical Materials Co., Ltd., China. The ZSM-5 powder was placed in a muffle furnace, heated to 873 K at a heating rate of 2.4 K/min, and then calcined for 4 h at 873 K to remove organic impurities in the molecular sieves. A standard sample of CHE ($\geq 98\%$, mass purity) was purchased from Shanghai Aladdin Biochemical Technology Co., Ltd., China, and chromatographic-grade acetonitrile was purchased from Fisher Scientific International Inc., America. Hydrochloric acid, phosphoric acid, methanol, and ammonia were purchased from Shanghai Titan Technology Co., Ltd., China; all these chemicals were analytical-grade reagents.

An Agilent-1260 high-performance liquid chromatograph from Agilent Co., Ltd. (America), equipped with a Waters C₁₈ reverse-phase column (250 \times 4.6 mm, 5 μ m), was used for quantitative and qualitative analysis. An ultraviolet-visible spectrophotometer from SHIMADZU Co., Ltd., (Japan) equipped with a 1 cm cuvette was used for wavelength scanning. An FE20 laboratory pH meter from METTLER TOLEDO Co., Ltd., (Switzerland) was used for pH analysis.

2.2. Analytical Methodologies. A sample (2.0 g) of *Toddalia asiatica* (L.) Lam. powder was weighed accurately, infiltrated with 40 mL aqueous methanol (60%, v/v) for 30 min, and then ultrasonically extracted for 50 min at 333 K. The above process was repeated 3 times, and the extracted liquid was filtered. The filtrate was collected, concentrated to 20 mL under reduced pressure, and adjusted to pH = 6 with 1 mol/L HCl aqueous solution. The concentration of CHE in the extracts was analyzed by high-performance liquid chromatography (HPLC) under the following chromatographic conditions: a mixture of acetonitrile and 0.2% aqueous phosphoric acid (27 : 83 v/v) was used as the mobile phase with a flow rate of 1.0 mL/min, the temperature of the column was 303 K, and the UV detector was operated at 273 nm. The standard curves are shown in Figure 2. Prior to injection, the solutions were filtered through a 0.45 μ m membrane; the injection volume was 20 μ L.

2.3. Determination of Optimal Adsorption Capacity. The adsorption capacity is mainly determined by the initial solution pH and adsorbent dosage. Therefore, the adsorption of CHE was performed by using batch experiments with different initial solution pH values and adsorbent dosages. The pH was carefully adjusted by using 3.65 wt.% HCl and 3.5 wt.% NH₄OH to values in the range of 2 to 10. ZSM-5 with an adsorption dosage of 2.0–10.0 g was transferred to a conical flask containing 15 mL of extract. The two-factor sample solutions were vibrated for 24 h in a thermostatic shaker bath at a constant temperature of 288 K, and the

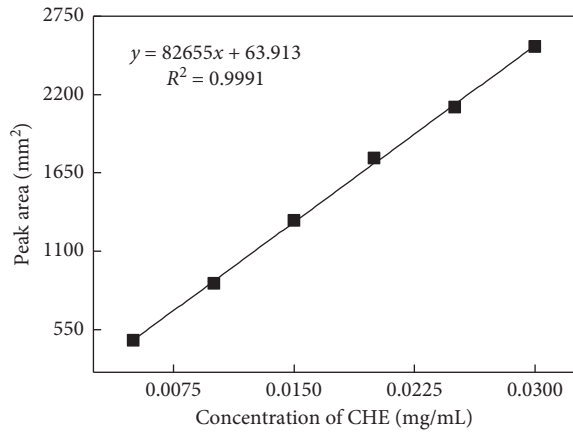


FIGURE 2: HPLC standard curve of CHE.

concentration of CHE in the solution was determined by using HPLC.

2.4. Adsorption Kinetics. A total of 2.0 g of ZSM-5 was added to 15 mL of solution at a concentration of 0.150 mg/mL, as described in Section 2.3, and the mixtures were stirred for 24 h by using a shaker at a constant temperature of 288 K. Samples were pipetted at certain intervals and determined by HPLC; the adsorption amount of ZSM-5 adsorbed at time t (q_t , mg/g) was calculated using the following equation:

$$q_t = \frac{(c_0 - c_t) \times V}{m}, \quad (1)$$

where c_0 and c_t (mg/mL) are the initial and time t concentrations of CHE in solution, respectively; V (mL) is the volume of the solution; and m (g) is the mass of ZSM-5.

2.5. Adsorption Isotherm. ZSM-5 (2.0 g) was added to 15 mL solutions containing CHE at concentrations from 0.050 to 0.500 mg/mL, and the mixtures were oscillated for 24 h until reaching adsorption equilibrium by using a shaker at constant temperatures of 288, 298, and 308 K. Known volumes of samples were pipetted and determined by HPLC. The equilibrium adsorption capacity (q_e , mg/g) of ZSM-5 was calculated using the following equation:

$$q_e = \frac{(c_0 - c_e) \times V}{m}, \quad (2)$$

where c_0 , V , m , and q_e are as described above and c_e (mg/mL) is the equilibrium concentration of ZSM-5.

3. Results and Discussion

3.1. HPLC Analysis. The CHE contents of the standard solutions, extracts, and eluents were determined by HPLC. HPLC spectra of CHE are shown in Figure 3. From Figure 3(a), the standard solution has a characteristic peak at 11.83 min, while Figure 3(b) shows a characteristic peak at 10.11 min for the extracts. Figure 3(c) shows the peak of CHE at 10.53 min, which was determined using 80% ethanol solution with a pH of 2 to elute ZSM-5 at adsorption

equilibrium. In addition, Figure 3(c) preliminarily proves that using ZSM-5 to enrich CHE from *Toddalia asiatica* (L.) Lam. is feasible.

3.2. Influence of pH. The hydrogen ion concentration is always considered one of the most important parameters in the adsorption process; it influences the surface binding sites or charges of the adsorbent and the degree of ionization/dissociation of CHE [25]. To study the influence of the initial solution pH on the adsorption of CHE, batch experiments at different pH values were carried out at 288 K with 15 mL of 0.150 mg/mL CHE and 2.0 g of adsorbent. Figure 4 shows that the adsorption capacity slightly increased with increasing initial pH and reached a maximum at pH 6. This trend occurred because at low pH, ether groups are protonated, which greatly weakens the binding capability between CHE and the active sites in molecular sieves. With further increases in pH, the adsorption capacity decreases sharply, mainly because of competitive adsorption; similar results have been shown in a previous study [26, 27].

3.3. Influence of Adsorbent Dosage. The influence of various amounts of ZSM-5 on adsorption capacity was studied in 15 mL of 0.15 mg/mL CHE methanol solution. The results are presented in Figure 5, which shows that the adsorption capacity decreases from 0.31 mg/g to 0.079 mg/g with an increase in adsorbent dosage from 2.0 g to 10.0 g due to the greater number of binding sites available. The adsorption rate increases substantially with increasing adsorbent dosage from 2.0 g to 6.0 g and increases slightly from 6.0 g to 10.0 g when CHE entirely occupies the available binding sites. Therefore, the amount of adsorbent was maintained at 2.0 g in the following experiments to optimize both the adsorption capacity and adsorption rate.

3.4. Adsorption Kinetics. The adsorption curves of ZSM-5 for CHE are plotted with adsorption capacity as the ordinate and time as the abscissa. As shown in Figure 6, the adsorption capacity increases rapidly during the initial 16 h and then gradually becomes flat until reaching equilibrium at 1.25 mg/g.

Adsorption kinetics models were used to illustrate the adsorption rate and mechanism of ZSM-5 [28]. Pseudo-first-order kinetics, pseudo-second-order kinetics, and intraparticle diffusion kinetics [29, 30] were used to evaluate the sorption kinetics; the equations are generally written as follows:

$$\ln(q_e - q_t) = \ln q_e - k_1 t,$$

$$\frac{t}{q_t} = \frac{t}{q_e} + \frac{1}{k_2 q_e^2}, \quad (3)$$

$$q_t = k_p t^{0.5} + C,$$

where k_1 (min^{-1}), k_2 ($\text{g} \cdot \text{mg}^{-1} \cdot \text{min}^{-1}$), and k_p ($\text{g} \cdot \text{mg}^{-1} \cdot \text{min}^{-1/2}$) are the pseudo-first-order kinetics, pseudo-second-order kinetics, and intraparticle diffusion kinetics rate constants of

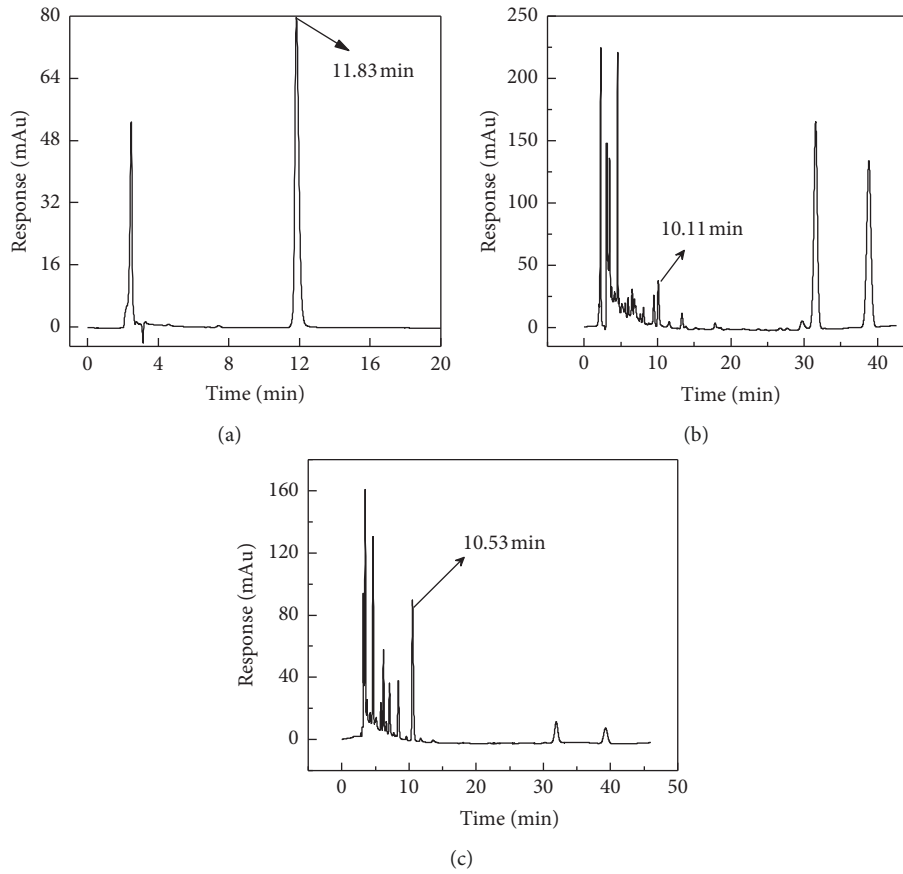


FIGURE 3: HPLC chromatograms of standard substance (a), extracts (b), and eluents (c).

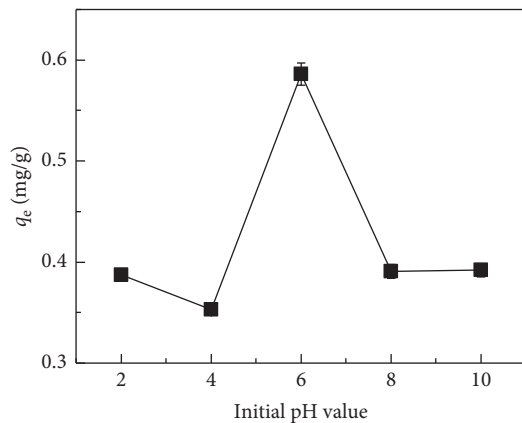


FIGURE 4: Influence of initial pH on adsorption capacity.

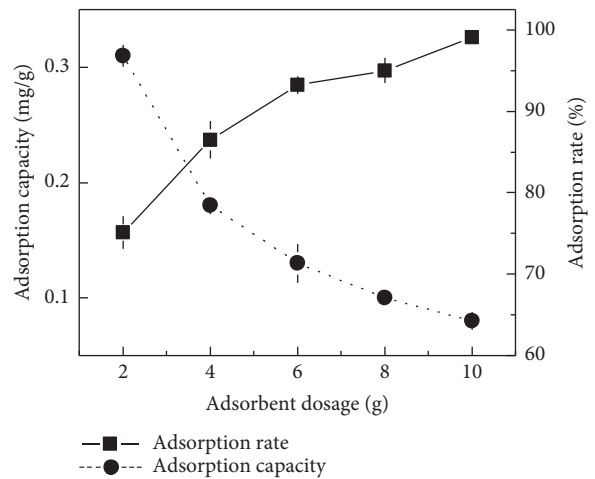


FIGURE 5: Effect of adsorbent dosage on adsorption capacity and adsorption rate.

adsorption, respectively; q_e (mg/g) is the equilibrium adsorption capacity; q_t (mg/g) is the amount of CHE adsorbed at time t ; and C is the constant of adsorption.

According to the kinetics equations, the pseudo-first order, pseudo-second order and intraparticle diffusion kinetics curves are given by $\ln(q_e - q_t) \sim t$, $t/q_t \sim t$, and $q_t \sim t^{0.5}$, respectively. The fitting curves of the three kinetics models and their parameters are given in Figure 7 and Table 1, respectively. From Figure 7(a) and Table 1, the CHE adsorption data fit well with the pseudo-second-order kinetics

model, as indicated by the high correlation ($R^2 = 0.9991$). This result indicates that chemisorption plays a major role in the adsorption process. From the fitting curve of the particle diffusion model in Figure 7(b), three stages exist during the diffusion of CHE to ZSM-5. k_{p1} , k_{p2} , and k_{p3} , which express the diffusion rates of the different stages in the adsorption process, are shown in Table 2 and follow the order

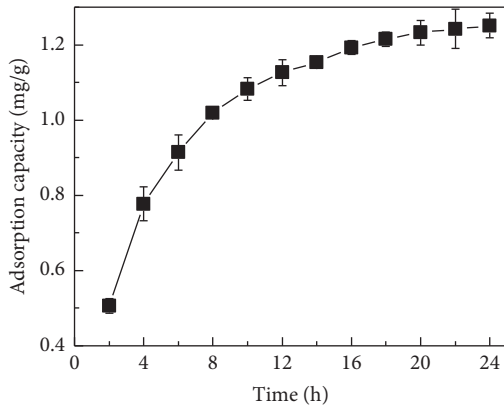


FIGURE 6: Adsorption kinetics curve.

$k_{p1} > k_{p2} > k_{p3}$. The first steeply sloped period is a rapid stage during which a large amount of CHE is rapidly adsorbed by the exterior surface of the molecular sieves. When the adsorption on the exterior surface reaches saturation, CHE molecules enter the pores of the adsorbent and are adsorbed by the interior surface of the molecular sieves. As the CHE molecules enter the pores, the diffusion resistance increases, which leads to a decrease in the diffusion rate. With the rapid decrease in CHE concentration, the intraparticle diffusion rate gradually falls and finally reaches equilibrium; therefore, the changes in k_{p1} , k_{p2} , and k_{p3} could be attributed to the different adsorption behaviors in the exterior surface adsorption stage, in the interior surface adsorption stage, and at equilibrium, respectively. The same result was obtained in a previous study [31]. In general, if the plot of q_t against $t^{1/2}$ gives a straight line and crosses the origin, intraparticle diffusion is the only rate-controlling step in the adsorption process. As shown in Figure 7(b), three straight lines were obtained, suggesting that intraparticle diffusion plays a major role but is not the only rate-controlling step in the adsorption process: external diffusion and boundary diffusion also influence the process.

3.5. Adsorption Isotherm. Adsorption isotherms are important for determining the adsorption behavior of an adsorbent. To simulate the adsorption behavior of molecular sieves for CHE, the adsorption curves of CHE on molecular sieves at different temperatures and solution concentrations were investigated. Figure 8 shows that the adsorption capacity increases with increasing solution concentration at a pH of 6, indicating that a high CHE concentration in solution is beneficial for adsorption by molecular sieves. Moreover, the results demonstrate that the molecular sieves show high affinity at lower temperatures.

To verify the adsorption process and clearly investigate the mechanism of adsorption, the Langmuir and Freundlich isotherms were applied to fit the experimental data in this study. The Langmuir isotherm model is based on the assumption that monolayer adsorption takes place onto a completely homogeneous surface that contains a limited number of active sites. The Freundlich isotherm is an empirical equation that describes adsorption onto a

heterogeneous surface through a multilayer adsorption mechanism, and the sites on the surface have different binding energies [32]. The linear forms of the Freundlich and Langmuir adsorption isotherm equations are given as follows:

$$\ln q_e = \ln K_F + \frac{1}{n} \ln c_e, \quad (4)$$

$$\frac{1}{q_e} = \frac{1}{q_m} + \frac{1}{q_m K_L c_e},$$

where q_e (mg/g) and q_m (mg/g) are the equilibrium and maximum adsorption capacity of CHE adsorbed by the molecular sieve, respectively; c_e (mg/mL) is the equilibrium concentration in solution; K_L (L/mg) and K_F (dm³/mg) are the Langmuir and Freundlich adsorption constants, respectively; and n is the Freundlich constant, which is temperature-dependent.

The fitting parameters were calculated by linear plotting and are shown in Table 3. The constants n and K_F were calculated from the slope and intercept, respectively, of $\ln q_e$ versus $\ln c_e$ from Figure 9(a). The values of q_m and K_L can be calculated from Figure 9(b), the linear plot of c_e/q_e versus c_e . To choose the best-fitting model, the correlation coefficient (R^2) was studied. Comparing the values of R^2 from Table 3, we can conclude that the Langmuir model fits well with the experimental data for CHE adsorption on molecular sieves, indicating that a monolayer adsorption process occurs. According to the best fitting of the Langmuir model, the maximum adsorption capacities of CHE at 288, 298, and 308 K are 2.327 mg/g, 2.072 mg/g, and 1.877 mg/g, respectively. Moreover, the separation factor or equilibrium parameter (R_L) is introduced to describe the favorability of the CHE adsorption process; the formula of R_L is shown as follows:

$$R_L = \frac{1}{1 + K_L c_0}, \quad (5)$$

where c_0 (mg/dm³) is the initial concentration of CHE. The favorability of the adsorption process is based on the value of R_L and can be irreversible ($R_L = 0$), favorable ($0 < R_L < 1$), linear ($R_L = 1$), or unfavorable ($R_L > 1$) [33]. The values of R_L shown in Table 3 are all positive; thus, the adsorption of CHE is favorable.

3.6. Adsorption Thermodynamics. Because the adsorption isotherm fits well with the Langmuir isotherm model at 288, 298, and 308 K, the adsorption enthalpy (ΔH), adsorption entropy (ΔS), and adsorption free energy (ΔG) of CHE on the ZSM-5 molecular sieves can be calculated using the Langmuir constant of K_L based on the following equations [34]:

$$\Delta G = -RT \ln K_a, \quad (6)$$

$$\ln K_a = -\frac{\Delta H}{RT} + \frac{\Delta S}{R},$$

where K_a (dimensionless) is the thermodynamic equilibrium constant (the K_a values were estimated from the parameters of the Langmuir model, as presented in previous literature

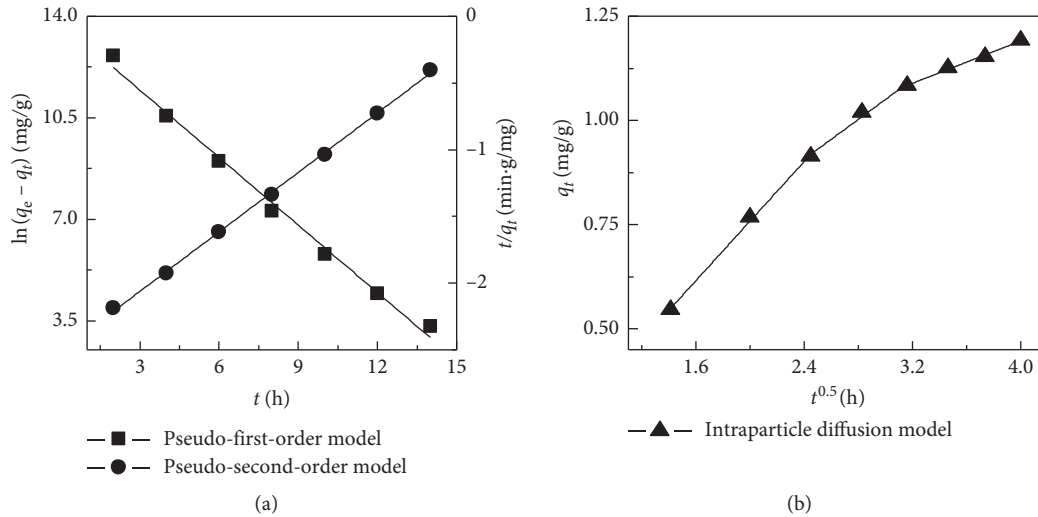


FIGURE 7: Fitting curves of various kinetics equations.

TABLE 1: Parameters of the pseudo-first-order and pseudo-second-order kinetics models.

Adsorbent	Pseudo-first-order kinetics model			Pseudo-second-order kinetics model		
	k_1 (min^{-1})	q_e (mg/g)	R^2	k_2 (g/mg·min)	q_e (mg/g)	R^2
CHE	0.0469	0.8446	0.9911	0.1959	1.4638	0.9991

TABLE 2: Fitting parameters of the intraparticle diffusion model.

Adsorbent	Intraparticle diffusion model					
	k_{p1} (g/mg $\text{min}^{1/2}$)	R^2	k_{p2} (g/mg $\text{min}^{1/2}$)	R^2	k_{p3} (g/mg $\text{min}^{1/2}$)	R^2
CHE	0.357	0.9969	0.238	0.9790	0.127	0.9910

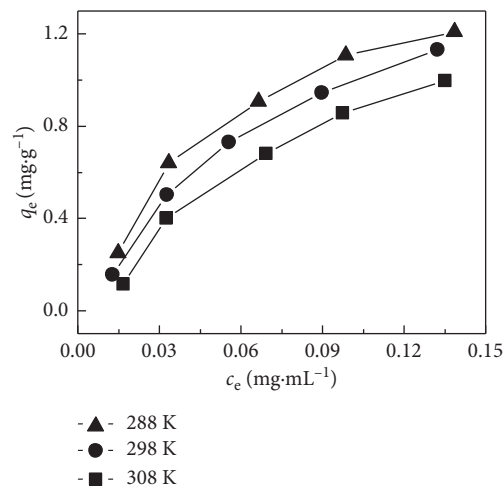


FIGURE 8: CHE adsorption isotherms of ZSM-5.

[35, 36]); R is the ideal gas constant, $8.314 \text{ J}/(\text{mol}\cdot\text{K})$; and T is the absolute temperature (K). The values of ΔH and ΔS are calculated from the slope and the intercept of the linear plot of $\ln K_L$ versus $1/T$, respectively. The results are summarized in Table 4. The values of ΔG for CHE are negative, which implies that the adsorption of CHE by molecular sieves can

happen spontaneously. Moreover, the values of ΔG increase gradually with decreasing adsorption temperature, which indicates that the lower the adsorption temperature is, the greater the affinity of binding sites and the more spontaneous the adsorption occurs. The negative value of ΔH implies that the adsorption of CHE is an exothermic process,

TABLE 3: Langmuir and Freundlich isotherm parameters of CHE on ZSM-5 at different temperatures.

Temperature (K)	Langmuir			Freundlich			
	Q_m (mg/g)	K_L (L/g)	R^2	R_L	K_F (dm ³ /g)	$1/n$	R^2
288	2.327	13.905	0.9812	0.0024	3.836	0.556	0.9362
298	2.072	9.311	0.9872	0.0036	4.373	0.649	0.9579
308	1.877	5.758	0.9717	0.0051	4.636	0.744	0.9497

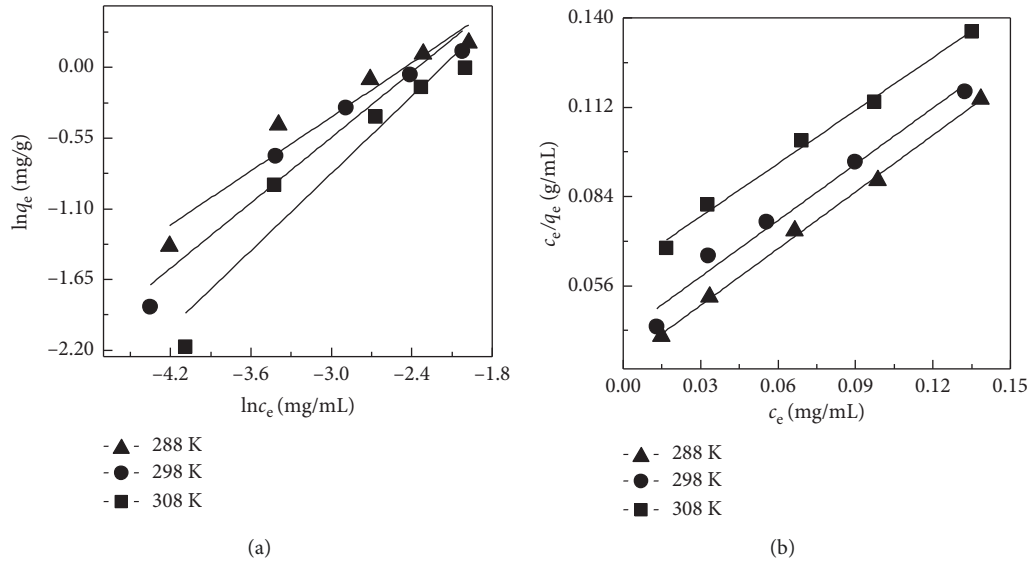


FIGURE 9: Fitting curves of the Freundlich model (a) and Langmuir model (b).

TABLE 4: Thermodynamic parameters for the adsorption of CHE on ZSM-5 at different temperatures.

Temperature (K)	ΔG (kJ/mol)	ΔH (kJ/mol)	ΔS (J/mol K)
288	-6.411		
298	-5.620	-67.232	-203.602
308	-4.556		

which demonstrates that decreasing the temperature is beneficial. The negative value of ΔS shows decreases in the degrees of freedom of the adsorbed species and the randomness at the solid/liquid interface.

4. Conclusions

This scientific study clearly suggests that ZSM-5 is suitable for adsorbing CHE from *Toddalia asiatica* (L.) Lam. Batch experiments revealed that the adsorption efficiency was affected by the solution pH, and the optimum initial solution pH was 6. The maximum adsorption capacity of CHE was found at a solid-liquid ratio of 2:15. The pseudo-second-order kinetics model and intraparticle diffusion model suitably describe the kinetics of the adsorption process, indicating that chemisorption plays a major role in the adsorption process and that intraparticle diffusion is not the only rate-controlling step in the adsorption process. The equilibrium adsorption data of CHE by ZSM-5 fit well with the Langmuir isotherm model, as indicated by the high

correlation coefficients. The maximum adsorption capacities obtained from the Langmuir isotherm model in the temperature range of 288 K to 308 K are 2.327, 2.072, and 1.877 mg/g. The thermodynamic parameters show a favorable, spontaneous, and exothermic process in the adsorption of CHE by molecular sieves. In conclusion, as shown by the adsorption mechanism of the ZSM-5 molecular sieve for CHE, this material is thought to be a promising adsorbent for purifying alkaloids (especially quaternary ammonium alkaloids) from medicinal herbs. In addition, a technique for isolating active components from the pretreatment process of biomass is provided.

Data Availability

The data used to support the findings of this study are available from the corresponding author upon request.

Conflicts of Interest

The authors declare that there are no conflicts of interest regarding the publication of this paper.

Acknowledgments

This work was supported by the National Natural Science Foundation of China (no. 31560105), Zhangjiajie Science and Technology Development Project (no. 2015FJ2151), and

Graduate Student Scientific Research Innovation Projects of Jishou University (no. JGY201844).

References

- [1] M. N. Catrinck, E. S. Ribeiro, R. S. Monteiro, R. M. Ribas, M. H. P. Barbosa, and R. F. Teofilo, "Direct conversion of glucose to 5-hydroxymethylfurfural using a mixture of niobic acid and niobium phosphate as a solid acid catalyst," *Fuel*, vol. 210, pp. 67–74, 2017.
- [2] F. Parveen and S. Upadhyayula, "Efficient conversion of glucose to HMF using organocatalysts with dual acidic and basic functionalities—a mechanistic and experimental study," *Fuel Processing Technology*, vol. 162, pp. 30–36, 2017.
- [3] Y. P. Shan, Y. H. Song, Y. Q. Liu, R. X. Liu, J. J. Du, and P. Zeng, "Adsorption of berberine by polymeric resin H103: kinetics and thermodynamics," *Environmental Earth Sciences*, vol. 73, no. 9, pp. 4989–4994, 2015.
- [4] Y. Z. Zhu, Y. Y. Pan, G. B. Zhang et al., "Chelerythrine inhibits human hepatocellular carcinoma metastasis in vitro," *Biological & Pharmaceutical Bulletin*, vol. 41, no. 1, pp. 36–46, 2018.
- [5] J. Jana, S. Mondal, P. Bhattacharjee et al., "Chelerythrine down regulates expression of VEGFA, BCL2 and KRAS by arresting G-Quadruplex structures at their promoter regions," *Scientific Reports*, vol. 7, no. 1, 2017.
- [6] W. J. Lin, J. J. Huang, Z. W. Yuan, S. L. Feng, Y. Xie, and W. Z. Ma, "Protein kinase C inhibitor chelerythrine selectively inhibits proliferation of triple-negative breast cancer cells," *Scientific Reports*, vol. 7, no. 1, 2017.
- [7] L. Y. Yao, Y. X. Zhu, C. Q. Liu, R. H. Jiao, Y. H. Lu, and R. X. Tan, "Preparative separation and purification of fumigaclavine C from fermented mycelia of *Aspergillus fumigatus* CY018 by macroporous adsorption resin," *Journal of Chromatography*, vol. 989, pp. 122–128, 2015.
- [8] D. Castillo, M. Sauvain, M. Rivaud, and V. Jullian, "In vitro and in vivo activity of benzo c phenanthridines against leishmania amazonensis," *Planta Medica*, vol. 80, no. 11, pp. 902–906, 2014.
- [9] A. Maurya and S. K. Srivastava, "Large-scale separation of clavine alkaloids from *Ipomoea muricata* by pH-zone-refining centrifugal partition chromatography," *Journal of Chromatography B*, vol. 877, no. 18–19, pp. 1732–1736, 2009.
- [10] H. D. Luo, M. Peng, H. Y. Ye et al., "Predictable and linear scale-up of four phenolic alkaloids separation from the roots of *Menispermum dauricum* using high-performance counter-current chromatography," *Journal of Chromatography B*, vol. 878, no. 22, pp. 1929–1933, 2010.
- [11] Y. H. Kwon, B. Min, S. W. Yang, D. Y. Koh, R. R. Bhave, and S. Nair, "Ion-Exchanged SAPO-34 membranes for krypton-xenon separation: control of permeation properties and fabrication of hollow fiber membranes," *Acs Applied Materials & Interfaces*, vol. 10, no. 7, pp. 6361–6368, 2018.
- [12] Y. Shen, F. M. Wang, W. Liu, and X. B. Zhang, "The preparation of Fe³⁺ ion-exchanged mesopore containing ZSM-5 molecular sieves and its high catalytic activity in the hydroxylation of phenol," *Journal of Porous Materials*, vol. 25, no. 6, pp. 1587–1595, 2018.
- [13] B. Li, X. L. Cui, D. O'Nolan et al., "An ideal molecular sieve for acetylene removal from ethylene with record selectivity and productivity," *Advanced Materials*, vol. 29, no. 47, 2017.
- [14] L. Zhang, Y. Li, H. C. Zhou, and M. D. Chen, "Performance of 1,8-diazabicyclo [5.4.0] undec-7-ene-Modified SBA-15 for selective adsorption of CO₂," *Energy & Fuels*, vol. 31, no. 3, pp. 3062–3068, 2017.
- [15] X. T. Zhang, N. He, C. Y. Liu, and H. C. Guo, "Pt-Cu alloy nanoparticles encapsulated in silicalite-1 molecular sieve: coke-resistant catalyst for alkane dehydrogenation," *Catalysis Letters*, vol. 149, no. 4, pp. 974–984, 2019.
- [16] L. D. Wang, S. Cui, Q. W. Li, J. Wang, and S. Liu, "Kinetics and mechanism of magnesium sulphite oxidation promoted by a novel cobalt-based molecular sieve catalyst," *Applied Catalysis A-General*, vol. 511, pp. 16–22, 2016.
- [17] N. Ohnishi and K. Hiraga, "Slow-scan CCD camera analysis of electron diffraction and high-resolution micrographs of zeolite TPA/ZSM-5," *Journal of Electron Microscopy*, vol. 45, no. 1, pp. 85–92, 1996.
- [18] S. Schallmoser, T. Ikuno, M. F. Wagenhofer et al., "Impact of the local environment of Bronsted acid sites in ZSM-5 on the catalytic activity in n-pentane cracking," *Journal of Catalysis*, vol. 316, pp. 93–102, 2014.
- [19] R. Vonballmoos and W. M. Meier, "Zoned aluminium distribution in synthetic zeolite ZSM-5," *Nature*, vol. 289, no. 5800, pp. 782–783, 1981.
- [20] X. H. Mu, D. Z. Wang, Y. R. Wang, M. Lin, S. B. Cheng, and X. T. Shu, "Nanosized molecular sieves as petroleum refining and petrochemical catalysts," *Chinese Journal of Catalysis*, vol. 34, no. 1, pp. 69–79, 2013.
- [21] H. Belarbi, Z. Lounis, R. Hamacha, A. Bengueddach, and P. Trens, "Textural properties of ZSM-5 nanocrystals prepared in alkaline potassium fluoride medium," *Colloids and Surfaces A-Physicochemical and Engineering Aspects*, vol. 453, pp. 86–93, 2014.
- [22] G. V. Briao, S. L. Jahn, E. L. Foletto, and G. L. Dotto, "Adsorption of crystal violet dye onto a mesoporous ZSM-5 zeolite synthesized using chitin as template," *Journal of Colloid and Interface Science*, vol. 508, pp. 313–322, 2017.
- [23] H. Y. Liu, Z. K. Zhang, Y. Y. Xu, Y. F. Chen, and X. Li, "Adsorption-Oxidation reaction mechanism of NO on Na-ZSM-5 molecular sieves with a high Si/Al ratio at ambient temperature," *Chinese Journal of Catalysis*, vol. 31, no. 9–10, pp. 1233–1241, 2010.
- [24] Y. L. Liu, S. Ke, Z. B. Xiao, and J. Guo, "Adsorption kinetics of lycorine and galantamine with molecular sieves ZSM-5," *Chemistry and Industry of Forest Products*, vol. 38, no. 3, pp. 122–128, 2018.
- [25] Z. H. Chen, J. N. Zhang, J. W. Fu et al., "Adsorption of methylene blue onto poly (cyclotriphosphazene-co-4,4'-sulfonyldiphenol) nanotubes: kinetics, isotherm and thermodynamics analysis," *Journal of Hazardous Materials*, vol. 273, pp. 263–271, 2014.
- [26] X. Z. Xu, S. X. Chen, and Q. H. Wu, "Surface molecular imprinting on polypropylene fibers for rhodamine B selective adsorption," *Journal of Colloid and Interface Science*, vol. 385, no. 1, pp. 193–201, 2012.
- [27] S. Liao, W. Zhang, W. Long, D. Hou, X. C. Yang, and N. Tan, "Adsorption characteristics, recognition properties, and preliminary application of nordihydroguaiaretic acid molecularly imprinted polymers prepared by sol-gel surface imprinting technology," *Applied Surface Science*, vol. 364, pp. 579–588, 2016.
- [28] L. Tang, G. D. Yang, G. M. Zeng et al., "Synergistic effect of iron doped ordered mesoporous carbon on adsorption-coupled reduction of hexavalent chromium and the relative mechanism study," *Chemical Engineering Journal*, vol. 239, pp. 114–122, 2014.

- [29] M. Tanyol, N. Kavak, and T. Gülben, "Synthesis of poly (AN-co-VP)/zeolite composite and its application for the removal of brilliant green by adsorption process: kinetics, isotherms, and experimental design," *Advances in Polymer Technology*, vol. 2019, Article ID 8482975, 12 pages, 2019.
- [30] J. S. He, A. A. Cui, F. Ni, S. H. Deng, F. Shen, and G. Yang, "A novel 3D yttrium based-graphene oxide-sodium alginate hydrogel for remarkable adsorption of fluoride from water," *Journal of Colloid and Interface Science*, vol. 531, pp. 37–46, 2018.
- [31] W. J. Yang, P. Ding, L. Zhou, J. G. Yu, X. Q. Chen, and F. P. Jiao, "Preparation of diamine modified mesoporous silica on multi-walled carbon nanotubes for the adsorption of heavy metals in aqueous solution," *Applied Surface Science*, vol. 282, pp. 38–45, 2013.
- [32] L. T. Tran, H. V. Tran, T. D. Le, G. L. Bach, and L. D. Tran, "Studying Ni (II) adsorption of magnetite/graphene oxide/chitosan nanocomposite," *Advances in Polymer Technology*, vol. 2019, Article ID 8124351, 9 pages, 2019.
- [33] L. Tang, Y. Cai, G. D. Yang et al., "Cobalt nanoparticles-embedded magnetic ordered mesoporous carbon for highly effective adsorption of rhodamine B," *Applied Surface Science*, vol. 314, pp. 746–753, 2014.
- [34] B. Erdem, A. Ozcan, and A. S. Ozcan, "Adsorption and solid phase extraction of 8-hydroxyquinoline from aqueous solutions by using natural bentonite," *Applied Surface Science*, vol. 256, no. 17, pp. 5422–5427, 2010.
- [35] Y. Liu, "Is the free energy change of adsorption correctly calculated?," *Journal of Chemical and Engineering Data*, vol. 54, no. 7, pp. 1981–1985, 2009.
- [36] X. X. Liu, W. P. Gong, J. Luo, C. T. Zou, Y. Yang, and S. J. Yang, "Selective adsorption of cationic dyes from aqueous solution by polyoxometalate-based metal-organic framework composite," *Applied Surface Science*, vol. 362, pp. 517–524, 2016.

Research Article

Efficient Production of Methyl Oleate Using a Biomass-Based Solid Polymeric Catalyst with High Acid Density

Anping Wang ^{1,2} Heng Zhang ¹ Hu Li ¹ and Song Yang ¹

¹State Key Laboratory Breeding Base of Green Pesticide & Agricultural Bioengineering, Key Laboratory of Green Pesticide & Agricultural Bioengineering, Ministry of Education, State-Local Joint Laboratory for Comprehensive Utilization of Biomass, Center for Research & Development of Fine Chemicals, Guizhou University, Guiyang, Guizhou 550025, China

²Key Laboratory for Information System of Mountainous Area and Protection of Ecological Environment of Guizhou Province, Guizhou Normal University, Guiyang, Guizhou 550025, China

Correspondence should be addressed to Hu Li; hli13@gzu.edu.cn and Song Yang; jhzx.msm@gmail.com

Received 12 June 2019; Revised 24 August 2019; Accepted 9 September 2019; Published 8 December 2019

Academic Editor: Minna Hakkarainen

Copyright © 2019 Anping Wang et al. This is an open access article distributed under the Creative Commons Attribution License, which permits unrestricted use, distribution, and reproduction in any medium, provided the original work is properly cited.

Biomass-based polymers are eco-friendly, nontoxic and biodegradable materials. In this work, in order to prepare green, low-cost and high-efficient catalysts under mild conditions, we chose biomass-based chitosan as raw material and prepared a new solid acidic catalyst by an acid functionalization method. FT-IR, XRD, SEM, TGA, BET, neutralization titration and other analytical methods were used to characterize the catalyst. The results showed that CS-SO₃H morphology exhibited a sphere of about 10 μm diameter, and the acid density was as high as 3.81 mmol/g. The catalyst exhibits good catalytic activity in the esterification of oleic acid and methanol, which is a model reaction of the pre-esterification process in the preparation of biodiesel from feedstocks with high acid values. Under the optimum reaction conditions (15/1 methanol/oleic acid mole ratio and 3 wt% catalyst dosage at 75°C for 3 h), the yield of methyl oleate can reach 95.7%. Even if the mass of oleic acid in the reactant increased to 20 g, solid acid showed good catalytic performance, and the yield of methyl oleate was 94.4%. After four times of reuse, the yield of the catalyst can still reach 85.7%, which indicates that the catalyst has good catalytic activity and stability, and has potential application prospects.

1. Introduction

Biodiesel is a green, biodegradable and renewable fuel. As a competitive alternative to fossil fuels, it attracts more and more attention [1–3]. The main component of biodiesel is free fatty acid methyl ester or ethyl ester, which is a mixture of various esters and determined by the composition diversity of raw materials [4]. Biodiesel was originally made from edible oils, such as soybean oil, rapeseed oil, and sunflower oil. However, the use of edible oil to produce biodiesel may affect food security in populous countries [5]. Therefore, researchers gradually explore the use of nonedible oil to synthesize biodiesel, such as *Jatropha* oil, *Euphorbia lathyris* oil [6], *Koeleria integrifoliola* oil [7] and so on. Meanwhile, waste cooking oils have gradually begun to recycle, which not only greatly reduces the cost of attractive raw materials, but also can solve the problem of environmental pollution [8, 9]. Unfortunately, nonedible oils and waste cooking oils generally

have high acid value, which is disadvantageous in the preparation of biodiesel.

In order to convert raw materials with high acid values into biodiesel efficiently and quickly, researchers have been exploring more effective catalysts to deal with this problem. Homogeneous acids and bases, such as H₂SO₄, NaOH, and KOH, were initially used in the preparation of biodiesel [10]. However, homogeneous catalysts are difficult to separate from the reaction products, which has an impact on the quality of biodiesel. Moreover, the catalyst cannot be recycled. Simultaneously, homogeneous catalysts can also cause corrosion to the reaction equipment. Therefore, heterogeneous catalysts have attracted the attention of researchers [11]. In addition, for the high acid value raw materials, alkali catalysis will lead to serious saponification, so pre-esterification is necessary before transesterification. The esterification and transesterification can be carried out simultaneously by acid catalysis in one pot [8]. Therefore, using acid materials to

catalyze the preparation of biodiesel from raw materials with high acid values is a good choice. Researchers reported a series of applications in the preparation of acidic catalysts for biodiesel, including $\text{SO}_3\text{H-ZnO}$ [12], $\text{SO}_4^{2-}/\text{ZrO}_2$ [13], supported acidic ionic liquids [8], HPW-PGMA-MNPs [14], C18-SiO₂-SO₃H [15], carbon-based solid acids [16], MOF-supported heteropoly acids [17], and other heterogeneous acid catalysts. However, solid acid catalysts generally need higher reaction temperature and longer reaction time to obtain high biodiesel yield by high acid value raw materials. Thereby, in order to reduce the production cost of biodiesel, it is necessary to explore novel and efficient solid acid catalysts, which can pre-esterification oils with high acid value under mild conditions or simultaneously perform esterification and transesterification by one-pot method.

With the development of the times, it is recognized that the development of renewable and biodegradable biomass-based catalysts are more in line with the concept of green chemistry [2]. Biomass-based catalysts are mainly obtained by carbonization and post-modification of biomass. However, high-temperature carbonization is not economical in practical application. Therefore, it is necessary to prepare functionalized biomass-based catalysts directly in a simple approach to meet the needs of production [18]. Chitosan is a kind of macromolecule polymer biomass material made from shrimp shell and crab shell, which has rich natural reserves. Chitosan has many advantages, such as biological function, compatibility, safety, and microbial degradation. It is widely used in medicine, food, chemical industry, cosmetics, water treatment and other fields [19, 20]. Chitosan has strong modifiability due to its active hydroxyl and amino groups. At the same time, chitosan is a cheap polymer, which makes it a natural advantage in industrial production as a catalyst.

A solid acid catalyst for biomass polymer was prepared from chitosan and chlorosulfonic acid, to obtain high acid density, stability, and high-efficiency catalyst because sulfonic acid catalyst was a kind of relatively stable catalytic material [11, 21, 22]. The preparation method is simple, mild and eco-friendly. Because oleic acid is an important free fatty acid, it can be used to simulate high acid value raw materials to produce fatty acid methyl ester by esterification, which can effectively detect the catalytic activity of the catalyst in the preparation of biodiesel by pre-esterification and one-pot reaction. Thus, methyl oleate was synthesized by the reaction of oleic acid (OA) with methanol (MeOH), and the catalytic performance of CS-SO₃H was evaluated.

2. Materials and Methods

2.1. Materials. Potassium hydroxide (KOH, AR, ≥85.0%), sodium chloride (NaCl, ≥99.5%), chlorosulfonic acid (AR, ≥97%), and oleic acid (AR, ≥99%, AV = 184.52 KOH mg/g) were obtained from Shanghai Macklin Biochemical Co. Ltd. Chitosan (>99%, The degree of deacetylation ≥95%) was purchased from Shanghai Aladdin Biochemical Technology Co. Ltd. Methanol (AR, ≥99.5%), ethanol (AR, ≥99.7%), petroleum ether (AR, 60–90°C), and dichloromethane (AR,

≥99.5%) were purchased from Chuandong Chemical Reagent Co. Ltd.

2.2. Preparation of Catalyst. The preparation method of chitosan sulfonic acid catalyst (CS-SO₃H) with high acid density was modified with reference to the literature [23]. Specifically, 5.0 g chitosan powder was added into 50 mL dichloromethane and stirred to form a suspension. Then, 5 mL chlorosulfonic acid was dispersed in 25 mL dichloromethane and slowly dripped into suspended chitosan (about 30 min) under vigorous stirring at room temperature. Subsequently, the mixture was stirred for 6 h at 25°C, filtered and washed to be neutral alternately with dichloromethane and absolute ethanol. Finally, the catalyst CS-SO₃H was obtained after drying overnight at 80°C.

2.3. Catalyst Characterization. Fourier-transform infrared (FT-IR) spectrum is mainly used for functional characterization of catalytic materials. Through the appearance of new functional groups, we can judge whether the catalyst has been successfully prepared. The used infrared spectrometer is Nicolet 360 FT-IR apparatus. Crystallinity and structure of catalytic materials were characterized by means of the Cu K α radiation X-ray diffractometer (XRD, Tongda TD-3500). Scanning electron microscopy (SEM) can provide morphological information of catalysts, including morphology, surface roughness, and voids. The scanning electron microscope we used was JSM-6700F (5 kV). Physical properties of polymer materials were determined at 77 K using Bruner-Emmett-Teller (BET) method and nitrogen adsorption-desorption device (ASAP 2460, Mcmerric Instruments Co. Ltd.). The instrument used for measuring the contact angle of catalyst water is from Dataphysics Corporation (OCA15EC, Germany). The thermal stability of the samples was determined by PerkinElmer TGA47 thermogravimetric analyzer in a nitrogen atmosphere.

The acid density is an important parameter of catalyst. It is generally evaluated by acid-base neutralization titration [11, 20, 24]. In this work, the acid density of CS-SO₃H is determined by the same method. In a general procedure, 40 mg catalyst was added into 20 mL 0.1 M NaCl solution. The suspension was stirred vigorously for 24 h, then centrifuged and separated. The solution after the catalyst removal was titrated to be neutral with 0.01 M NaOH solution. Phenolphthalein is an indicator of neutralization titration. The acid density of the catalyst was obtained by calculating the average value of the three parallel measurements.

2.4. Esterification of Oleic Acid. Methyl oleate was synthesized from OA and MeOH, and the catalytic activity of CS-SO₃H was tested. Usually, a 15 mL pressure bottle is used as a reaction vessel (Beijing Synthware Glass Instrument Co. Ltd.). Methanol (1.70 g, 53 mmol), oleic acid (1.00 g, 3.5 mmol), and 0.03 g CS-SO₃H were added to the reaction vessel. The reactor was placed into an oil bath at 75°C and lasted for 3 h under magnetic stirring (600 rpm). Subsequently, the mixture was cooled to room temperature and the catalyst was removed by centrifugation. Water and unreacted MeOH were removed by vacuum distillation. Nuclear magnetic resonance (NMR,

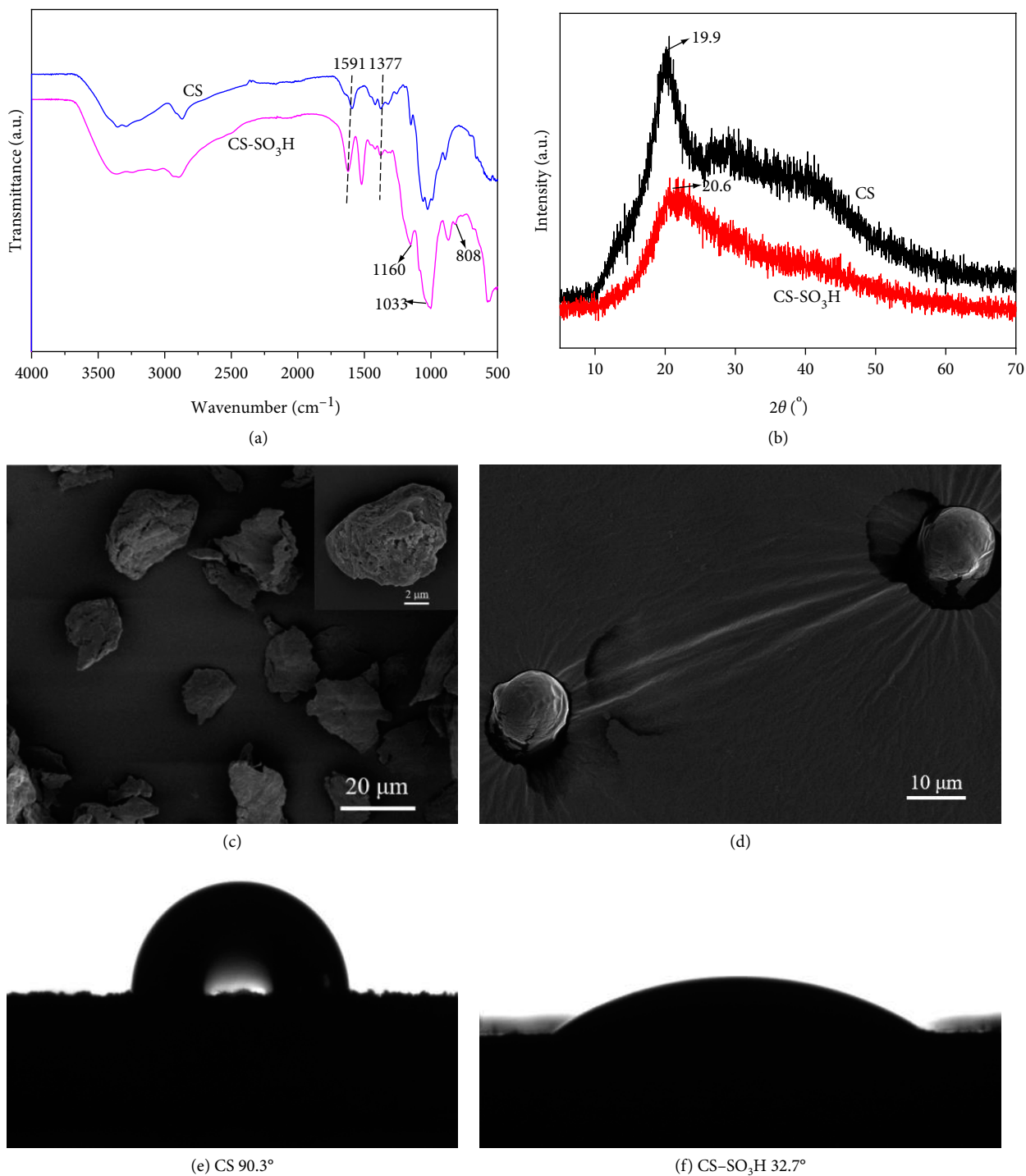


FIGURE 1: The CS and CS-SO₃H FT-IR spectra (a), XRD (b), SEM (c) and (d), water contact angle (e) and (f).

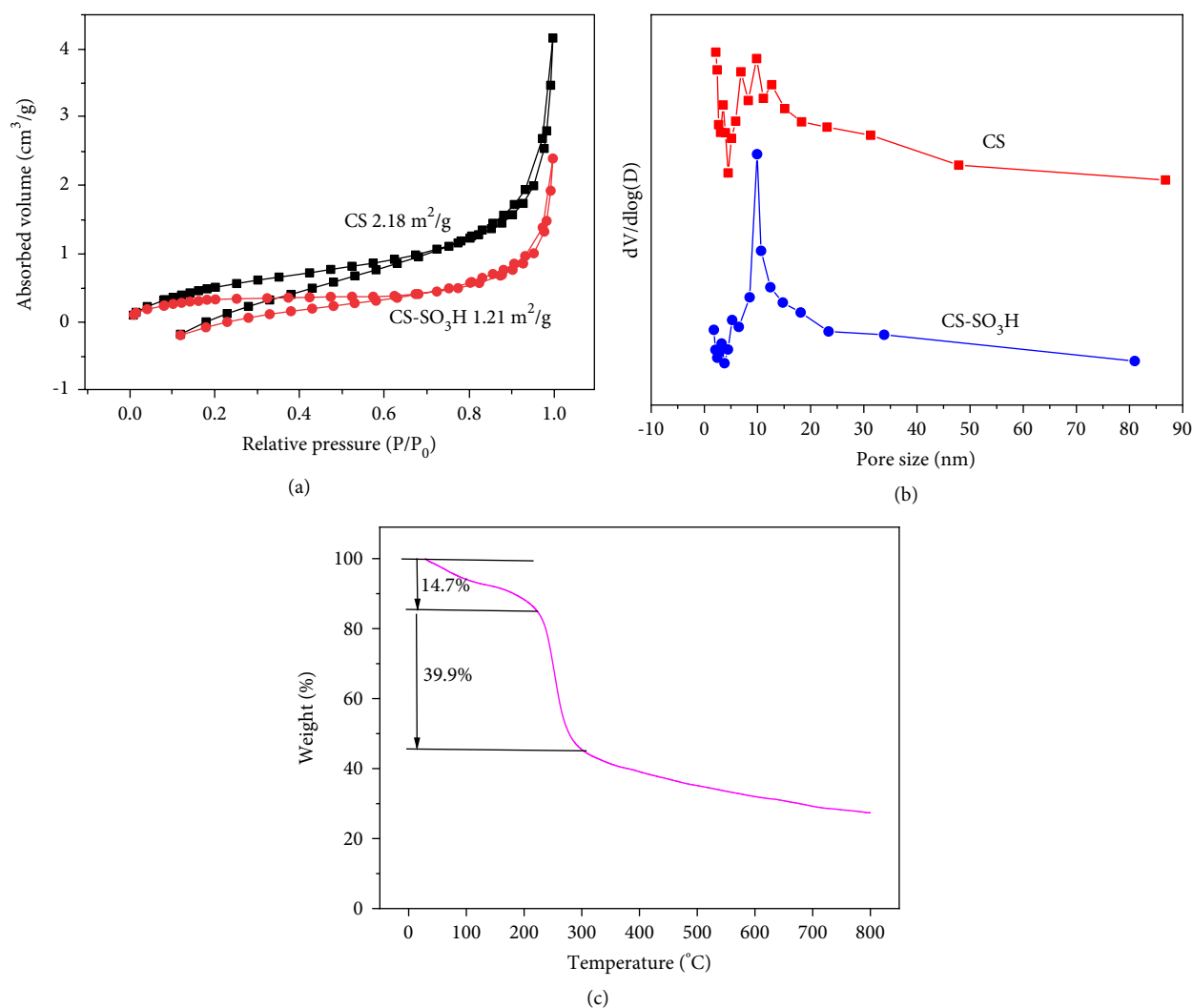
500 MHz₂) was used as an instrument for measuring the yield of FAME, and CDCl₃ is used as a solvent.

2.5. Expanded Reaction Scale for the Production of Methyl Oleate. In order to ensure that the catalyst has good catalytic performance in large-scale preparation of methyl oleate, the amount of oleic acid was increased to 20 g, with the temperature of 75°C, the MeOH to OA molar ratio of 15 : 1, and the time of 3 h. The yield was determined by NMR after post-treatment.

2.6. Hot Filtration and Water Tolerance Tests. In order to study heterogeneous catalytic behavior of catalysts, thermal filtration experiments were used to verify the catalytic performance. Under the optimal conditions, two groups of parallel experiments were carried out. One group continued to react after filtrating and removing the catalyst after 0.5 h, then sampled and tested the yield at 0.5 h, 1 h, 2 h, and 3 h, respectively. The control group did not do any treatment and with the yield being measured at the same time point.

TABLE 1: The BET and acid density comparison different catalysts.

Sample	S_{BET} (m^2/g)	Pore volume (cm^3/g)	Pore diameter (nm)	Total acid density ($\text{mmol H}^+ \cdot \text{g}^{-1}$)	Ref.
HS/C-SO ₃ H	470	0.40	4.2	2.10	[11]
FCHC-SO ₃ H	41.4	0.085	6.4	1.20	[18]
β -Cyclodextrin-SO ₃ H	0.18	-	4.74	3.00	[21]
Bamboo acid	0.25	-	-	1.74	[30]
CS	2.18	0.006	11.4	-	This work
CS-SO ₃ H	1.21	0.003	11.1	3.81	This work

FIGURE 2: (a) Nitrogen adsorption-desorption isotherms of CS and CS-SO₃H, (b) BJH pore-size distributions of CS and CS-SO₃H, and (c) thermogravimetric analysis of the CS-SO₃H catalyst.

Water tolerance tests were determined by adding a certain amount of water (0–10% of oleic acid mass) to the reaction system, and then the change of methyl oleate yield was detected.

2.7. Reusability. The reusability test was still carried out under optimum conditions, and then the catalyst was washed repeatedly with MeOH and petroleum ether to remove

adhering impurities. Subsequently, the solvent on the catalyst surface was removed at 80°C and applied in the next cycle.

3. Results and Discussion

3.1. Catalyst Characterization. As in Figure 1(a), the FT-IR spectra show that the absorption bands at 1591 and 1377 cm⁻¹

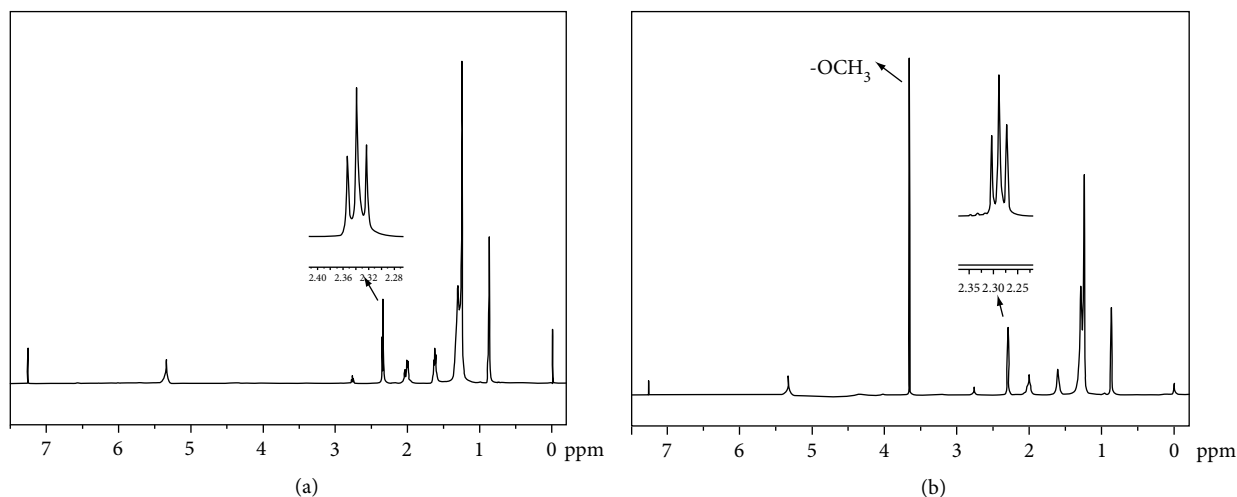


FIGURE 3: The ^1H spectra of oleic acid (a), and methyl oleate (b).

correspond to the peaks of N-H and C-O functional groups, respectively. Those belong to the characteristic peaks of chitosan. The peaks at 1160 and 1033 cm^{-1} are characteristic absorption bands of $-\text{SO}_3\text{H}$ group [25]. This is consistent with Dawodu et al. [21] report that the absorption bands at 1178 and 1026 cm^{-1} are attributed to $\text{O}=\text{S}=\text{O}$ stretching vibrations. Compared with the FT-IR spectra of CS and CS- SO_3H , a new absorption band appeared at 808 cm^{-1} of CS- SO_3H , which belongs to the characteristic peak of C-O-S [26–28]. This indicates that $-\text{SO}_3\text{H}$ functional group has been grafted onto $-\text{OH}$ of chitosan, and the preparation of the catalyst is successful.

XRD spectra (Figure 1(b)) show that chitosan was amorphous powder, and the characteristic peak of chitosan appeared at 19.9° [23]. The position of the diffraction peak of CS- SO_3H is at 20.6° , which indicates that the structure of sulfonated SO_3H has changed.

As can be seen from Figure 1(c), CS has irregular morphology and rough surface with a size of about $10\text{--}20\ \mu\text{m}$, which conforms to the structural characteristics of polymers. Figure 1(d) shows that after sulfonation, CS- SO_3H becomes a more regular spherical structure with a relatively smooth surface and a size of about $10\ \mu\text{m}$. This indicates that the sulfonic acid functional groups are mainly concentrated on the surface of the catalyst, resulting in changes in the surface morphology.

In the production of methyl oleate, hydrophobic materials can catalyze raw materials containing water. If hydrophobic materials are strong, the yield of methyl oleate will be higher. The water contact angle of CS is 90.3° and CS- SO_3H is 32.7° (Figures 1(e) and 1(f)). Because chitosan itself is insoluble in water, and the sulfonic acid group belongs to the hydrophilic group, which results in a smaller contact angle. When the contact angle is greater than 90° , it is generally considered that catalyst has good hydrophobic properties. While the contact angle is between 30° and 90° , it is thought that the material has certain wettability, but the wettability is not good [8, 29]. However, in the process of preparing methyl oleate, a certain contact angle can meet the needs of production. Therefore,

the water tolerance of catalyst was explored in the follow-up study.

Table 1, Figures 2(a) and 2(b) show that the specific surface area of CS and CS- SO_3H decreases from 2.18 to $1.21\text{ m}^2/\text{g}$, the pore volume reduces from 0.006 to $0.003\text{ cm}^3/\text{g}$, while the mean pore size remains unchanged at 11 nm . This is mainly due to the fact that the surface area of biomass-based polymer CS is relatively small. However, the pore size distribution of chitosan from 2 to 50 nm , while that of sulfonated chitosan pore diameter distribution from 2 to 20 nm , indicating that the sulfonation process changes the pore structure of chitosan. As shown in Figure 2(c), thermogravimetric analysis shows that the mass loss of CS- SO_3H is 14.7% when the temperature is lower than 223°C , which may be mainly due to the loss of water in the catalyst. Subsequently, in the range of $223\text{--}305^\circ\text{C}$, the mass of catalyst decreased sharply, indicating that polymeric network was decomposed and carbon materials were gradually formed [28]. However, the mass of CS- SO_3H decreased less after 305°C , which proved that the carbon material tended to be stable, and the decomposition of residual organic components reduced slightly. Overall, the thermal stability of CS- SO_3H is acceptable and has no effect on catalytic esterification.

Because the active amino and hydroxyl groups on chitosan can react with chlorosulfonic acid, the same unit can contain $2\text{--}4$ sulfonic groups, so CS- SO_3H catalyst has high acid density. At the same time, because of the small specific surface area, the $-\text{SO}_3\text{H}$ are mainly concentrated on the surface of the polymer acidic materials.

3.2. Yield Analysis of Methyl Oleate. NMR ^1H spectroscopy is an effective and simple method for quick detection of methyl oleate yields [29–32]. Generally, TMS is used as the internal standard marker for 0 point, and CDCl_3 is used as the solvent. As can be seen from Figures 3(a) and 3(b), oleic acid and methyl oleate ^1H NMR spectra are basically the same. The only difference is that methyl oleate has a significant new single peak at 3.66 ppm , which is $-\text{OCH}_3$ peak after esterification. Meanwhile, the triple peaks at 2.30 ppm did not change before

TABLE 2: The methyl oleate yield comparison different catalysts.

Catalyst	Total acid density (mmol H ⁺ ·g ⁻¹)	Methyl oleate yield (%)
Blank	-	0.4
CS	-	0.9
CS-SO ₃ H	3.81	95.7

and after the reaction, which is a typical α -CH₂ peak. Therefore, the yields of methyl oleate can be determined by unchanged α -CH₂ and emerging -OCH₃ peak areas. The following formula is used to evaluate methyl oleate yield.

$$C = 100 \times \left(\frac{2A_{Me}}{3A_{CH_2}} \right), \quad (1)$$

where A_{Me} represents the integral area of -OCH₃ and A_{CH_2} is the area of α -CH₂.

3.3. Esterification of Oleic Acid to Methyl Oleate. The cost of preparing methyl oleate is a primary consideration in industrial production. Therefore, the parameters of the OA and MeOH esterification reaction were optimized. The reaction temperature (55–95°C), reaction time (1–5 h), MeOH/OA molar ratio (5/1–25/1), and catalyst dosage (1–5 wt% oleic acid) were studied by single factor experiment. Under the optimized conditions, the yield was examined and compared with the results of chitosan catalysis and blank experiments (Table 2).

3.3.1. Reaction Temperature. High temperature is conducive to accelerating the reaction rate and reaching equilibrium quickly [33]. However, excessive temperature increases the production cost. Therefore, it is the first thing to determine the appropriate reaction temperature through experiments. The yield of methyl oleate increased from 75.2% to 95.9% due to the change in temperature (55–75°C) (Figure 4(a)). With the increase of temperature to 95°C, the yield reached 97.9%, and the change of yield was not obvious. The reaction temperature can be determined at 75°C.

3.3.2. Reaction Time. Esterification reaction needs enough time to ensure mass transfer, but once the equilibrium state is reached, increasing reaction time has little effect on the yield [34]. As shown in Figure 4(b), the yield of methyl oleate varies greatly with time. When the time is within 1–3 h, the yield ranges from 81.3% to 95.9%. However, when time is 4 h and 5 h, the yield of methyl oleate did not increase significantly (96.3%–97.6%). Therefore, it is more reasonable to select a reaction time of 3 h for the following optimization.

3.3.3. Methanol/Oleic Acid Molar Ratio. As can be seen from Figure 4(c), with the increase in a molar ratio of MeOH/OA, the yield of methyl oleate gradually increases. The molar ratio of MeOH/OA has little effect on the yield of methyl oleate. The yield of 73.3% can be obtained at the molar ratio of 5 : 1. The yield of 95.8% is obtained when the molar ratio is 15 : 1. When the highest molar ratio is 25 : 1, the yield reaches 96.6%, almost

unchanged. While esterification itself is a type of reversible reaction, more methanol can accelerate the reaction rate before reaching equilibrium. However, a 15 : 1 molar ratio is desirable in view of cost.

3.3.4. Catalyst Dosage. In the esterification reaction, a relatively large number of active sites can promote the positive direction of the reaction [18]. As shown in Figure 4(d), When the amount of catalyst was increased from 1% to 3% the weight of OA, methyl oleate yield increased from 84.8 to 95.2%. However, when the amount of catalyst was increased to 4% and 5%, the yield hardly changed. Therefore, a suitable amount of catalyst will accelerate the reaction rate, and the yield will reach a certain level, and increasing the amount of the catalyst has no practical significance for the reaction. Moreover, from the viewpoint of actually controlling the production cost, 3 wt% of the catalyst is the optimal condition.

In summary, considering the cost of production, the optimized reaction conditions are as follows: temperature 75°C, time 3 h, methanol/oleic acid molar ratio 15/1, catalyst dosage 3 wt%, and the yield of methyl oleate is 95.7%. As a contrast, the yield of the blank experiment without a catalyst is only 0.4%, while that of the control group with chitosan as a catalyst is 0.9% (Table 2). Therefore, it can be concluded that CS-SO₃H catalyst has an excellent catalytic effect and is a simple, economical and green catalyst for methyl oleate production.

3.4. Expanded Reaction Scale for the Production of Methyl Oleate. High yield could be obtained with fewer substrates, but when the amount of substrates multiplied, the catalytic activity may be affected by mass transfer resistance [35–37]. In order to ensure that the catalyst still has excellent catalytic performance in the presence of a large number of substrates, the large-scale reaction was carried out. Under the optimized conditions of the oleic acid amount of 20 g, the temperature of 75°C, the methanol to oleic acid molar ratio of 15 : 1, and the reaction time of 3 h, a high methyl oleate yield of 94.4% could be obtained. It shows that chitosan sulfonic acid catalyst still has a good catalytic effect in large scale reactions. This provides a basis for the development of new polymer-based high-efficiency acid catalysts.

3.5. Hot Filtration and Water Tolerance Tests. Thermal filtration is a simple and easy way to distinguish the types of catalysts. By comparing the yields after thermal filtration, the homogeneous/heterogeneous solid catalysts can be quickly judged [38]. Generally speaking, the heterogeneous behavior of catalysts is measured under the same conditions of comparative experiments. One group filtered the catalyst after 0.5 h and kept the reaction for another 2.5 h, while the other group did not have any treatment under the same conditions (Figure 5(a)). The results show that after removal of the catalyst, the yield remains basically unchanged, that is, the active site of the catalyst is not lost. This proves that CS-SO₃H is an excellent heterogeneous biomass-based polymer catalyst.

Owing to the esterification reaction is reversible, water will be formed in the reaction process. However, water, as a by-product of esterification, will lead to inactivation of the active site of the acid catalyst with poor water resistance, thus

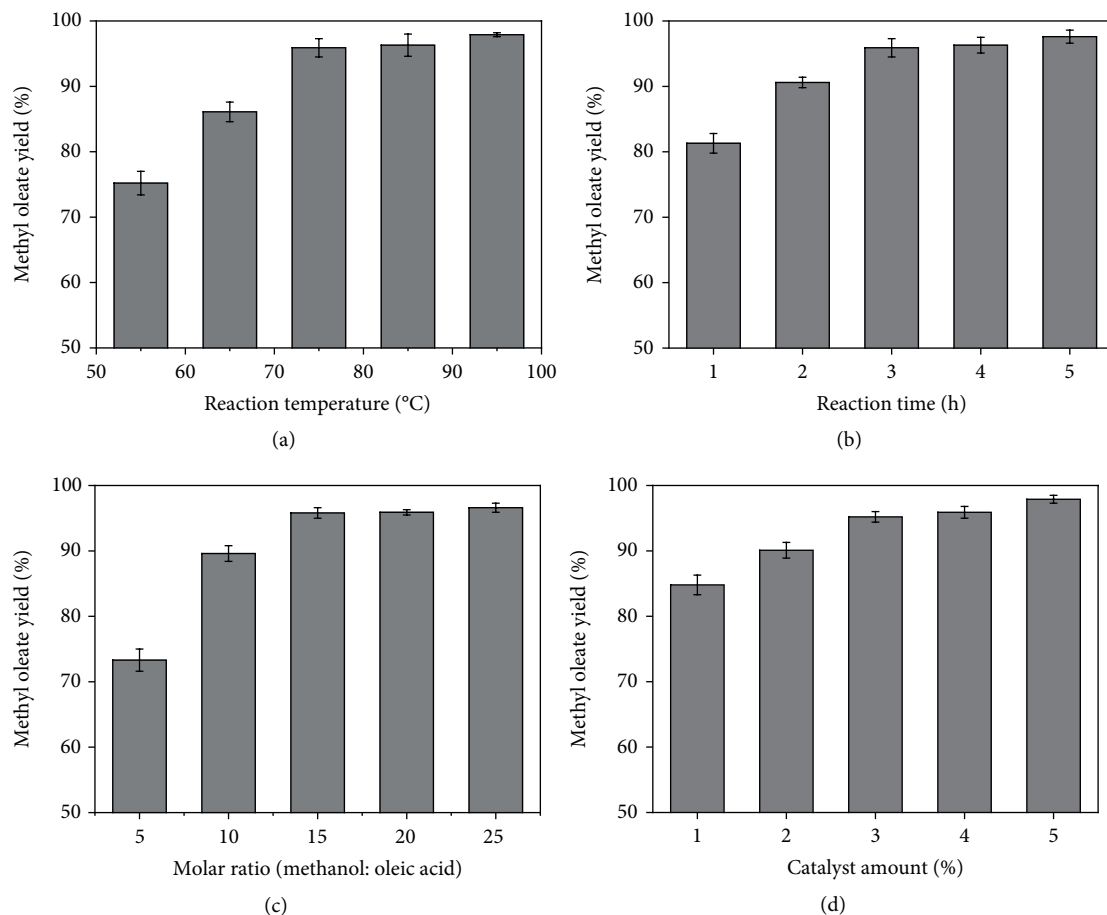


FIGURE 4: Performance optimization of oleic acid (AV = 184.52 mg KOH/g) with the CS-SO₃H catalyst: (a) reaction temperature, (b) reaction time, (c) methanol/oleic acid molar ratio, and (d) catalyst amount.

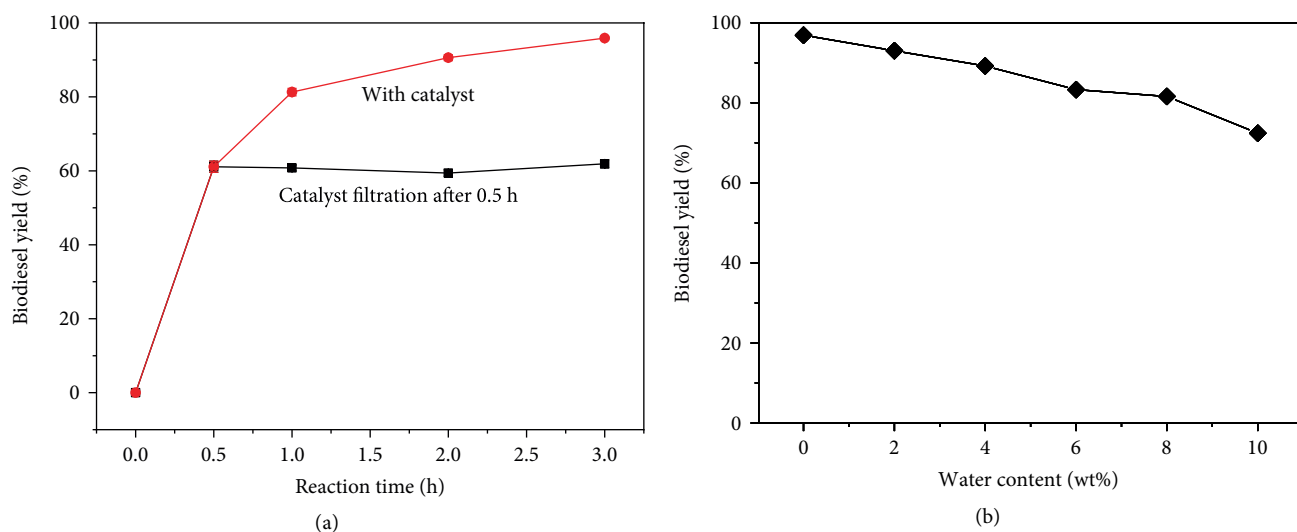


FIGURE 5: (a) Hot filtration test of CS-SO₃H in the esterification of oleic acid; (b) Water tolerance study of the CS-SO₃H catalyst. Reaction conditions: temperature 75°C, the CS-SO₃H catalyst of 3 wt%, time of 3 h, and methanol/oil molar ratio 15/1.

reducing the reaction rate, resulting in a lower yield of ester in certain reaction time. This will lead to poor reusability of the catalyst. Thus, the water tolerance of the catalyst is good,

which is beneficial to esterification [8]. We added a certain amount of water into the system to determine the water tolerance of the catalyst. At the same time, it can also achieve the

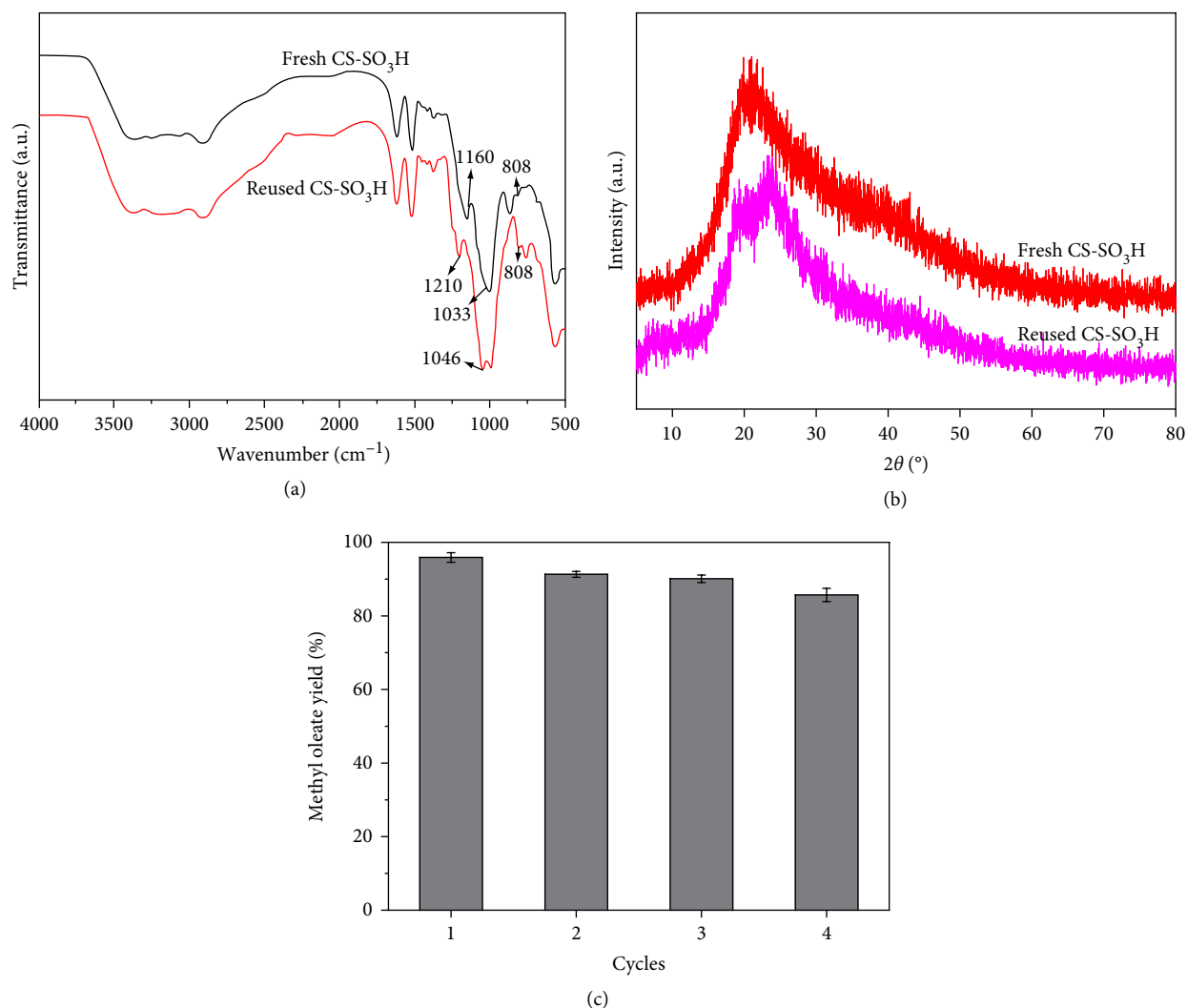
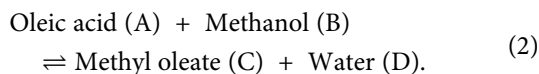


FIGURE 6: The fresh and reused CS-SO₃H (a) FT-IR; (b) XRD; (c) reusability of the CS-SO₃H catalyst. Reaction conditions: reaction temperature 75°C, the CS-SO₃H catalyst of 3 wt%, reaction time of 3 h, and methanol/oil molar ratio 15/1.

same effect for feedstocks which contain a small amount of water.



As can be seen from Figure 5(b), when the water content is 4 wt% of oil quality, the yield of methyl oleate is very close to 90%. When the water content is 8 wt%, the yield of methyl oleate can still reach 80%. With water content reaching 10 wt%, the yield can be reduced to 72.4%. This indicates that the catalyst has excellent water tolerance.

3.6. Reusability of Catalyst. For heterogeneous catalysts, their recyclability can not only reduce the production cost but also maximize environmental protection [14]. Therefore, it is necessary to explore the reusability of catalysts. The reusability of catalysts was determined under the optimal conditions. After each reaction cycle, the catalyst was centrifuged and washed alternately with petroleum ether and ethanol three times to remove the organic matter adhering on the catalyst.

After drying overnight at 80°C, the regenerated catalyst was used again for the next reaction.

As can be seen from Figure 6(a), the active site of sulfonic acid still exists, but the characteristic infrared absorption band moves from 1160 and 1033 cm⁻¹ to 1210 and 1046 cm⁻¹. This indicates that the catalyst is affected by impurities, and it is necessary to remove by repeated use of petroleum ether scrubbing. The absorption band at 808 cm⁻¹ belongs to C-O-S, which indicates that -SO₃H is still bonded to chitosan [26–28]. By comparing the XRD peaks of CS-SO₃H before and after the reaction (Figure 6(b)), no significant change in the shape of the peaks was observed, indicating that the catalyst was stable. The methyl oleate yield can still reach 85.7% after the catalyst is reused for four times (Figure 6(c)). Generally speaking, the sulfonic acid catalyst prepared by grafting method has good catalytic activity and stability, and the leaching amount of the active site is relatively small [25, 28]. For example, after five cycles of use, the yield of HS/C-SO₃H catalyst is still as high as 90% [11]. Moreover, the CS-SO₃H catalyst prepared by us has a high acid density

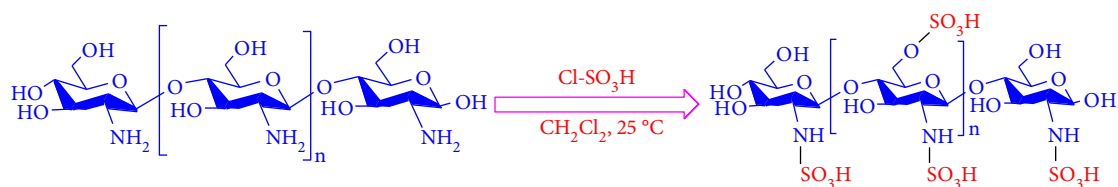
SCHEME 1: Synthesis of the biomass-based acid catalyst CS-SO₃H.

TABLE 3: Comparison of the performance of different heterogeneous catalysts in esterification.

NO.	Catalyst	Feedstock	Reaction conditions	Methyl oleate yield (Conversion) (%)	Reuse cycle (Conversion after last run)	Ref.
1	HS/C-SO ₃ H	Oleic acid	$T=80^{\circ}\text{C}$, CA = 3.6 wt%, M/O = 10:1, $t = 5$ h	96.9	5 (90)	[11]
2	FCHC-SO ₃ H	Oleic acid	$T = 80^{\circ}\text{C}$, CA = 4 wt%, M/O = 15:1, $t = 3$ h	96.7	5 (84.3)	[18]
3	Bamboo Ph-SO ₃ H	Oleic acid	$T=85^{\circ}\text{C}$, CA = 12 wt%, E/O = 7:1, $t = 3\text{h}^{\text{a}}$	96.0	5 (28)	[39]
4	Sugarcane bagasse -SO ₃ H	Oleic acid	$T = 50^{\circ}\text{C}$, CA = 0.1 wt%, M/O = 20:1, $t = 24$ h	85.1	5 (66.6)	[40]
5	Sulfonated carbon	FFA ^b	$T = 68^{\circ}\text{C}$, CA = 6 wt%, M/O = 15:1, $t = 3$ h	94.4	5 (60)	[41]
6	CS-SO ₃ H	Oleic acid	$T = 75^{\circ}\text{C}$, CA = 3 wt%, M/O = 15:1, $t = 3$ h	95.7	4 (85.7)	This work

^aThe reaction substrates are ethanol and oleic acid. ^bFFA denotes free fatty acids.

(3.81 mmol/g), which makes the catalyst maintain good reusability.

As can be seen from Table 3, entry 1 and 2 are bio-matrix composite catalysts with good reusability. Relative to entry 3, 4, 5, the reuse efficiency of biomass-based catalysts is poor. This is mainly due to the sulfonation reagent being generally sulfuric acid. Although it has a high acid density, the active sites are easy to leach in the reaction, resulting in a low reuse rate. However, CS-SO₃H is a stable biomass-based polymer material because it is directly bonded by chlorosulfonic acid and CS in the form of a covalent bond, rendering the catalyst of strong stability. After four cycles, the yield of CS-SO₃H can still reach 85.7%. Compared with entry 1 and 2, the yield of CS-SO₃H after reuse is roughly the same, but the synthesis method of CS-SO₃H is simpler and milder. This is an advantage for the polymer catalyst. Meanwhile, the reaction temperature of CS-SO₃H in esterification reaction is mild, the reaction time is short, and the amount of catalyst needed is less. This may be mainly due to the high acid density which provides more active sites and speeds up the reaction rate (Scheme 1).

4. Conclusion

In this paper, a simple method was used to prepare biomass-based polymer catalyst CS-SO₃H under mild conditions. The results showed that the catalyst had a high acid density (3.81 mmol/g), good catalytic performance in the esterification of OA and MeOH, and could efficiently prepare methyl oleate. Under the optimum reaction conditions, the yield of methyl

oleate was up to 95.7%. In addition, the catalyst has good stability and reusability. After four cycles, the yield of methyl oleate can still as high as 85.7%. This indicates that CS-SO₃H has good catalytic performance in the pre-esterification and esterification of biodiesel. Moreover, the preparation of catalysts from biomass raw materials not only greatly reduces the cost, but also can be used as a solution for the treatment of biomass waste. Therefore, the preparation of biomass-based polymer materials with high activity is of great significance in the production of biodiesel and has good application prospects in the field of cleaner production.

Data Availability

The data used to support the findings of this study are available from the corresponding author upon request.

Conflicts of Interest

The authors declare that they have no conflicts of interest.

Acknowledgments

This study was financially supported by the National Natural Science Foundation of China (21576059, 21666008 & 21908033), Key Technologies R&D Program of China (2014BAD23B01), Fok Ying-Tong Education Foundation (161030), and Guizhou Science & Technology Foundation ([2018]1037 & [2017] 5788).

References

- [1] R. Shan, L. Lu, Y. Shi, H. Yuan, and J. Shi, "Catalysts from renewable resources for biodiesel production," *Energy Conversion and Management*, vol. 178, pp. 277–289, 2018.
- [2] S. H. S. Abdullah, N. H. M. Hanapi, A. Azid et al., "A review of biomass-derived heterogeneous catalyst for a sustainable biodiesel production," *Renewable and Sustainable Energy Reviews*, vol. 70, pp. 1040–1051, 2017.
- [3] A. F. Lee, J. A. Bennett, J. C. Manayil, and K. Wilson, "Heterogeneous catalysis for sustainable biodiesel production via esterification and transesterification," *Chemical Society Reviews*, vol. 43, no. 22, pp. 7887–7916, 2014.
- [4] I. M. Atadashi, M. K. Aroua, A. A. Aziz, and N. M. N. Sulaiman, "Production of biodiesel using high free fatty acid feedstocks," *Renewable and Sustainable Energy Reviews*, vol. 16, no. 5, pp. 3275–3285, 2012.
- [5] H. Zhang, Q. Zhou, F. Chang et al., "Production and fuel properties of biodiesel from *Firmiana platanifolia* Lf as a potential nonfood oil source," *Industrial Crops and Products*, vol. 76, pp. 768–771, 2015.
- [6] R. Wang, M. A. Hanna, W. W. Zhou et al., "Production and selected fuel properties of biodiesel from promising nonedible oils: *Euphorbia lathyris* L., *Sapiumsebiferum* L. and *Jatropha curcas* L.," *Bioresource Technology*, vol. 102, no. 2, pp. 1194–1199, 2011.
- [7] H. Zhang, H. Li, H. Pan et al., "Efficient production of biodiesel with promising fuel properties from *Koelreuteria integrifoliola* oil using a magnetically recyclable acidic ionic liquid," *Energy Conversion and Management*, vol. 138, pp. 45–53, 2017.
- [8] H. Zhang, H. Li, H. Pan et al., "Magnetically recyclable acidic polymeric ionic liquids decorated with hydrophobic regulators as highly efficient and stable catalysts for biodiesel production," *Applied Energy*, vol. 223, pp. 416–429, 2018.
- [9] P. Syal, V. V. Verma, and R. Gupta, "Targeted mutations and MD simulations of a methanol-stable lipase YLIP9 from *Yarrowia lipolytica* MSR80 to develop a biodiesel enzyme," *International Journal of Biological Macromolecules*, vol. 104, pp. 78–88, 2017.
- [10] W. Xie and F. Wan, "Basic ionic liquid functionalized magnetically responsive Fe₃O₄@ HKUST-1 composites used for biodiesel production," *Fuel*, vol. 220, pp. 248–256, 2018.
- [11] Y. Wang, D. Wang, M. H. Tan et al., "Monodispersed hollow SO₃H-functionalized carbon/silica as efficient solid acid catalyst for esterification of oleic acid," *ACS Applied Materials & Interfaces*, vol. 7, no. 48, pp. 26767–26775, 2015.
- [12] S. Soltani, U. Rashid, S. I. Al-Resayes, and I. A. Nehdi, "Sulfonated mesoporous ZnO catalyst for methyl esters production," *Journal Cleaner Production*, vol. 144, pp. 482–491, 2017.
- [13] L. Li, B. Yan, H. Li et al., "SO₄²⁻/ZrO₂ as catalyst for upgrading of pyrolysis oil by esterification," *Fuel*, vol. 226, pp. 190–194, 2018.
- [14] T. A. Ngu and Z. Li, "Phosphotungstic acid-functionalized magnetic nanoparticles as an efficient and recyclable catalyst for the one-pot production of biodiesel from grease via esterification and transesterification," *Green Chemistry*, vol. 16, no. 3, p. 1202, 2014.
- [15] B. Yang, L. Leclercq, J. M. Clacens, and V. Nardello-Rataj, "Acidic/amphiphilic silica nanoparticles: new eco-friendly Pickering interfacial catalysis for biodiesel production," *Green Chemistry*, vol. 19, no. 19, pp. 4552–4562, 2017.
- [16] K. Nakajima and M. Hara, "Amorphous carbon with SO₃H groups as a solid Brønsted acid catalyst," *ACS catalysis*, vol. 2, no. 7, pp. 1296–1304, 2012.
- [17] W. Xie and F. Wan, "Immobilization of polyoxometalate-based sulfonated ionic liquids on UiO-66-2COOH metal-organic frameworks for biodiesel production via one-pot transesterification-esterification of acidic vegetable oils," *Chemical Engineering Journal*, vol. 365, pp. 40–50, 2019.
- [18] A. Wang, H. Li, H. Pan et al., "Efficient and green production of biodiesel catalyzed by recyclable biomass-derived magnetic acids," *Fuel Processing Technology*, vol. 181, pp. 259–267, 2018.
- [19] W. L. Xie and J. L. Wang, "Immobilized lipase on magnetic chitosan microspheres for transesterification of soybean oil," *Biomass Bioenergy*, vol. 36, pp. 373–380, 2012.
- [20] P. A. Russo, M. M. Antunes, P. Neves et al., "Mesoporous carbon-silica solid acid catalysts for producing useful bio-products within the sugar-platform of biorefineries," *Green Chemistry*, vol. 16, no. 9, pp. 4292–4305, 2014.
- [21] F. A. Dawodu, O. Ayodele, J. Xin, S. Zhang, and D. Yan, "Effective conversion of nonedible oil with high free fatty acid into biodiesel by sulphonated carbon catalyst," *Applied Energy*, vol. 114, pp. 819–826, 2014.
- [22] Y. Zhang, W. T. Wong, and K. F. Yung, "Biodiesel production via esterification of oleic acid catalyzed by chlorosulfonic acid modified zirconia," *Applied Energy*, vol. 116, pp. 191–198, 2014.
- [23] B. S. Reddy, A. Venkateswarlu, G. N. Reddy, and Y. R. Reddy, "Chitosan-SO₃H: an efficient, biodegradable, and recyclable solid acid for the synthesis of quinoline derivatives via Friedländer annulation," *Tetrahedron Letters*, vol. 54, no. 43, pp. 5767–5770, 2013.
- [24] T. C. dos Santos, E. C. Santos, J. P. Dias, J. Barreto, F. L. Stavale, and C. M. Ronconi, "Reduced graphene oxide as an excellent platform to produce a stable brønsted acid catalyst for biodiesel production," *Fuel*, vol. 256, p. 115793, 2019.
- [25] R. S. Thombal, A. R. Jadhav, and V. H. Jadhav, "Biomass derived β-cyclodextrin-SO₃H as a solid acid catalyst for esterification of carboxylic acids with alcohols," *RSC Advances*, vol. 5, no. 17, pp. 12981–12986, 2015.
- [26] Y. Xiang, M. Yang, Z. Guo, and Z. Cui, "Alternatively chitosan sulfate blending membrane as methanol-blocking polymer electrolyte membrane for direct methanol fuel cell," *Journal of Membrane Science*, vol. 337, no. 1–2, pp. 318–323, 2009.
- [27] Z. Yao, C. Zhang, Q. Ping, and L. L. Yu, "A series of novel chitosan derivatives: synthesis, characterization and micellar solubilization of paclitaxel," *Carbohydrate Polymers*, vol. 68, no. 4, pp. 781–792, 2007.
- [28] C. S. Caetano, M. Caiado, J. Farinha et al., "Esterification of free fatty acids over chitosan with sulfonic acid groups," *Chemical Engineering Journal*, vol. 230, pp. 567–572, 2013.
- [29] A. Wang, H. Li, H. Zhang, H. Pan, and S. Yang, "Efficient Catalytic Production of Biodiesel with acid-base bifunctional rod-Like Ca-B oxides by the sol-gel approach," *Materials*, vol. 12, no. 1, p. 83, 2019.
- [30] H. Yu, S. Niu, C. Lu, J. Li, and Y. Yang, "Preparation and esterification performance of sulfonated coal-based heterogeneous acid catalyst for methyl oleate production," *Energy Conversion and Management*, vol. 126, pp. 488–496, 2016.
- [31] G. Pathak, D. Das, K. Rajkumari, and L. Rokhum, "Exploiting waste: towards a sustainable production of biodiesel using *Musa acuminata* peel ash as a heterogeneous catalyst," *Green Chemistry*, vol. 20, no. 10, p. 2365, 2018.
- [32] M. C. Nongbe, T. Ekou, L. Ekou, K. B. Yao, E. Le Grogneac, and F.-X. Felpin, "Biodiesel production from palm oil using

- sulfonated graphene catalyst,” *Renewable Energy*, vol. 106, pp. 135–141, 2017.
- [33] H. Pan, H. Li, X. F. Liu et al., “Mesoporous polymeric solid acid as efficient catalyst for trans esterification of crude *Jatropha curcas* oil,” *Fuel Processing Technology*, vol. 150, pp. 50–57, 2016.
- [34] Y. Ning and S. Niu, “Preparation and catalytic performance in esterification of a bamboo-based heterogeneous acid catalyst with microwave assistance,” *Energy Conversion and Management*, vol. 153, pp. 446–454, 2017.
- [35] Y. Zhou, S. L. Niu, and J. Li, “Activity of the carbon-based heterogeneous acid catalyst derived from bamboo in esterification of oleic acid with ethanol,” *Energy Conversion and Management*, vol. 114, pp. 188–196, 2016.
- [36] K. Malins, J. Brinks, V. Kampars, and I. Malina, “Esterification of rapeseed oil fatty acids using a carbon-based heterogeneous acid catalyst derived from cellulose,” *Applied Catalysis A: General*, vol. 519, pp. 99–106, 2016.
- [37] Z. Gao, S. Tang, X. Cui, S. Tian, and M. Zhang, “Efficient mesoporous carbon-based solid catalyst for the esterification of oleic acid,” *Fuel*, vol. 140, pp. 669–676, 2015.
- [38] R. Cano, A. F. Schmidt, and G. P. McGlacken, “Direct arylation and heterogeneous catalysis; ever the twain shall meet,” *Chemical Science*, vol. 6, no. 10, pp. 5338–5346, 2015.
- [39] S. Niu, Y. Ning, C. Lu, K. Han, H. Yu, and Y. Zhou, “Esterification of oleic acid to produce biodiesel catalyzed by sulfonated activated carbon from bamboo,” *Energy Conversion and Management*, vol. 163, pp. 59–65, 2018.
- [40] K. P. Flores, J. L. O. Omega, L. K. Cabatingan, A. W. Go, R. C. Agapay, and Y.-H. Ju, “Simultaneously carbonized and sulfonated sugarcane bagasse as solid acid catalyst for the esterification of oleic acid with methanol,” *Renewable Energy*, vol. 130, pp. 510–523, 2019.
- [41] A. B. Fadhil, A. M. Aziz, and M. H. Al-Tamer, “Biodiesel production from *Silybum marianum* L. seed oil with high FFA content using sulfonated carbon catalyst for esterification and base catalyst for transesterification,” *Energy Conversion and Management*, vol. 108, pp. 255–265, 2016.